# Needle puncture forces in liver blood vessels: towards vein implantation in a liver phantom.

Thesis by Sander van der Velden.

*October 2018*

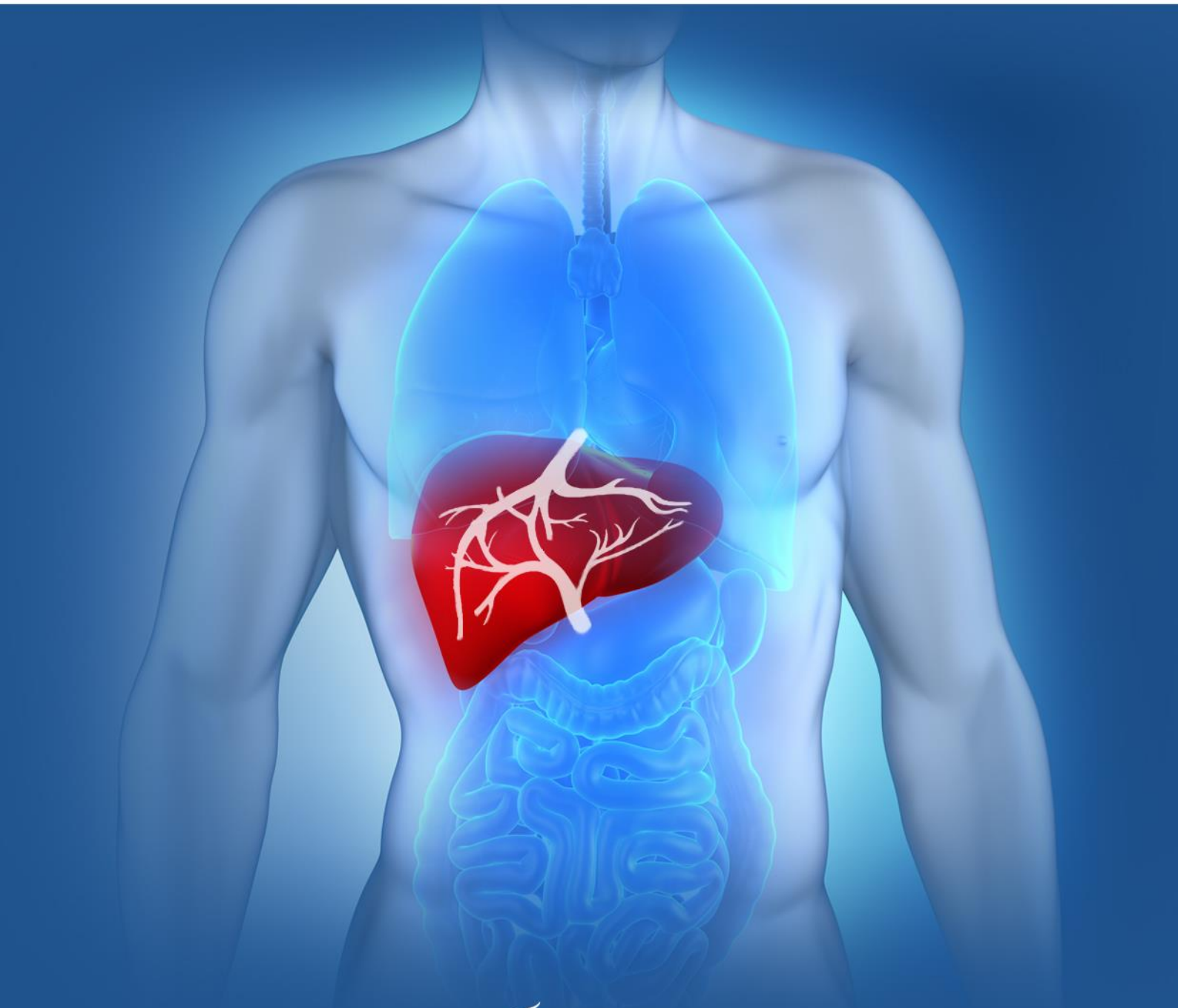

TU Delft

# Needle puncture forces in liver blood vessels: towards vein implantation in a liver phantom.

By

Sander van der Velden

in partial fulfilment of the requirements for the degree of

**Master of Science**
in Biomedical Engineering

at the Delft University of Technology,
to be defended publicly on Thursday November 1, 2018 at 14:00.

| | | |
|---|---|---|
| Supervisors: | Dr. J.J. van den Dobbelsteen | TU Delft |
| | Ir. T.L. de Jong | TU Delft |
| Thesis committee: | Dr. J.J. van den Dobbelsteen | TU Delft |
| | Ir. T.L. de Jong | TU Delft |
| | Dr. J. Zhou | TU Delft |

*This thesis is confidential and cannot be made public until December 31, 2019.*

An electronic version of this thesis is available at http://repository.tudelft.nl/.

TU Delft

# Preface

After my bachelor in Mechanical Engineering, I started my master Biomedical Engineering at the TU Delft, due to my interest in medical topics. For my graduation project, I have done research on needle interaction forces in human liver blood vessels to collect data for the improvement of a liver phantom. The combination of theoretical work and experimental research has made it an interesting and enjoyable project for me. The results of my work would not have been possible without the help and support of some people that I would like to thank here.

I would like to start by thanking my supervisors Tonke de Jong and John van den Dobbelsteen for their help during my entire graduation project. I really enjoyed your enthusiastic and positive way of guiding me. When needed, you were always available to share your knowledge and point me in the right direction. That is very much appreciated. I would like to thank Gert-Jan Kleinrensink and Yvonne Steinvoort, for the provided opportunities to do research at the Erasmus MC. It was a nice and informative experience for me to do experiments with livers. Furthermore, I would like to thank Jang Zhang and Jan Vos for helping me prepare the blood vessels from the livers during the experiments.

Finally, I would like to thank my parents for their support during my entire study at the TU Delft.

*Sander van der Velden*
*Delft, October 2018*

# Table of Contents

# --- Summary ---

# Needle puncture forces in liver blood vessels: towards vein implantation in a liver phantom.

Sander van der Velden, Delft University of Technology

***Abstract*— Treatment of liver diseases is often done by means of interventional radiology and thereby needles are widely used. These needles are under constant development and therefore needle-tissue interaction data are necessary. The goal of this study is to provide data on needle forces during puncturing of liver blood vessels. These data can be used to mimic blood vessels in a polyvinyl alcohol (PVA) liver phantom, intended for needle development and training purposes. Needle insertion experiments were done on human livers, by puncturing portal veins, hepatic veins, hepatic arteries and liver tissue. The resulting force data show that peak forces are higher during puncturing of liver veins (median=2.20 N, interquartile range=1.46 N to 3.67 N) than during puncturing of liver tissue (median=0.38 N, interquartile range=0.31 N to 0.51 N). The force data were used to find a blood vessel mimicking material. Silicone, with the addition of a mesh fabric, was found to mimic the peak forces of liver veins during needle insertion. A silicone blood vessel was created with use of a 3D-printed blood vessel structure made of water-soluble PVA. The addition of the mesh fabric, furthermore ensures proper bonding between the silicone blood vessel and the PVA liver tissue. The methods described in this study can be used to implant artificial veins in a PVA liver phantom.**

***Index Terms*— Blood vessels, liver phantom, needle insertion forces.**

## I. Introduction

The liver is an important and complex organ and treatment of liver diseases is often done by means of interventional radiology. In interventional radiology, minimally invasive procedures are performed using radiologic image guidance to diagnose and treat diseases. Needles are widely used in interventional radiology and interventional radiologists thereby use imaging techniques, such as ultrasound, for needle guidance. Needles are under constant development and they need to be tested for needle-tissue interaction forces, needle bending and steerability for example. Due to safety and ethical reasons, it is difficult to test needles on patients and therefore an appropriate alternative is needed. Animals and human cadavers are currently used for development and training purposes, but a realistic liver phantom would be preferable. A liver phantom needs to mimic the human liver by internal structure, mechanical properties and imaging properties. This way, the needle-tissue interaction during needle interventions can be mimicked using a liver phantom. Besides the use for the development of needles, a liver phantom can be used as a training device for needle interventions.

A recent study by De Jong et al. [1] provided a material, polyvinyl alcohol (PVA), that mimics the forces of liver tissue during needle-tissue interaction. The heterogeneity of the liver tissue is mimicked by subjecting the PVA to freeze-thaw cycles and that way a liver phantom was created [2]. The liver phantom can be further improved by implanting blood vessels. During needle interventions, puncturing of these blood vessels could result in different forces on the needle and thus in different needle movement and haptic feedback.

### A. Related work

Little research has been done on needle-blood vessel interaction forces, certainly in the field of interventional radiology. An indication of these forces can be found using studies with both animal tissue and blood vessels that are located outside the liver. Studies on needle-blood vessel interaction in the liver were found using porcine livers [3-6], in which peak forces between 0.4 N and 1.3 N were measured. Furthermore, human blood vessels located outside the liver were used for needle insertion experiments [7-10]. Puncturing of the jugular vein resulted in peak forces between 1.35 N and 2.02 N [10] and manually puncturing the femoral artery resulted in peak forces between 0.13 N and 8.89 N [9]. Finally, studies were found using animal blood vessels located outside the liver [8, 11-16]. Puncturing of porcine jugular veins resulted in forces between 0.3 N and 1.3 N [11].

These results can be compared with needle-liver interaction forces. One study used human livers and showed forces between 0.1 N and 0.65 N (median = 0.18 N) [1]. This gives a good indication of the forces during puncturing of a human liver. Most other studies were done using porcine livers, both in vivo [17-20] and ex vivo [3-6, 21-33]. One of the research groups examined both liver tissue and liver blood vessels in ex vivo porcine liver [5]. The results showed that puncturing of blood vessels in porcine liver results in higher forces than puncturing of liver tissue. This gives a good indication that blood vessels result in higher puncture forces than liver tissue.

However, no data are available on needle interaction forces using human liver blood vessels. Furthermore, most of the data found in literature are difficult to compare due to the use of different experimental methods.

### B. Goal and approach of the study

The goal of this study is to provide insight into the needle forces during puncturing of blood vessels from the human liver. The resulting data are used to mimic veins in a PVA liver phantom, designed for needle interventions.

First, needle insertion experiments are done to collect force data during puncturing of blood vessels from the human liver.

These data are then used to find a blood vessel mimicking material that mimics these forces during needle puncturing. The final step is to use that material to create a blood vessel structure that can be implanted in a PVA liver phantom.

## II. Methods and Materials

### A. Needle insertion experiment with human livers

Data were collected during three experiments, in which blood vessels from three human livers were extracted from the liver and punctured with a needle. The livers were made available at the department of Neuroscience at the Erasmus MC in Rotterdam. The livers were fresh-frozen and expected to be healthy. Needle forces were collected by puncturing portal veins, hepatic veins, hepatic arteries and liver tissue. Experiments with liver tissue were done to compare the blood vessel forces to the liver tissue forces.

#### 1) Experimental setup and specimens

The experimental setup consisted of a linear stage (EGSL-BS-45-200-3P, Festo BV, Delft, The Netherlands) that moves in vertical direction. A force sensor (LSB200-FSH00104, FUTEK Advanced Sensor Technology Inc., Irvine, CA, USA) and a needle were attached to the linear stage to measure the forces during movement of the needle (Figure 1A). 18G two-part trocar needles (Cook Medical, Bloomington, IN, USA) were used during the experiments. This type of needle is commonly used during radiologic interventions. The blood vessels were cut open (Figure 1B) and placed between two identical aluminum plates. These plates had seven holes in them, with a diameter of 7 mm and a distance of 10 mm between the centers. Through these holes the needle punctured the blood vessel wall. The holes on the outside of the aluminum plates were used to fix the plates with bolts and nuts, in order to hold the blood vessel in place. The aluminum plates were then placed in a construction that was mounted underneath the needle. This construction could be manually moved in horizontal direction to align the needle with the holes in the plates (Figure 1C). This way, multiple insertions could be done for a single blood vessel sample.

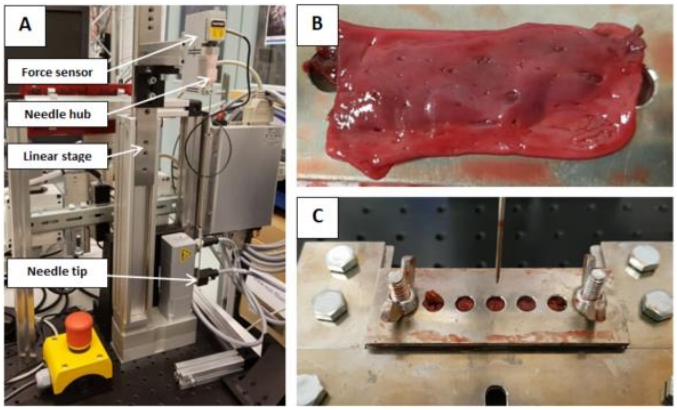


Fig 1. (A) the experimental setup, containing the force sensor and the needle, which are both mounted on the linear stage. (B) a liver vein that is retrieved from the liver and cut open. (C) a liver vein fixed between two aluminum plates and mounted underneath the needle.

The different blood vessels were carved out of the liver using scalpels. Preliminary experiments showed the necessity of including a layer between 2 mm and 5 mm of liver tissue on the outside of the blood vessel wall, to prevent damaging the vessel. Each part of a blood vessel that was extracted, was classified as a different sample. For each sample, the type of blood vessel and the approximate location in the liver were noted. In addition, samples were taken that included only a 5 mm layer of liver tissue. Finally, the samples were placed in a saline solution until they were used for measurements.

#### 2) Peak force measurement

The needle was inserted and retracted automatically at 5 mm/s. The needle insertion experiments were controlled and analyzed using Matlab R2014b (The MathWorks Inc., Natick, MA, USA). During the insertion, data on needle force, needle displacement and time were recorded.

Due to the layer of liver tissue that was still attached to the blood vessel wall, there were two possible orientations of the blood vessel sample during a measurement. The sample could be punctured with the vessel wall on the top or with the vessel wall on the bottom. This was randomized and the influence of the orientation was examined.

### B. Blood vessel mimicking material

#### 1) Material characteristics

The blood vessel mimicking material needs to mimic the needle forces during puncturing of human liver veins. We therefore chose the desired peak forces to be in the interquartile range (IQR) of the peak forces resulting from the liver blood vessel experiment.

It must be considered that the material needs to be formed into the shape of a blood vessel. The typical wall thickness of the larger liver veins is about 0.5 mm [34]. For the blood vessel mimicking material we chose the thickness to be between 0.5 mm and 1.0 mm, to ensure a decent representation. Furthermore, the material needs to be implanted into a PVA phantom. A possibility of bonding with PVA is therefore necessary. Finally, the blood vessel mimicking material must not compromise the ability to use the liver phantom with ultrasound for needle guidance.

Soft human tissues are commonly mimicked by polymers, like agarose, gelatin, polyvinyl alcohol (PVA), polyvinyl chloride (PVC) and silicone [35]. Three polymers were included in this study, PVA, PU and silicone, because they are expected to have characteristics as mentioned in this section.

#### 2) Needle insertion forces

Needle insertion experiments were done on PVA, PU and silicone, using the same experimental setup and insertion methods as described in Section II-A. Different samples are shown in Figure 2A. Preliminary tests showed that puncturing of PVA samples (Selvol PVOH 165, Sekisui Chemical Group, NJ, USA) resulted in peak forces that were too low. Samples of 7m% PVA were used with 2-8 freeze-thaw cycles of 8 hours freezing and 8 hours thawing. Puncturing of PU-rubber (PMC-780 Dry, Smooth-On Inc., Macungie, PA, USA) resulted in a force pattern that differed too much from the

force pattern during puncturing of a liver vein. This was primarily due to a high and fluctuating friction force.

Two types of silicone, with different layer thicknesses, were used to examine the puncture forces: Dragon Skin 20 (Smooth-On Inc., Macungie, PA, USA) and Smooth-Sil 950 (Smooth-On Inc., Macungie, PA, USA). Thi-Vex (Smooth-On Inc., Macungie, PA, USA) was added during the production of the silicone. Thi-Vex increases the viscosity of the silicone so it can be more easily applied to non-horizontal surfaces. The addition of Thi-Vex does not influence the needle force.

Preliminary tests showed that Dragon Skin 20, with a Shore A hardness of 20, resulted in peak forces that were too low. Therefore, Smooth-Sil 950, with a Shore A hardness of 50, was selected. To further increase the peak forces, a mesh fabric was added to the silicone. In addition to this feature, the mesh fabric ensures bonding between the silicone and PVA (described in Section II-D). The mesh fabric can be applied during the hardening process of the silicone or afterwards using Sil-Poxy glue (Smooth-On Inc., Macungie, PA, USA). The addition of glue does not affect the needle forces.

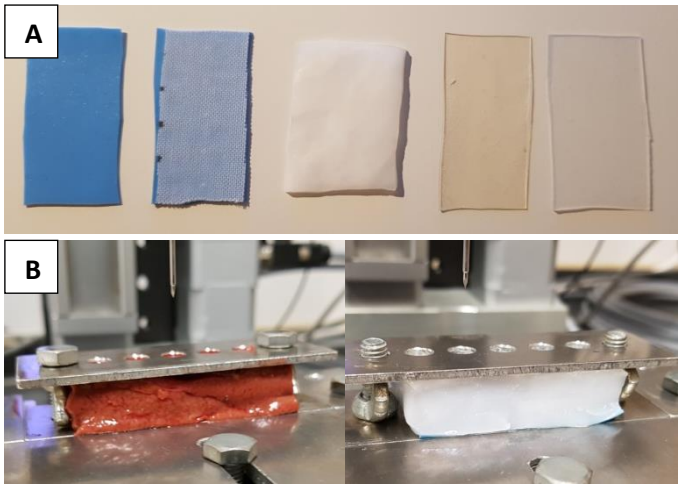


Fig. 2. (A) Samples of blood vessel mimicking materials used for needle insertion experiments. From left to right: Smooth-Sil 950 silicone, Smooth-Sil 950 silicone with mesh fabric, PVA (7m%, 4 freeze-thaw cycles), PMC-780 Dry PU-rubber, Dragon Skin 20 silicone. (B) Samples used for force profile experiments. Left: 15 mm layer of liver tissue with liver vein attached. Right: 15 mm layer of PVA with silicone and mesh fabric attached.

### *C. Blood vessel structure recreation*

It is possible to create thin-walled hollow tubes using the silicone, both with and without mesh fabric. A more complex blood vessel structure can be 3D-printed using water-soluble PVA. The silicone can then be smeared on the structure and, after the silicone is hardened, the structure is placed in water. The water-soluble PVA will dissolve and a thin-walled silicone blood vessel structure will remain. This method was tested using a simplified model of the portal vein. Therefore, a 3D-model of the liver veins was made with 3DSlicer 4.8.1 [36], using a CT-scan of the abdomen. Figure 3 shows the anterior view of both the portal vein and the hepatic vein models in MeshLab [37], that can be used to edit the models.

### *D. Implantation in PVA*

Bonding between the blood vessel and the PVA liver tissue is necessary to keep the blood vessel in place during needle interaction. The silicone itself does not bond with PVA. Therefore a mesh fabric was added to the silicone, to create a physical link with both the silicone and the PVA. The mesh was added to flat-surfaced silicone layers and thin-walled silicone tubes, both with and without Sil-Poxy glue. PVA (4m%) was then poured over the samples and they were subjected to 2 freeze-thaw cycles of 8 hours freezing and 8 hours thawing. After that, the bonding was examined.

Furthermore, the current liver phantom is intended to be used with ultrasound needle guidance. An ultrasound test was done using the silicone tubes with mesh fabric, embedded in PVA. This was done to check whether both the blood vessels and the needle tip are visible during puncturing.

Finally, the force profile of a needle insertion was examined using both human liver blood vessel samples and PVA and silicone samples. The same experimental setup and insertion methods are used as described in Section II-A. First, 18 needle insertions were done in human liver blood vessels with about 15 mm of liver tissue still attached to the blood vessel (Figure 2B). Then, needle insertions were done using samples with a layer of silicone and mesh fabric with a 15 mm layer of PVA attached (4m%, 2 freeze-thaw cycles of 8 hours freezing and 8 hours thawing). For the silicone, two different layer thicknesses were used: 0.6 mm and 1.1 mm. All experiments were done with the (artificial) blood vessel wall on the bottom.

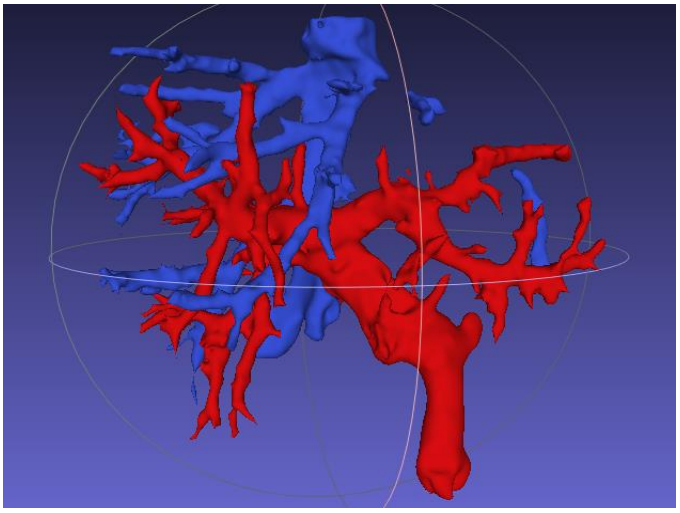

Fig. 3. Anterior view of the 3D-model of the portal vein (red) and hepatic vein (blue) in MeshLab. The left hepatic vein is partially missing.

## III. Results

### *A. Needle insertion experiment*

#### *1) Peak forces*

A total of 231 measurements were done. Figure 4 shows a boxplot with the peak forces per blood vessel type or liver tissue. All data of the three different livers are combined, because there were no clear differences between the three livers. There is no clear difference between the peak forces of the portal vein (median=1.98 N, IQR=1.45 N to 2.97 N) and the hepatic vein (median=2.51 N, IQR=1.54 N to 4.40 N), although the variability of the hepatic vein is slightly larger. Puncturing liver veins results in higher forces than puncturing liver tissue (median=0.38 N, IQR=0.31 N to 0.51 N). The

results of the combined data of the hepatic vein and portal vein (median=2.20 N, IQR=1.46 N to 3.67 N) are shown in Figure 5. The range of desired peak forces (IQR) for the blood vessel mimicking material is shown by the red dotted lines.

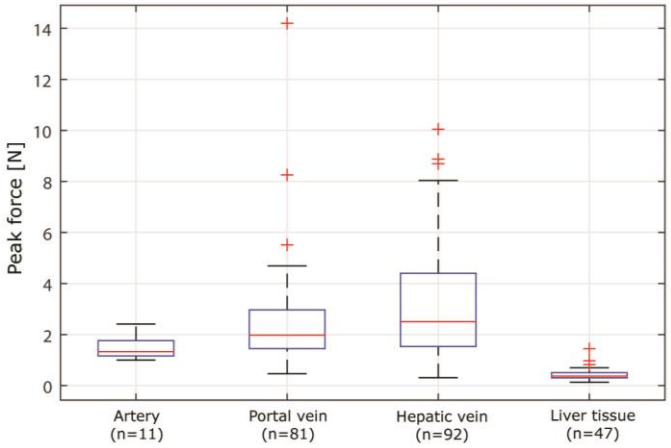


Fig 4. Boxplot of the peak forces per blood vessel type or liver tissue. The data for all three human livers are combined.

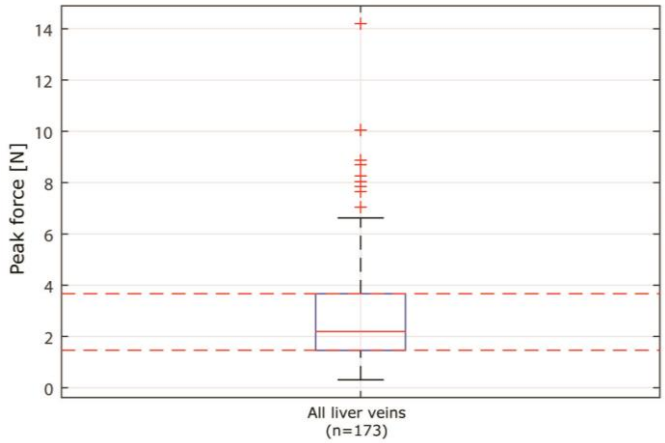


Fig. 5. Boxplot of the peak forces of the measurements of all portal veins and hepatic veins combined. The red dotted lines show the range of the desired peak forces for the blood vessel mimicking material.

*2) Blood vessel location and orientation*

In general, puncturing of the proximal blood vessels results in slightly higher forces than puncturing of the distal blood vessels. However, this is not always the case, certainly not for the portal vein. This is shown in Appendix C of the thesis.

No clear differences can be seen in the peak forces when looking at the two different orientations of the blood vessel wall. This is shown in Section 3.2.4 of the thesis.

### *B. Blood vessel mimicking material*

Figure 6 shows a boxplot of the peak forces using Smooth-Sil 950 silicone. The peak forces are in the desired range when using a 0.9 mm to 1.1 mm silicone layer (median=1.68 N, IQR=1.63 N to 1.71 N) or a 0.9 mm to 1.2 mm silicone layer with mesh fabric (median=3.00 N, IQR=2.46 N to 3.42 N). For a 0.6 mm to 0.8 mm silicone layer with mesh fabric, the peak forces are almost all in the desired range (median=1.63 N, IQR=1.46 N to 1.73 N).

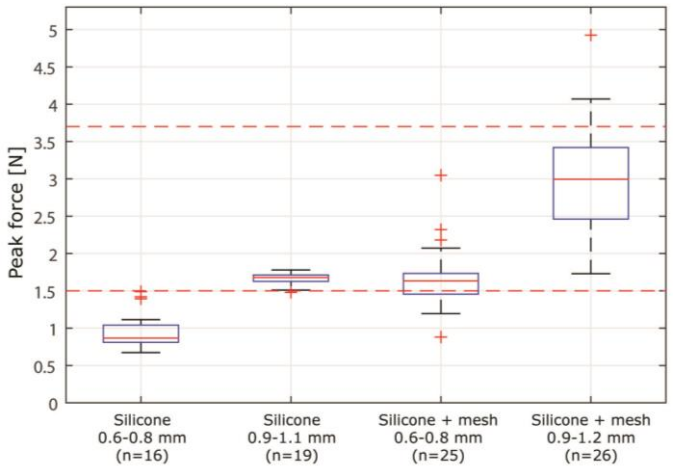


Fig. 6. Boxplot of the peak forces of Smooth-Sil 950 silicone, with and without mesh fabric, using different silicone thicknesses.

### *C. Blood vessel structure recreation*

The result of the silicone portal vein is shown in Figure 7. The mesh fabric can be applied using glue. The water-soluble PVA structure is inside the vein and can be dissolved in water.

Fig. 7. Silicone blood vessel created with a simplified, 3D-printed, portal vein model.

### *D. Implantation in PVA*

The addition of mesh fabric to the silicone, both with and without glue, ensured a proper bonding with the PVA. This was the case for both the flat silicone layers and the silicone tubes. During puncturing with a needle, the silicone remained bonded to the PVA as well.

The results of the ultrasound scan are shown in Figure 8. It shows that both the blood vessels and the needle are visible and ultrasound needle guidance is therefore possible.

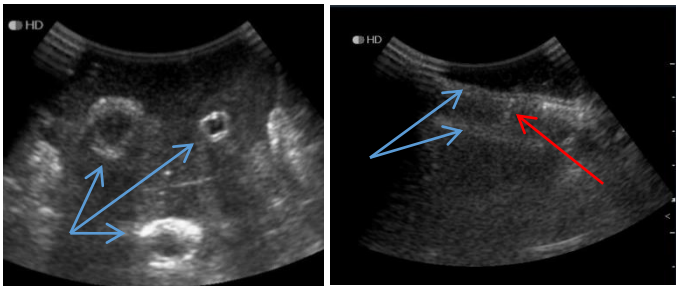

Fig. 8. Ultrasound scans of three silicone tubes embedded in PVA. The blue arrows indicate the silicone blood vessel wall and the red arrow indicates the needle tip (in-plane) after puncturing the silicone blood vessel wall.

Figure 9 shows a typical example of the force profile during needle insertion and retraction in a liver sample and two phantom samples. The friction force during retraction of the needle is higher for the 1.1 mm silicone sample compared to the human liver sample. For the 0.6 mm silicone sample, the friction force during insertion is lower than for the human liver sample. During puncturing of the silicone and mesh fabric, in general, a double peak is shown followed by a downward peak.

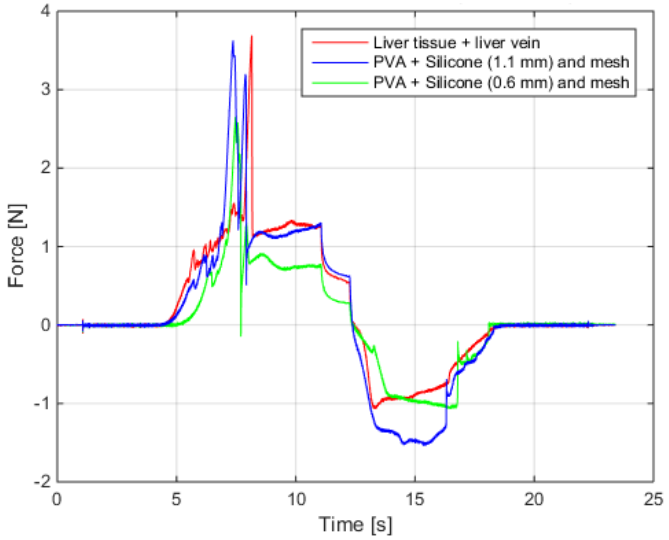


Fig. 9. A typical example of the force profiles of needle insertions into human liver samples and phantom samples. The human liver samples consist of a 15 mm layer of liver tissue with a single liver vein wall attached. The phantom samples consist of a 15 mm layer of PVA (4m%, 2 freeze-thaw cycles) with a 1.1 mm or 0.6 mm layer of silicone and mesh fabric attached.

## IV. Discussion

### A. *Needle insertion experiment*

Needle insertion experiments were done using three human livers, to examine the peak forces during puncturing of liver blood vessels. The livers were examined with a durometer to compare the hardness of the different livers. Needle insertions were done on portal veins, hepatic veins, hepatic arteries and on the liver tissue. The location and the orientation of the blood vessel were examined as well.

The liver hardness was examined using a Shore OO durometer (Dalian Teren Instruments Co., Ltd, Dalian, China). This was done to get an indication of the liver hardness and to compare the different livers. The results of the durometer showed that there were no clear differences between the three livers. Therefore, no significant differences in needle forces are expected between the livers due to their hardness.

The results of the peak forces, show that puncturing of a blood vessel results in a higher force than puncturing of the surrounding liver tissue. The large variability and the outliers, might be due to the fact that the blood vessels contain a lot of branches. When the needle punctures at a branch, this can result in a higher force due to local thickening of the blood vessel wall. Furthermore, it was expected that arteries would result in higher peak forces than veins, because of their relatively thick walls. However, the results show that this is not the case. This might be due to the smaller vessel diameter of the arteries and the different layer composition of the arteries and veins. Arteries relatively contain more smooth muscle tissue and veins more collagenous tissue [34].

The orientation of the blood vessel wall has no influence on the peak force during puncturing. Thus, the peak force does not change if the vessel is punctured from the inside instead of from the outside. In general, puncturing of the proximal blood vessels results in higher peak forces than puncturing of the distal blood vessels. This is probably due to the fact that the proximal veins are larger, contain more blood and thus have a thicker wall.

To conclude, it must be considered that in vivo blood vessels might have different mechanical properties than ex vivo blood vessels. Puncturing in vivo blood vessels could therefore result in different needle forces [38,39]. The same applies to needle insertions into blood vessels from sick livers, like cirrhotic livers. Finally, different needle insertion parameters, such as the needle diameter, the insertion velocity and the insertion angle, can influence the needle force as well.

### B. *Mimicking liver veins*

The Smooth-Sil 950 silicone was chosen as blood vessel mimicking material. The addition of a mesh fabric and a silicone thickness between 0.6 mm and 1.2 mm, resulted in the desired range of peak forces. In addition, the mesh fabric ensures a proper bonding between the silicone and PVA and ultrasound needle guidance remains possible.

A blood vessel structure can be precisely created with a 3D-printer using water-soluble PVA. The 3D-printed structure can remain in the silicone vessel during further production of the PVA liver phantom. This ensures that the structure of the silicone blood vessels remains in the correct shape and position when the PVA is poured in the liver mold. A downside of the 3D-printing method is that it takes quite some time to dissolve all of the water-soluble PVA from the silicone blood vessel. Furthermore, it is difficult to remove the support structure, used during the 3D-printing, because it is made of the same material as the blood vessel structure. This problem might partially be solved by using different settings for the support structure.

The force profile of the phantom samples resembles the force profiles of the human liver samples. It needs to be mentioned that the layer of PVA in the 0.6 mm silicone sample was about 2 mm thinner than the liver tissue samples. This explains why the force starts to rise later when using the 0.6 mm silicone samples. This might also result in less friction. The double peak at the silicone samples is probably the result of the mesh fabric in combination with the inner and outer needle. The downward peak might be due to oscillation of the thin silicone layer just after it is punctured.

### C. *Steps towards an improved liver phantom*

To implant veins in the liver phantom, several steps need to be made. First, 3D-models of the desired vein structures must be designed. The structures can then be 3D-printed using water-soluble PVA and used to create the silicone blood vessels. This can be done by applying the silicone with a brush. However, this method makes it difficult to create an even layer of silicone. It can be considered to submerge the entire structure in silicone without the addition of Thi-Vex.

Then, the structure needs to be kept in motion to prevent the silicone from dripping off during the hardening process. Another option is to develop a mold in which the silicone can be poured around the water-soluble PVA structure.

The mesh fabric can be applied in two ways. Either by gluing it onto the silicone, or by placing in onto the silicone during the hardening process. The latter is time-dependent and therefore more difficult. However, this method can be used to create a more even layer of silicone by applying pressure to the mesh while the silicone is still soft.

To implant the veins into a PVA liver phantom, a liver mold must be designed in which the silicone blood vessel structures can be placed. It needs to be ensured that the vessels remain in the correct shape and position during the pouring of the PVA into the liver mold. After the PVA has been poured, freeze-thaw cycles can be applied. Finally, the entire liver phantom can be placed in water to dissolve the water-soluble PVA structure inside the silicone blood vessels.

## V. Conclusion

Experiments were conducted to examine the needle forces during puncturing of blood vessels from the liver. The results show that puncturing of blood vessels results in higher needle forces than puncturing of the surrounding liver tissue. The acquired force data were used to find a blood vessel mimicking material, Smooth-Sil 950 silicone. A mesh fabric was added to the silicone to ensure proper bonding with the PVA liver phantom and to acquire the desired peak forces during needle insertion. A simplified structure of the portal veins was created with a 3D-printer using water-soluble PVA. That structure was used to create a silicone blood vessel. The described methods can be used to implant artificial veins in a PVA liver phantom.


## Acknowledgment

I thank prof. Gert-Jan Kleinrensink and Yvonne Steinvoort, Neuroscience department of the Erasmus MC, for offering the opportunities to do experiments with livers at the Erasmus MC. Furthermore I thank Jang Zhang and Jan Vos, medical students and the Erasmus University, for their assistance during the liver experiments.


## References


[1] De Jong, T.L., et al., PVA matches human liver in needle-tissue interaction. Journal of the mechanical behavior of biomedical materials, 2017. 69: p. 223-228.

[2] De Jong, T.L., Adrichem, D.R., Dankelman, J., Van den Dobbelsteen, J.J., Design of a PVA liver phantom with respiratory motion for simulation of needle interventions, CARS, Berlin, Germany, 2018 (extended abstract in: Int J CARS Proceedings, S66 -67)

[3] Elgezua, I., Y. Kobayashi, and M.G. Fujie, Survey on current state-of-the-art in needle insertion robots: Open challenges for application in real surgery. Procedia CIrP, 2013. 5: p. 94-99.

[4] Elgezua, I., et al. Event classification in percutaneous treatments based on needle insertion force pattern analysis. in Control, Automation and Systems (ICCAS), 2013 13th International Conference on. 2013. IEEE.

[5] Elgezua, I., et al., Online Event Classification for Liver Needle Insertion Based on Force Patterns, in Intelligent Autonomous Systems 13. 2016, Springer. p. 1145-1157.

[6] Jiang, S., et al., Experimental study of needle–tissue interaction forces: effect of needle geometries, insertion methods and tissue characteristics. Journal of biomechanics, 2014. 47(13): p. 3344-3353

[7] Zhai, J., et al., A sensor for needle puncture force measurement during interventional radiological procedures. Medical Engineering and Physics, 2013. 35(3): p. 350-356.

[8] Okuno, D., et al. Development of an automatic blood sampling system: control of the puncturing needle by measuring forces. in Engineering in Medicine and Biology Society, 1998. Proceedings of the 20th Annual International Conference of the IEEE. 1998. IEEE.

[9] Healey, A.E., et al., In vivo force during arterial interventional radiology needle puncture procedures. Stud Health Technol Inform, 2005. 111: p. 178-84.

[10] Pepley, D., et al. Measurement of syringe needle forces for a haptic robotic training device. in 2017 Design of Medical Devices Conference. 2017. American Society of Mechanical Engineers.

[11] Kobayashi, Y., et al., Development of a needle insertion manipulator for central venous catheterization. The International Journal of Medical Robotics and Computer Assisted Surgery, 2012. 8(1): p. 34-44.

[12] Kobayashi, Y., et al., Use of puncture force measurement to investigate the conditions of blood vessel needle insertion. Medical Engineering and Physics, 2013. 35(5): p. 684-689.

[13] Kobayashi, Y., et al., Preliminary in vivo evaluation of a needle insertion manipulator for central venous catheterization. ROBOMECH Journal, 2014. 1(1): p. 18.

[14] Saito, H. and T. Togawa, Detection of needle puncture to blood vessel using puncture force measurement. Medical and Biological Engineering and Computing, 2005. 43(2): p. 240-244.

[15] Saito, H., K. Mitsubayashi, and T. Togawa, Detection of needle puncture to blood vessel by using electric conductivity of blood for automatic blood sampling. Sensors and Actuators A: Physical, 2006. 125(2): p. 446-450.

[16] Clement, R.S., et al., Effects of axial vibration on needle insertion into the tail veins of rats and subsequent serial blood corticosterone levels. Journal of the American Association for Laboratory Animal Science, 2016. 55(2): p. 204-212.

[17] Maurin, B., et al., In vivo study of forces during needle insertions, in Perspective in Image-Guided Surgery. 2004, World Scientific. p. 415-422.

[18] Barbé, L., et al., In vivo model estimation and haptic characterization of needle insertions. The International Journal of Robotics Research, 2007. 26(11-12): p. 1283-1301.

[19] Washio, T. and K. Chinzei. Needle force sensor, robust and sensitive detection of the instant of needle puncture. in International Conference on Medical Image Computing and Computer-Assisted Intervention. 2004. Springer.

[20] Shah, S., et al., Robotically assisted needle driver: evaluation of safety release, force profiles, and needle spin in a swine abdominal model. International Journal of Computer Assisted Radiology and Surgery, 2008. 3(1-2): p. 173-179.

[21] Kobayashi, Y., et al. Modeling of conditions where a puncture occurs during needle insertion considering probability distribution. in Intelligent Robots and Systems, 2008. IROS 2008. IEEE/RSJ International Conference on. 2008. IEEE.

[22] Kobayashi, Y., et al. In vitro validation of viscoelastic and nonlinear physical model of liver for needle insertion simulation. in Biomedical Robotics and Biomechatronics, 2008. BioRob 2008. 2nd IEEE RAS & EMBS International Conference on. 2008. IEEE.

[23] Kobayashi, Y., et al. Developing a planning method for straight needle insertion using probability-based condition where a puncture occurs. in Robotics and Automation, 2009. ICRA'09. IEEE International Conference on. 2009. IEEE.

[24] Wang, W., et al., Experimental analysis of robot-assisted needle insertion into porcine liver. Bio-medical materials and engineering, 2015. 26(s1): p. S375-S380.

[25] Wang, Y., et al., Optimal needle design for minimal insertion force and bevel length. Medical Engineering and Physics, 2014. 36(9): p. 1093-1100.

[26] Wang, Y., et al., The needle with lancet point: geometry for needle tip grinding and tissue insertion force. Journal of Manufacturing Science and Engineering, 2013. 135(4): p. 041010.

[27] Kobayashi, Y., J. Okamoto, and M.G. Fujie. Physical properties of the liver and the development of an intelligent manipulator for needle insertion. in Robotics and Automation, 2005. ICRA 2005. Proceedings of the 2005 IEEE International Conference on. 2005. IEEE.
[28] Kobayashi, Y., J. Okamoto, and M.G. Fujie. Physical properties of the liver for needle insertion control. in Intelligent Robots and Systems, 2004.(IROS 2004). Proceedings. 2004 IEEE/RSJ International Conference on. 2004. IEEE.
[29] Hing, J.T., A.D. Brooks, and J.P. Desai. Reality-based needle insertion simulation for haptic feedback in prostate brachytherapy. in Robotics and Automation, 2006. ICRA 2006. Proceedings 2006 IEEE International Conference on. 2006. IEEE.
[30] Hing, J.T., A.D. Brooks, and J.P. Desai, A biplanar fluoroscopic approach for the measurement, modeling, and simulation of needle and soft-tissue interaction. Medical image analysis, 2007. 11(1): p. 62-78.
[31] Bao, X., et al., Experiment study on puncture force between MIS suture needle and soft tissue. Biosurface and Biotribology, 2016. 2(2): p. 49-58.
[32] Yang, T., et al., Identification of tissue types and boundaries with a fiber optic force sensor. Science China Information Sciences, 2014. 57(12): p. 1-7.
[33] Mahvash, M. and P.E. Dupont, Mechanics of dynamic needle insertion into a biological material. IEEE Transactions on Biomedical Engineering, 2010. 57(4): p. 934-943
[34] Marieb, E.N. and K. Hoehn, Human anatomy & physiology. 2014: Pearson Education.
[35] Hungr, N., et al., A realistic deformable prostate phantom for multimodal imaging and needle-insertion procedures. Medical physics, 2012. 39(4): p. 2031-2041.
[36] Fedorov A., Beichel R., Kalpathy-Cramer J., Finet J., Fillion-Robin J-C., Pujol S., Bauer C., Jennings D., Fennessy F.M., Sonka M., Buatti J., Aylward S.R., Miller J.V., Pieper S., Kikinis R. 3D Slicer as an Image Computing Platform for the Quantitative Imaging Network. Magn Reson Imaging. 2012 Nov;30(9):1323-41. PMID: 22770690. PMCID: PMC3466397.
[37] P. Cignoni, M. Callieri, M. Corsini, M. Dellepiane, F. Ganovelli, G. Ranzuglia, MeshLab: an Open-Source Mesh Processing Tool, Sixth Eurographics Italian Chapter Conference, page 129-136, 2008.
[38] Barbé, L., et al., In vivo model estimation and haptic characterization of needle insertions. The International Journal of Robotics Research, 2007. 26(11-12): p. 1283-1301.
[39] Majewicz, A., et al., Behavior of tip-steerable needles in ex vivo and in vivo tissue. IEEE Transactions on Biomedical Engineering, 2012. 59(10): p. 2705-2715.

# --- Thesis ---

# List of figures and tables

# 1. Introduction

## 1.1 Context

The liver is an important and complex organ and treatment of liver diseases is often done by means of interventional radiology. In interventional radiology, minimally invasive procedures are performed using radiologic image guidance to diagnose and treat diseases. This type of procedures has a lot of benefits for the patient compared to open surgery, for example less pain and recovery time. However, it introduces some difficulties for the medical doctor, due to a lack of visibility and limited instrument movability. Needles are widely used in interventional radiology and interventional radiologists thereby use imaging techniques, such as ultrasound, for needle guidance. Needles are under constant development and they need to be tested for needle-tissue interaction forces, needle bending and steerability for example. Due to safety and ethical reasons, it is difficult to test needles on patients and therefore an appropriate alternative is needed. Animals and human cadavers are currently used for development and training purposes, but a realistic phantom would be preferable. An appropriate liver phantom needs to mimic the human liver by internal structure, mechanical properties and imaging properties. This way, the needle-tissue interaction during real needle interventions can be mimicked using a liver phantom. Besides the use for the development of needles, a liver phantom can be used as a training device. Interventional radiologists use haptic feedback during puncturing of different kinds of tissue, to help determine the location of the needle. Good interpretation of haptic feedback is therefore crucial and can be obtained by experience and thus practice. To gain experience in the use of this haptic feedback, medical doctors and students can use a liver phantom to practice needle interventions.

## 1.2 Problem statement

A recent study by De Jong et al. [1] provided a material, polyvinyl alcohol (PVA), that mimics the forces of liver tissue during needle-tissue interaction. With that material a liver phantom was created [2], shown in Figure 1. However, to further develop the liver phantom, more research is needed. For instance, a liver contains a lot of blood vessels that might have different mechanical properties than the liver tissue itself. During needle interventions, puncturing of these blood vessels could therefore result in different forces on the needle and thus in different needle movement and haptic feedback. If that is the case, the liver phantom could be further developed by adding artificial blood vessels to the phantom. These vessels then need to mimic the needle interaction forces during puncturing of liver blood vessels.

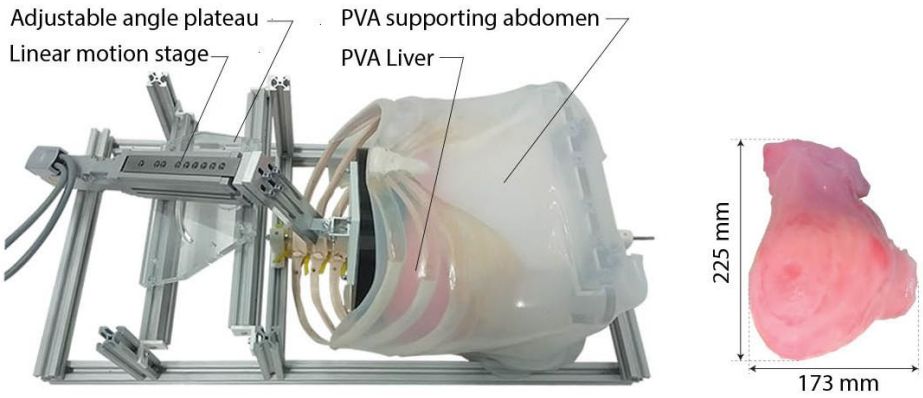


**Figure 1 Setup of the PVA liver phantom with respiratory motion (left) and the PVA liver (right). Retrieved from [2].**

## 1.3 Goal and approach of the study

The goal of this study is to provide insight into the needle forces during puncturing of blood vessels from the human liver. The resulting force data are used to improve a PVA liver phantom, designed for needle interventions, by implanting artificial blood vessels. An overview of the approach of the study is shown in Figure 2, in which the four steps towards the improved liver phantom are shown. The first step is to determine if the addition of a separate blood vessel wall in the phantom is an improvement. Therefore we need to know if puncturing a liver blood vessel results in different needle insertion forces than puncturing of the surrounding liver tissue. At first, this is examined via a literature study to find needle force data on needle-blood vessel interaction and needle-liver interaction. If the literature study does not result in sufficient data, experiments are done to collect the required force data. During the second step, we need to find a blood vessel mimicking material that mimics these needle forces when punctured. The third step is to use the blood vessel mimicking material to create the structure of the blood vessels in the liver. The fourth and final step is to implant the blood vessel structure into PVA tissue. If all is completed, these steps can be used to improve the existing PVA liver phantom via the addition of artificial blood vessels. The improved phantom then better mimics the human liver during needle-tissue interaction, which is beneficial for the development of new needles and for training purposes. If the blood vessel mimicking material, selected in the second step, turns out to be not suitable to create the blood vessel structure or not suitable to implant in the PVA phantom, we need to go back to the second step and select a different blood vessel mimicking material.

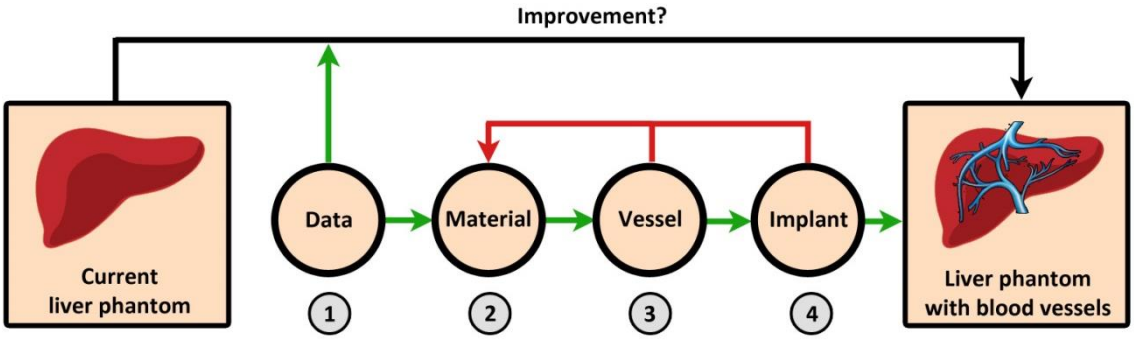


**Figure 2 Overview of the approach of the study, including the four main steps towards the improvement of the liver phantom.**

## 1.4 Outline of the thesis

The thesis starts with some theoretical background information in Chapter 2, intended for better understanding of the subject. In this chapter, the most important results of the literature study are discussed as well. In Chapter 3, an experiment is presented in which data are collected on needle forces during the insertion in blood vessels from the liver. Chapter 4 describes the selection of a blood vessel mimicking material and Chapter 5 explains how that material is used to create the structure of the liver blood vessels. Finally, the implantation of a blood vessel structure in PVA is described in Chapter 6, followed by a discussion and a conclusion.

# 2. Background information

This chapter provides background information on the topics that are discussed in this thesis. It starts with information about the human liver. The function of the liver is described, followed by its anatomy and examples of liver pathologies and interventions. In the next section, information is presented on the function and anatomy of human blood vessels. Then, a brief overview of needle-tissue interaction in general is presented, including needle forces, needle characteristics and tissue characteristics. The next three sections give a brief overview of the most important results of the literature study [3]. This includes needle interaction forces in blood vessels, needle interaction forces in the liver and the mechanical properties of blood vessels. The chapter ends with a brief introduction on ultrasound imaging.

## 2.1 The liver

### 2.1.1 Function

The liver is the human's largest internal organ and has multiple functions in the human body [4]. It processes nutrients from the blood stream and produces many proteins and chemicals that are essential for proper functioning of the human body. Detoxification of the blood, to get rid of harmful substances like alcohol and drugs, is done by the liver as well. Furthermore, the liver is responsible for breaking down hemoglobin, insulin and other hormones. The liver is also considered a gland, because it plays a role in the production and secretion of bile to help digest fat. Finally the liver acts as a storing unit for vitamins and other chemicals.

### 2.1.2 Anatomy

The liver is located in the right upper part of the abdomen, under the diaphragm, and according to its outside appearance the liver can be grossly divided into four primary lobes: right lobe, left lobe, caudate lobe and quadrate lobe. For describing the functional anatomy, the liver can be divided into eight independent segments according to the Couinaud classification, as shown in Figure 3 [5]. The layout of these segments is based on the fact that they all have their own vascular flow, biliary drainage and lymphatic drainage. The liver's blood supply is obtained by two sources: the portal vein and the hepatic artery. The portal vein delivers blood from the gastrointestinal tract and the spleen to the liver and the hepatic artery supplies oxygenated blood from the heart. Blood is transported back to the heart via the hepatic veins and the inferior vena cava. The liver contains a part of the biliary tract, where bile is secreted by the liver into small ducts so it can be stored in the gallbladder.

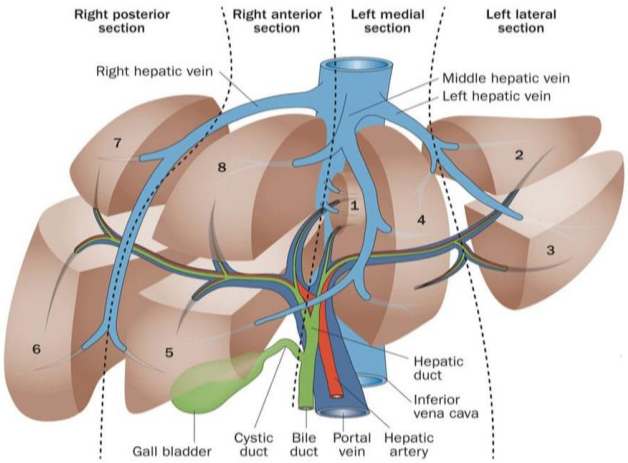


**Figure 3 Overview of different blood vessels in the human liver and different segments by the Couinaud classification. Retrieved from [5].**

### 2.1.3 Pathologies and interventions

There are different diseases and infections that can affect the liver's functionality, like hepatitis and alcohol induced liver disease. These kinds of diseases can lead to degradation of the liver, like

forming of scar tissue, which can eventually lead to cirrhosis. A cirrhotic liver can lose a part of its functionality and therefore cause portal hypertension. This means that the blood pressure in the portal vein increases due to lack of blood flow through the liver. Portal hypertension can be treated with use of the transjugular intrahepatic portosystemic shunt (TIPS) procedure, where a stent is placed between the portal vein and the hepatic vein to help retain the blood flow. TIPS is a typical procedure of interventional radiology where a needle is used to puncture the liver and its blood vessels. During the TIPS procedure a needle is inserted in the neck through the jugular vein to reach the liver via the hepatic vein. The needle then punctures the hepatic vein, goes through the liver tissue and punctures the portal vein. Eventually a stent can be placed between the blood vessels. It is a very difficult procedure and a realistic liver phantom, that includes blood vessels, could help interventional radiologists and students gain experience during practice.

## 2.2 Blood vessels

### 2.2.1 Function

Blood vessels are part of the circulatory system and transport blood throughout the human body. Blood carries chemicals and nutrients that are needed in all parts of the body so that it can function properly. Blood also removes waste products and plays an important role in the immune system, by distributing white blood cells throughout the body. Furthermore, blood vessels play a role in thermoregulation by adjusting the amount of blood that flows through a vessel. The human body regulates the blood flow via vasodilation and vasoconstriction, using the muscle cells in the blood vessels.

There are three main types of blood vessels: arteries, capillaries and veins. Arteries carry blood away from the heart and they branch into smaller arterioles and finally into the capillaries. These capillaries then enable the exchange of chemicals between the blood and the cells. After that they merge into larger venules and later into veins that carry the blood back towards the heart. Blood is transported in two different circuits: the systemic circuit and the pulmonary circuit, both shown in Figure 4 [6]. In the systemic circuit, the arteries transport oxygenated blood throughout the body. The oxygen is than delivered to the cells and the deoxygenated blood returns to the heart via the systemic veins. In the pulmonary circuit on the other hand, the arteries carry the deoxygenated blood from the heart to the lungs for the exchange of gasses, like oxygen and carbon dioxide. The pulmonary veins then carry the oxygenated blood back to the heart, where it can be transported throughout the rest of the body again.

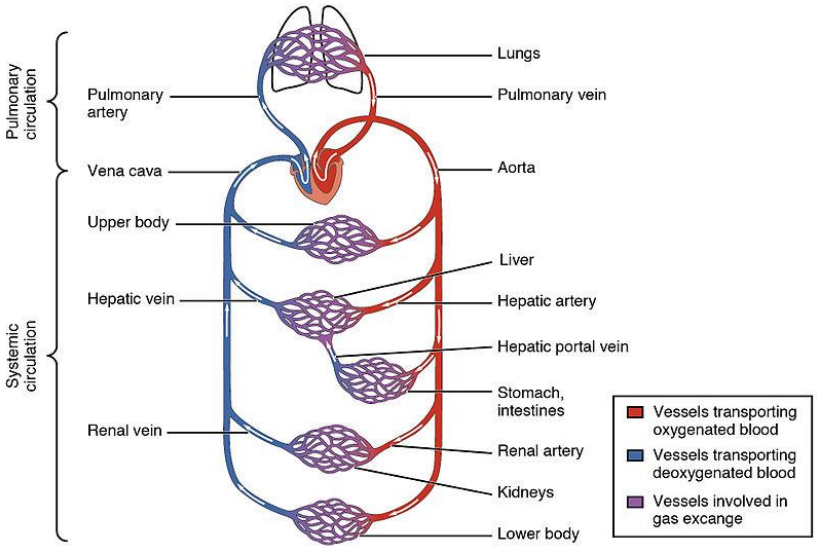


**Figure 4 Overview of the blood circulation in the pulmonary and systemic circuit. Retrieved from [6].**

## 2.2.2 Anatomy

Arteries and veins consist of a lumen, the part through which the blood flows, and a vessel wall with three layers: the tunica externa, tunica media and tunica intima. However, there are some differences in the composition of these layers between arteries and veins. Figure 5 shows the average size and the relative tissue makeup of the different blood vessels and Figure 6 shows the structure of the different layers. In general, arteries have thicker walls with smaller lumens and veins have thinner walls with larger lumens. Blood pressure is generally higher in arteries than in veins, because arteries receive blood closer to the heart and thus with greater pressure. To ensure that the blood keeps flowing in the right direction, veins can contain valves. This is mostly the case in limbs and veins inferior to the heart to overcome the effects of gravity. The three different layers of the blood vessels are further described below.

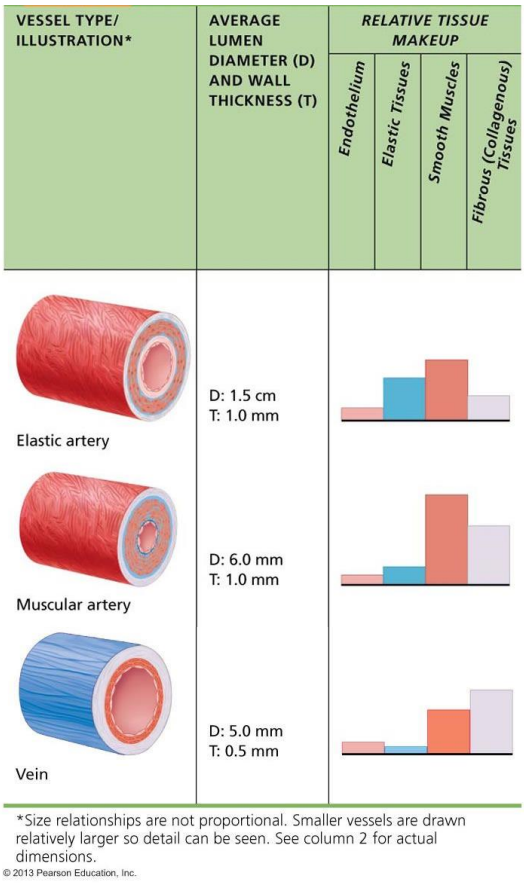


**Figure 5 Summary of blood vessel anatomy. Adapted from [4].**

The tunica intima is the thin inner layer and contains the endothelium that surrounds the lumen of all blood vessels. The endothelium ensures that there is minimal friction between the blood and the vessel so that the blood runs smoothly through the vessels. In larger vessels the endothelium is supported by a membrane and connective tissue, called the subendothelial layer.

The tunica media is the middle layer of a blood vessel and it consists of smooth muscle cells and elastin sheets. The smooth muscle cells are used to regulate the diameter of the blood vessels via dilation or constriction. This way, the tunica media plays an important role in blood pressure and blood circulation. The tunica media is usually the thickest layer in arteries and it is thicker than the tunica media in veins. Arteries regulate the oxygenated blood flow and receive blood close to the heart. This means that they have to deal with a larger blood pressure than veins. Close to the heart the arteries are more elastic and further away from the heart they are more muscular.

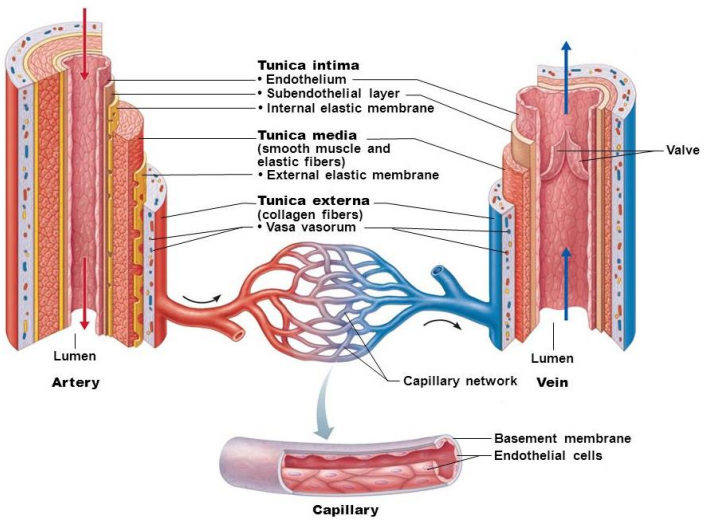


**Figure 6 General structure of human arteries, veins and capillaries. Retrieved from [4].**

The tunica externa is the outermost layer of the blood vessel wall and it is mostly composed of collagen fibers that protect and reinforce the vessel. It

attaches to surrounding tissues to keep the blood vessel in place. In general, the tunica externa is the thickest layer in veins. The tunica externa of larger blood vessels contains a vasa vorum. The vasa vorum consists of very small blood vessels, which feed the outer layer of the large blood vessel.

## 2.3 Needle tissue interaction

Needles are widely used in interventional radiology. A medical needle typically consists of a tube, called a cannula, with a sharp tip on one end and a plastic needle hub on the other end. An example is shown in Figure 7. The hollow space inside the needle is called the lumen. During the interaction between a needle and tissue, there are different forces acting on the needle. In this research, the main focus is on the axial peak force. This is the maximal force that is acting on the needle hub in the direction of the needle during puncturing of a tissue. The axial peak force could be an useful tool to determine what kind of tissue is being punctured during needle-tissue interaction. However, there are lots of parameters that influence the axial needle peak force and therefore need to be considered.

**Figure 7 Both ends of a two-part trocar needle used in interventional radiology. Retrieved from www.cookmedical.com on September 20, 2018.**

### 2.3.1 Needle forces

The insertion of a needle into a tissue can be described by three different phases: boundary displacement, tip insertion and tip and shaft insertion [7]. A typical force-time graph of a two-part needle insertion into a porcine liver is presented by Zhai et al. [8] and shown in Figure 8. The boundary displacement starts when the needle makes contact with the tissue (A). During this phase, the boundary of the tissue moves along with the needle tip but no penetration occurs. The axial needle force is now starting to increase. This type of force is referred to as puncture force or stiffness force [39]. At the point of contact between the tissue and the needle tip, the stresses in the tissue then increase until a certain threshold is reached. At that moment, the needle tip punctures the tissue boundary and the second phase, tip insertion, is reached (B-C). During this second phase, the opening in the tissue boundary gets larger because of the increasing cross-sectional area of the needle tip and eventually the outer needle part. This causes the axial needle force to further increase until the entire needle tip and the outer part of the needle starts to penetrate the tissue (D). At this point a clear peak force is visible and this is the total puncture force. After that we see a clear drop of force and the tip and shaft insertion phase starts (E). During this last insertion phase, the needle

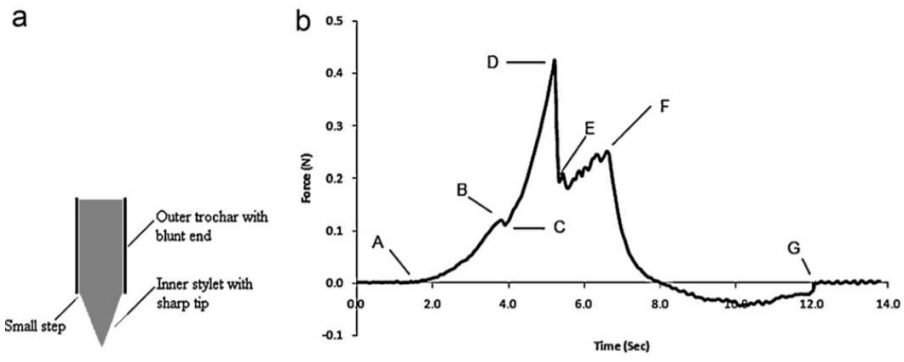


**Figure 8 Typical example of needle insertion into a porcine liver. (a) Two-part needle and (b) force-time graph. Retrieved from [8].**

force consists of an approximately constant cutting force and an increasing friction force (E-F). The cutting force is needed to cut through the tissue and the friction force is due to the increasing contact area of the needle shaft and the surrounding tissue. When the insertion of the needle is stopped, the axial needle force drops slightly due to relaxation. During retraction of the needle, there is an opposite needle force due to the friction between the needle shaft and the surrounding tissue (F-G).

### 2.3.2 Needle characteristics and insertion parameters

Needles can be described by several characteristics that influence the needle-tissue interaction. Two main characteristics are the needle diameter and the needle tip shape. The needle diameter is expressed as needle gauge (G) and a larger gauge number indicates a smaller needle diameter. The outer diameter of a needle ranges approximately between 0.19 mm (34G) and 5.16 mm (6G) [9]. The needle tip shape can vary as well. The most common tip shapes are shown in Figure 9, although there are many variations. Furthermore, the lubrication and sharpness of the needle can influence the axial needle force. When using a needle, there are multiple insertion parameters that affect the needle-tissue interaction. For example the insertion velocity, the insertion angle, the axial rotation and whether the needle is inserted automatically or manually can all influence the needle force. All these variables therefore need to be considered while conducting a needle-tissue interaction experiment.

**Figure 9 Different needle tip shapes. From left to right: blunt, beveled, conical, Sprotte, diamond, Tuohy. Retrieved from [7].**

### 2.3.3 Tissue characteristics and mechanical properties

During a needle insertion experiment different tissues can be used, that can be roughly divided into artificial and biological tissues. When using biological tissue for example, further distinction can be made between in vivo and ex vivo tissue. Different types of tissues can have different mechanical properties, that might affect the axial needle force. Like mentioned before, our main focus in on the peak forces that arise during puncturing of a blood vessel or other tissue. The elasticity of the tissue will influence this puncture force or stiffness force. Soft human tissue however, is in general non-homogenous and viscoelastic so it has an elastic component and a viscous component [10]. Therefore the material cannot be accurately described by a single elastic modulus, because the modulus depends on the applied strain and the behavior of the material is time dependent. The fact that soft human tissue is viscoelastic should be taken into account when trying to determine its elasticity. Furthermore, the fracture toughness of the tissue and the friction also affect the needle force by influencing the cutting force and friction force respectively.

## 2.4 Needle interaction forces in blood vessels

A literature research was conducted to find data on needle-blood vessel interaction forces. It can be concluded that little research has been done on needle-blood vessel interaction forces, certainly in the field of interventional radiology. The primary focus was on needle-blood vessel interaction in human livers, but no data on this subject were found in literature. To be able to get an indication of the magnitude of these forces, the focus was extended to needle interaction with both animal tissue

and blood vessels located outside the liver. Studies on needle-blood vessel interaction were found using porcine livers [11-14], in which peak forces between 0.4 and 1.3 N were measured. An example of the experimental setup is shown in Figure 10 [11]. Furthermore, human blood vessels located outside the liver were used for needle insertion experiments [8, 15-17]. Puncturing of the jugular vein resulted in peak forces between 1.35 and 2.02 N [17] and manually puncturing the femoral artery resulted in peak forces between 0.13 and 8.89 N [16]. Finally, studies were found using animal blood vessels located outside the liver [15, 18-23]. Puncturing of porcine jugular veins resulted in forces between 0.3 and 1.3 N [18]. The results of studies using rabbit's ear veins and rat's tail veins were considered as less fit for an indication of the needle forces due to the smaller vein size and needle diameter used in the experiments. The results of the literature study give an indication of the expected forces during puncturing of human liver blood vessels. However, experimental data still need to be collected to get a good estimation of these needle forces.

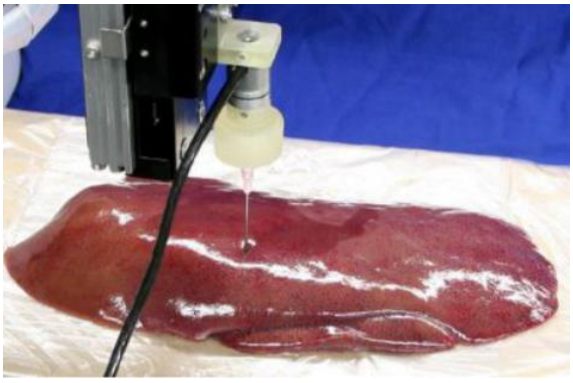

**Figure 10 Experimental setup for needle insertions in porcine liver and its blood vessels. Retrieved from [11].**

All articles on needle interaction forces in blood vessels are schematically listed in Appendix A.

## 2.5 Needle interaction forces in the liver

Studies on needle-liver interaction forces can be used to compare the blood vessel forces to the liver forces. The results give an indication of whether it is an improvement to implant blood vessels into the existing liver phantom. When looking at the different articles, one study used human livers and showed forces between 0.1 and 0.65 N (median = 0.18 N) [1]. This gives a good indication of the forces during puncturing of a human liver, although the results of this study might include some blood vessel punctures as well. Most other studies were done using porcine livers, both in vivo [24-27] and ex vivo [11-14, 28-40]. One of the research groups examined both liver tissue and liver blood vessels in ex vivo porcine liver [13]. The results show that puncturing blood vessels in the porcine liver resulted in higher forces than puncturing porcine liver tissue (Figure 11). This gives a good indication that blood vessels do result in higher puncture forces than the surrounding liver tissue. In literature it is furthermore mentioned that in vivo liver tissue has different mechanical properties than ex vivo tissue [25], which could result in higher needle forces. However, this cannot already be concluded from the results of the different studies using porcine livers. The in vivo studies resulted in forces between 0.4 and 1.5 N and the ex vivo studies resulted in forces between 0.1 and 1.9 N. Finally, the studies using ex vivo bovine [16, 41-46] livers seem to result in somewhat larger forces, ranging between 0.5 and 3.5 N. It needs to be considered that the different studies used different experimental methods, which makes it hard to compare studies.

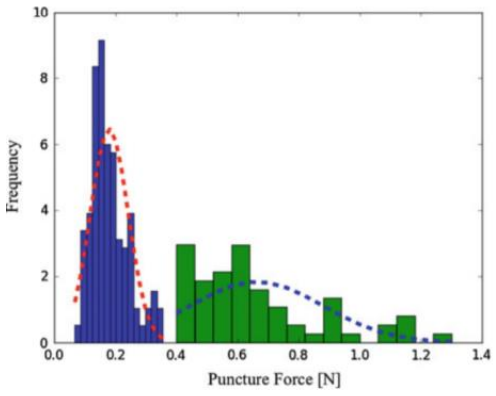


**Figure 11 Force distribution for puncturing of porcine liver tissue (blue) and liver veins or arteries (green). Retrieved from [13].**

All articles on needle interaction forces in the liver are schematically listed in Appendix B.

## 2.6 Mechanical properties of blood vessels

A lot of research has been done on the mechanical properties of blood vessels and it is a complex subject. Many different methods were used to quantify elasticity and stiffness [47-49], which makes it hard to compare different studies. In general, there are a few aspects that can influence the elasticity and stiffness that need to be considered when examining needle-blood vessel interaction. The collagen fibers in the blood vessel wall seem to have the largest influence on the elasticity due to the higher Young's modulus compared to the elastin fibers and the smooth muscles [50]. This needs to be considered when using different types of blood vessels, because different vessels contain different amounts of collagen fibers. Furthermore, the mechanical properties can differ per individual due to for example aging [51, 52] and diseases, like atherosclerosis [48].

## 2.7 Ultrasound

Ultrasound is an imaging technique that can be used for needle guidance during interventions. The current PVA liver phantom is designed to be used with ultrasound guidance, so the addition of artificial blood vessels must not compromise this ability. During ultrasound imaging, a transducer is used to generate sound waves on a frequency above the threshold for human hearing [53]. This transducer can also detect the ultrasound echoes that are reflected. The transducer consist of piezoelectric crystals, which are able to produce sound waves when an electric field is applied. They also work the other way around, so that an electric field is produced when they get hit by a sound wave. The sound waves that are emitted by the transducer travel through the tissues and lose amplitude, and thus energy, which is called attenuation. Attenuation is the combined effect of absorption, reflection and refraction of the sound waves. During absorption, the ultrasound beam's energy is transferred to the medium through heat generation, which accounts for most of the attenuation. The sound waves are reflected by boundaries between tissues with different acoustic impedances. The amount of reflection depends on the relative difference in acoustic impedance between the tissues or mediums. For example, large differences in acoustic impedance occur at air/soft tissue and bone/soft tissue boundaries, causing high reflection at the boundaries. When the returning echoes hit the transducer, an electric signal is created. By using the speed of sound and the time it took for the echo to return, the distance of the tissue boundary is calculated. This way, a real-time two-dimensional image of the scanned tissue can be created, with the energy of the returning wave determining the brightness of the image at that location. This way, tissues and mediums are presented according to their brightness. Anechoic means no returning echoes and a black representation, like in fluids. Hyperechoic means that the returning echoes have higher energy than the surrounding tissue, which results in a more white representation. An example of an ultrasound image of the liver and its blood vessels can be seen in Figure 12.

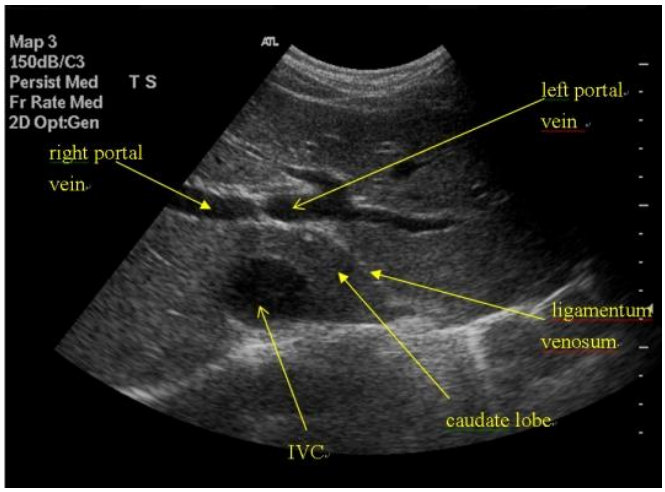


**Figure 12 Ultrasound image of the liver and some of its blood vessels. Retrieved from: http://www.droid.cuhk.edu.hk on September 20, 2018.**

# 3. Needle insertion force experiment

The resulting data of Section 2.4 and Section 2.5 were not sufficient to conclude that the liver phantom needs a separate blood vessel wall and not sufficient to find a blood vessel mimicking material. Therefore a needle insertion experiment was done at the Erasmus MC in Rotterdam, to collect data on needle forces during insertions into blood vessels from the human liver and the liver tissue itself. This chapter describes the design and the results of the experiment, followed by a discussion and a conclusion.

## 3.1 Design of the experiments

Data were collected during three experiments, in which blood vessels from three human livers were extracted from the liver and punctured with a needle. These livers were fresh-frozen and expected to be healthy. Prior to these experiments, two test experiments were conducted using ex vivo porcine livers to practice on the extraction of blood vessels from the liver and to test the experimental setup. During the human liver experiments, needle forces were collected by puncturing liver veins, liver arteries and liver tissue. Puncturing liver tissue was done to compare the results of the blood vessel forces to the liver tissue forces. This way, it can be examined if puncturing of a blood vessel results in a higher force than puncturing of liver tissue. This section now describes the experimental setup and the experimental protocol that were used during the experiment.

### 3.1.1 Experimental setup

The experimental setup was developed at the TU Delft and consisted of a linear stage (EGSL-BS-45-200-3P, Festo BV, Delft, The Netherlands) that moves in vertical direction. A force sensor (LSB200-FSH00104, FUTEK Advanced Sensor Technology Inc., Irvine, CA, USA) and a needle were attached to the linear stage to measure the forces during movement of the needle. 18G two-part trocar needles

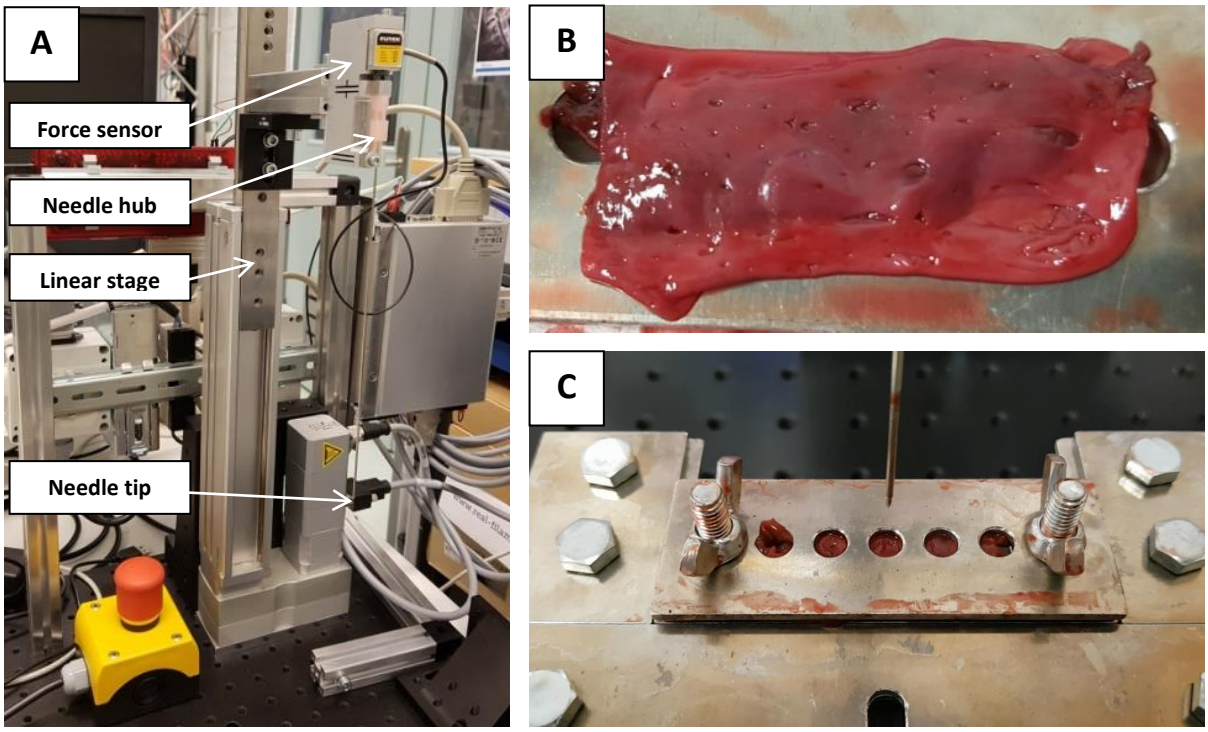


**Figure 13 (A) The experimental setup, containing the force sensor and the needle, which are both mounted on the linear stage. (B) A liver vein that is cut open after it was carved out of the liver. (C) A liver vein fixed between aluminum plates and mounted underneath the needle.**

(Cook Medical, Bloomington, USA) were used during the experiments. This type of needle is commonly used during radiologic interventions. The experimental setup is shown in Figure 13A. After a blood vessel was extracted from the liver, it was cut open, as shown in Figure 13B. Then it was placed between two identical aluminum plates. These plates had seven holes in them, with a diameter of 7 mm and a distance of 10 mm between the centers. Through these holes the needle punctured the blood vessel wall. The holes on the outside of the aluminum plates were used to fix the plates with bolts and nuts, in order to hold the blood vessel in place. The aluminum plates were then placed in a construction that was mounted underneath the needle, as can be seen in Figure 13C. This construction was mounted on another linear stage that could be manually moved in horizontal direction. This way, the holes in the plates were aligned with the needle and multiple needle insertions were done for a single blood vessel sample. For larger blood vessel samples, the sample was repositioned between the aluminum plates for multiple series of punctures.

### 3.1.2 Experimental protocol

#### Durometer

During the experiments with human liver, the liver hardness was first examined using a shore OO durometer (Dalian Teren Instruments Co., Ltd, Dalian, China). The results of the durometer were used as an indication of the hardness of the liver and to compare the different livers. At the start of each experiment, the liver was placed with the anterior part facing up. Two series of manual measurements were done. First, 20 measurements were done without putting any force on the durometer. Although this is not the intended way to use the durometer, it was done to ensure a constant force on the durometer, due to the gravitational force of the durometer itself. Then 20 more measurements were done with an almost constant force on the durometer. This force was applied manually and is therefore not exactly constant.

#### Blood vessel extraction and location

After the durometer measurements, the blood vessels were extracted from the liver. There are three main types of liver blood vessels: hepatic veins, portal veins and hepatic arteries. All these blood vessels were studied for needle insertion forces during this experiment and were thus extracted from the liver. First, the different blood vessels were located and then they were carved out of the liver using scalpels. During the porcine liver experiments, it was concluded that it was difficult to extract the blood vessels without any liver tissue still attached to the vessel wall. Removing all liver tissue from the blood vessel meant scraping over the vessel with the scalpel. This might damage the blood vessel wall and could therefore influence the puncture forces during the needle insertion experiment. For the experiments with human livers, it was therefore decided to keep a layer of 2-5 mm of liver tissue on the outside of the blood vessel wall. Each part of a blood vessel that was extracted, was classified as a different sample. For each sample, the type of blood vessel (hepatic vein, portal vein or artery) and the approximate location in the liver were noted. Then, the sample was marked with a colored pin to keep track of the different samples. In addition, there were samples that included only liver tissue. These samples were used for needle force experiments as well, to compare them to the results of the measurements using blood vessels. Finally, the sample was placed in a saline solution until it was randomly selected for measurements. Each sample was used for multiple consecutive measurements and then the next sample was selected.

### Peak force measurement

The needle was inserted and retracted at 5 mm/s. The needle insertion experiments were controlled and analyzed using Matlab R2014b (The MathWorks, Inc., Natick, Massachusetts, USA). During all insertions, data on needle force, needle displacement and time were recorded and saved. A typical example of a force-time graph during the insertion of a needle into a blood vessel wall, is shown in Figure 14. The different points on the force profile are explained in the description of the figure. Our main focus is on the peak force that is needed to puncture the blood vessel wall. The peak force is determined as the maximal force at the top in point B.

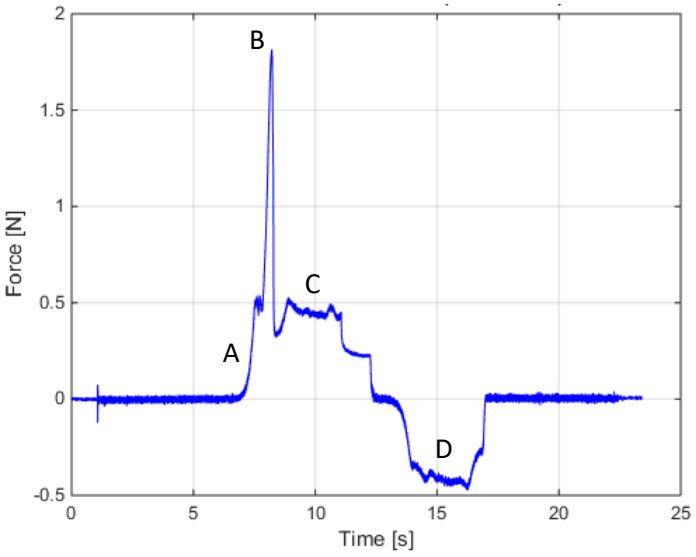


**Figure 14 A typical example of a force-time graph during a needle insertion into a blood vessel wall. At point A, the needles makes first contact with the vessel wall. Point B is the peak force during puncturing of the vessel wall. At point C the needle has punctured the blood vessel wall and the force is due to friction between the needle shaft and the vessel wall. Point D indicates the friction during retraction of the needle.**

### Blood vessel orientation

All blood vessels had a 2-5 mm layer of liver tissue attached to them during the measurements. This meant that there were two possible orientations of the blood vessel during the measurement: the blood vessel wall on top or the blood vessel wall on the bottom. This was randomized during all measurements to check whether the orientation has influence on the puncture force.

For all individual runs of the experiment, the following characteristics were noted: run number, sample (which includes type of blood vessel and location in the liver), orientation (bottom or top) and any specific details that were observed during the insertion of the needle.

## 3.2 Results

### 3.2.1 Durometer

The results of the durometer measurements for all three human livers are shown in Figure 15. The

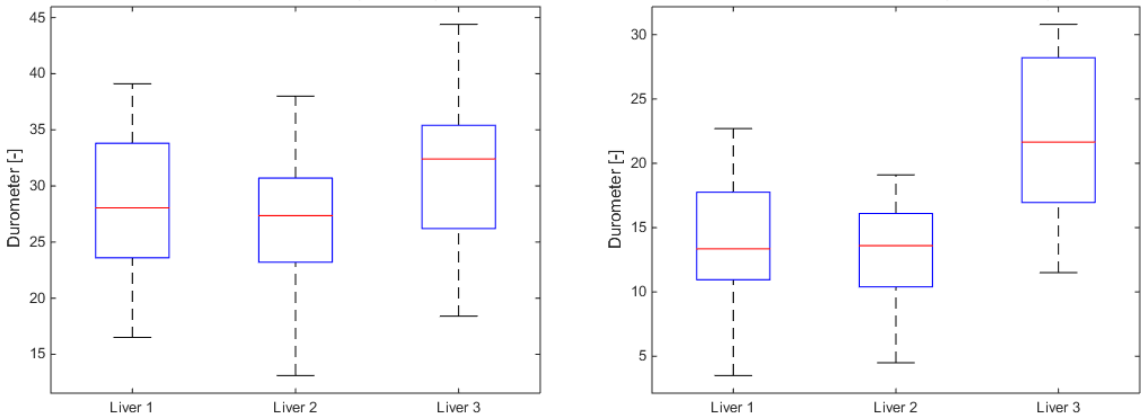


**Figure 15 Boxplots of the durometer results for the three human livers, both with pressure (left) and without pressure on the durometer (right). For all boxplots: n=20.**

left figure shows the results when an almost constant pressure is manually applied to the durometer. The right figure shows the results when no pressure is applied to the durometer. If we compare the different livers, we see that there is no clear difference between them, when using the durometer with a constant pressure. When looking at the results of the durometer without pressure, we see that liver 3 shows higher values in comparison with liver 1 and 2.

### 3.2.2 Peak forces

Using three different human livers, a total of 231 needle force measurements were done. Figure 16 shows a boxplot of the peak forces blood vessel type or liver tissue. All data of the three different livers are combined, because there were no clear differences in the peak forces between the livers, as shown in Appendix C. The results of the median and interquartile range (IQR) show that there is no clear difference between the peak forces of the portal vein (median=1.98 N, IQR=1.45 N to 2.97 N) and the hepatic vein (median=2.51 N, IQR=1.54 N to 4.40 N), although the variability of the hepatic vein is slightly larger. The peak forces during puncturing of hepatic arteries (median=1.33 N, IQR=1.16 N to 1.77 N) are slightly lower than for the veins. We can see that puncturing of all liver blood vessels results in higher forces than puncturing of the liver tissue (median=0.38 N, IQR=0.31 N to 0.51 N).

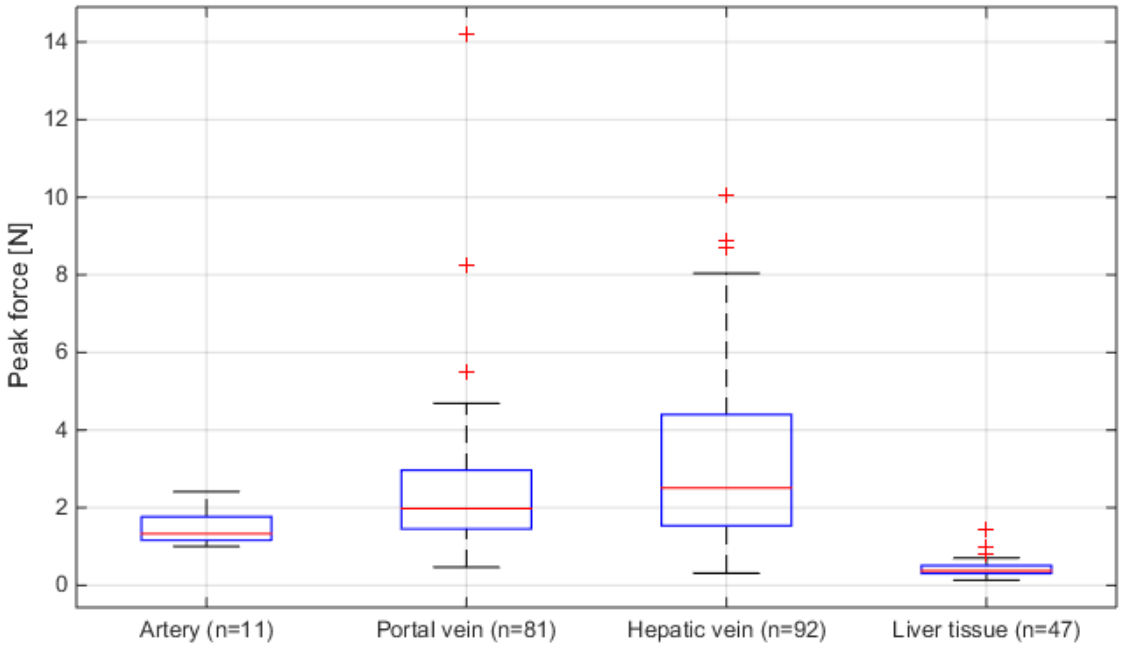


**Figure 16 Boxplot of the peak forces per type of blood vessel or liver tissue for all three human livers combined.**

### 3.2.3 Blood vessel location

During the extraction of the blood vessels from the liver, the approximate location of the vessel was noted. In general, puncturing of the proximal blood vessels results in slightly higher forces than puncturing of the distal blood vessels. However, this is not always the case, certainly not with the portal vein. Details are presented in Appendix C.

### 3.2.4 Tissue orientation

There were two possibilities for the tissue orientation: with the blood vessel wall on the top or on the bottom. The results per tissue orientation, of all the portal vein and the hepatic vein measurements,

are shown in Figure 17. No clear differences can be seen in the peak forces between the measurements with the blood vessel wall on top or with the blood vessel wall on the bottom.

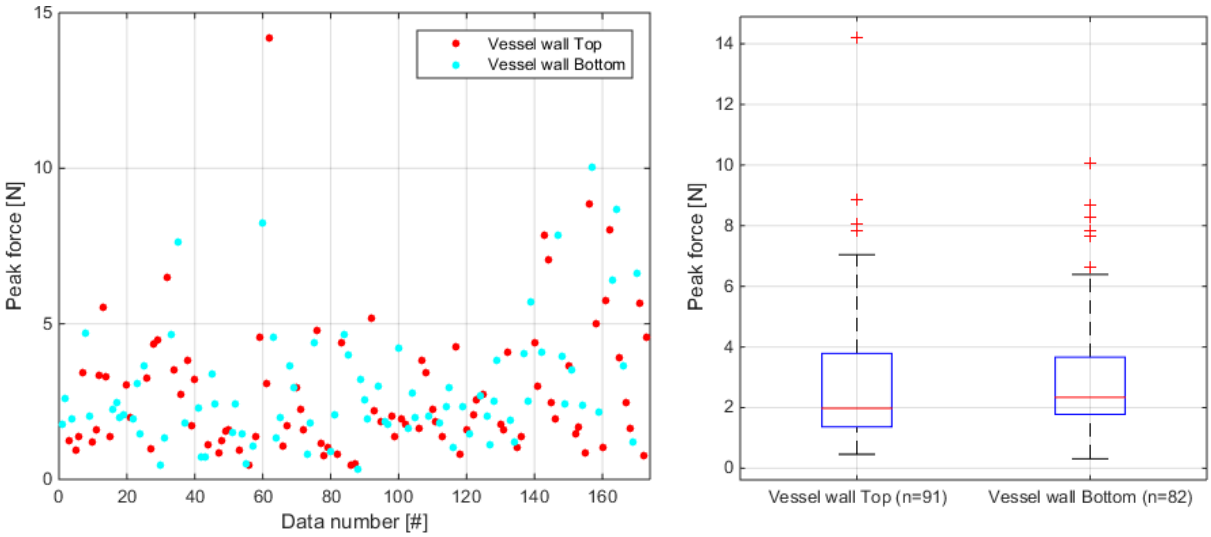


**Figure 17 The Peak forces per tissue orientation during all measurements using the portal vein and hepatic vein. The peak forces are shown in a scatter plot (left) and two boxplots (right).**

## 3.3 Discussion of the experiment

Needle insertion experiments were done using three human livers, to examine the peak forces during puncturing of liver blood vessels. First, the liver hardness was examined with use of a durometer to be able to compare the different livers on their hardness. Then, needle insertions were done in portal veins, hepatic veins, hepatic arteries and in the liver tissue itself. The location and the orientation of the blood vessel were examined as well during the measurements.

The results of the durometer show a lot of variance, both with pressure on the durometer and without pressure on the durometer. This is expected to be due to the different measurement locations on the liver. In general, some parts of the liver are harder than other parts. The large variance might also be due to the fact that the durometer was applied manually. The third liver resulted in slightly higher durometer values, when no pressure was applied. While manually examining the surface of the third liver, it felt a little dehydrated and therefore harder than the surface of the first two livers. The inside of the liver, however, felt approximately the same in all livers. Based on the durometer results, no significant differences in needle forces are expected between the livers due to their hardness.

The results of the peak forces, show that puncturing of a blood vessel from the liver results in a higher force than puncturing of the surrounding liver tissue. This shows that it is an improvement to include a separate blood vessel wall in the liver phantom. Furthermore, the peak forces of the portal vein and the hepatic vein show some outliers with relatively high forces. Although the reason for these high forces is not really clear, they might be due to the fact that blood vessels contain a lot of branches. These branches can be seen in Figure 13B. When the vessel is punctured exactly at a branch, this might result in a higher force due to the local thickening of the blood vessel wall. It was expected that the arteries would result in higher peak forces than the veins because of their thick walls. However, the results show that this is not the case. This might be due to the smaller vessel diameter of the arteries and the different layer composition of the arteries and veins. Arteries

relatively contain more smooth muscle tissue and veins more collagenous tissue, as shown in Figure 5. When looking at the results of the arteries, we do need to consider that only a few measurements were done. This is due to the fact that arteries were hard to locate and retrieve from the liver due to their small diameter.

When comparing both tissue orientations, we see that there is no clear difference in the puncture forces. This means that the peak force does not change if the vessel is punctured from the inside instead of from the outside. In general, the proximal blood vessel samples resulted in higher peak forces than the distal blood vessel samples. This is expected due to the fact that proximal vessel are in general larger, because they have to contain more blood. Therefore, they have a thicker wall and that results in higher puncture forces.

To conclude, a few other things need to be considered when looking at the results. First of all, the peak forces might be different when puncturing blood vessels that are fully surrounded by liver tissue and not extracted before puncturing. Then, however, it would be harder to determine the exact structure that is punctured at a certain moment. Furthermore, in vivo blood vessels might have different mechanical properties than ex vivo blood vessels and could therefore result in different needle forces [25, 54]. The same applies to needle insertions into blood vessels from sick livers, like cirrhotic livers. Finally, we need to consider that the needle insertion parameters, such as the needle diameter, the insertion velocity and the insertion angle, can influence the needle force during puncturing of a blood vessel as well.

## 3.4 Conclusion of the experiment

For the development of a liver phantom for needle interventions, we want to incorporate blood vessels in the liver phantom. Therefore a blood vessel mimicking material is needed which represents blood vessels during needle-tissue interaction. Experiments were conducted at the Erasmus MC in Rotterdam to examine the needle forces during puncturing of blood vessels from the liver. The results show that puncturing of blood vessels from the liver results in higher needle forces than puncturing of the surrounding liver tissue. This means that it is an improvement to include blood vessels in the existing liver phantom. The first step towards the improvement of the liver phantom is therefore completed, as shown in Figure 18. The resulting force data are used to find a blood vessel mimicking material to develop the artificial blood vessels for the liver phantom.

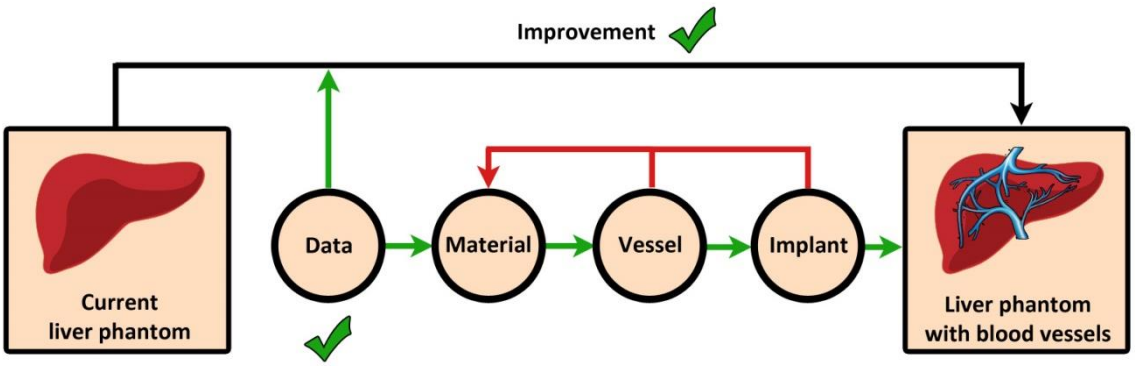


**Figure 18 The first step towards the improved liver phantom is completed by collecting data on needle-blood vessel interaction and needle-liver interaction. The next step is to find a blood vessel mimicking material.**

# 4. Blood vessel mimicking material

The next step towards the implantation of blood vessels in the liver phantom, is to find a blood vessel mimicking material. This material needs to mimic the peak forces during puncturing of a blood vessel from the human liver, as examined in Chapter 3. In Figure 19, all the measurements of the hepatic vein and the portal vein are combined (median=2.20 N, IQR=1.46 N to 3.67 N). This was done, because the peak forces during puncturing of the hepatic vein and portal vein are similar. For our blood vessel mimicking material we chose our desired peak forces to be in the IQR. This range is shown in Figure 19 by the red dotted lines. During the search for a suitable material, it must be considered that the material needs to be formed into the shape of a blood vessel. The typical vessel wall thickness of the larger liver veins is about 0.5 mm [4]. For the blood vessel mimicking material we therefore choose the thickness to be between 0.5 mm and 1.0 mm, to ensure a decent representation of the real blood vessel wall thickness. Furthermore, it must be considered that the material eventually needs to be implanted into the existing PVA phantom. A possibility of bonding with the PVA is therefore necessary. Finally, the blood vessel mimicking material must not compromise the ability to use the liver phantom with ultrasound for needle guidance.

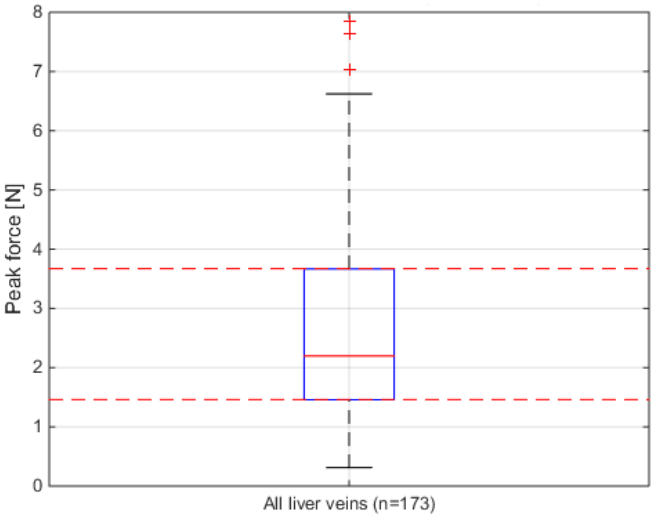


**Figure 19 Boxplot of the peak force data of all liver veins of the three livers combined.**

In the first section of this chapter, different materials are discussed that might be suitable as a blood vessel mimicking material, according to findings in literature. The most promising materials are then tested for their suitability, primarily by looking at the peak forces and the force profile during needle insertion experiments. The results of the needle insertion experiments with the blood vessel mimicking materials are presented in the second section of this chapter. In the final section of this chapter, the most promising blood vessel mimicking material is selected for further use.

## 4.1 Materials based on literature

In literature, we find that soft human tissues are commonly mimicked by polymers, like agarose, gelatin, polyvinyl alcohol (PVA), polyvinyl chloride (PVC) and silicone [55]. In general, polymers are macromolecules that consist of long and repeating chains of smaller molecules, called monomers. The process of forming polymers from monomers is called polymerization. Polymers come in a lot of varieties with different properties. These differences are the result of the type of molecules that are bonded and the way they are bonded. Polymers can be roughly divided into natural polymers and synthetic polymers. Furthermore, a distinction can

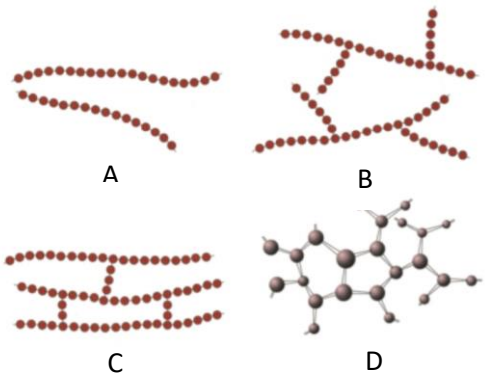


**Figure 20 Different polymer structures: (A) linear, (B) branched, (C) crosslinked, (D) network. Adapted from [56].**

be made based on the structure of the polymer. The polymer can be linear, branched, crosslinked or structured as a network, as can be seen in Figure 20 [56]. The network structure can be seen as a highly crosslinked polymer structure. Crosslinking can be achieved both chemically and physically and will influence the properties of the material. In general, crosslinking of the polymer results in an increased mechanical strength. In this section, different polymers are described that could be used as a blood vessel mimicking material, because they are expected to have characteristics as described in the introduction of this chapter.

### 4.1.1 Polyvinyl alcohol (PVA)

Polyvinyl alcohol (PVA) is a synthetic polymer that is produced by the polymerization of vinyl acetates. These polymerized vinyl acetates are then partially hydrolyzed. During the hydrolysis, the acetate groups in the vinyl acetate are replaced with hydroxyl groups. This can be seen in Figure 21. Due to the only partial hydrolysis of the polyvinyl acetates, some of the polyvinyl acetates monomers remain in the PVA polymer. The degree of polymerization is the number of linked monomers. This includes both the vinyl alcohol monomers and the vinyl acetate monomers. The degree of hydrolysis is the amount of vinyl alcohol monomers in relation to the total amount of monomers in the PVA.

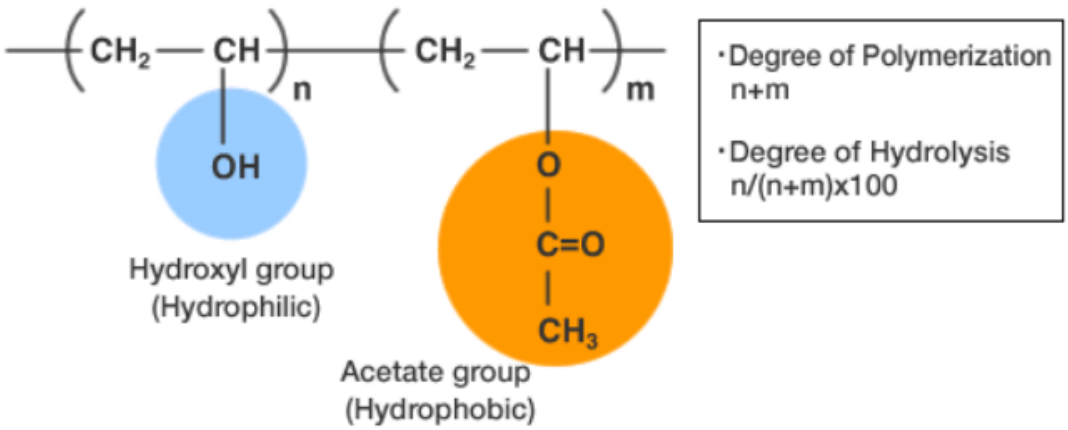


**Figure 21 Structure of PVA, resulting from the partial hydrolysis of polymerized vinyl acetates. Both the degree of polymerization and the degree of hydrolysis are shown with n = the number of vinyl alcohol monomers and m = the number of vinyl acetate monomers. Retrieved from http://www.j-vp.co.jp on September 23, 2018.**

PVA can be used to create PVA hydrogels, which are commonly used as a tissue mimicking material. The PVA can then be crosslinked by subjecting it to freeze-thaw cycles. The freeze-thaw cycles result in hydrogen bonding of hydroxyl groups in the PVA, which causes the crosslinks. The material made by this process is considered a PVA cryogel. The amount of crosslinks in the PVA cryogel can be influenced by the number of freeze-thaw cycles, the concentration of PVA in the solution, the thawing rate and the freeze time [57]. In general, more freeze-thaw cycles will results in a higher amount of crosslinks and a higher Young's Modulus [58, 59]. In literature, we see examples where PVA is used as a blood vessel mimicking material. However, these examples do not include force data during needle insertions. We do find a blood vessel phantom with a 1 mm vessel wall thickness intended for ultrasound studies [60]. Another PVA blood vessel phantom, intended for MR-imaging, was created using a wall thickness of 3.175 mm [61]. The samples underwent 1-10 freeze-thaw cycles and it was reported that the vessel wall thickness shrunk due to these freeze-thaw cycles. Furthermore, PVA was suggested as a useful material for blood vessel biomodeling, due to the similar viscoelasticity as a blood vessel from a dog [62].

### 4.1.2 Silicone

Silicone is a synthetic polymer that is made up of siloxane, which is a chain of alternating silicon and oxygen atoms, in combination with carbon and/or hydrogen atoms. One of the most common examples is polydimethylsiloxane (PDMS), shown in Figure 22. The difference in the structural forms of the silicone can result in a wide arrange of properties. Based on the length of the polymer chain and the degree of crosslinking, silicones can be roughly divided into five classes: fluids, compounds, lubricants, resins and rubbers [63]. Our main interest is in the silicone rubbers, which come in different hardnesses. One of the most common types of silicone used for tissue mimicking is room temperature vulcanizing (RTV) silicone, which can be easily molded into different shapes. In general, silicones are chemically inert, stable at both low and high temperatures and resistant to water and oxidation. In literature, silicone was used to mimic a blood vessel structure intended for needle puncture during ultrasound guidance [64]. Silicone tubes were furthermore embedded in gelatin to mimic blood vessels [65]. In other research, needle insertion force data were found using thin silicone layers. Cutting forces up to 1 N were observed during puncturing of silicone membranes of 0.4 and 0.8 mm thickness, embedded in a PVC block, using a 15G needle [66]. Needle insertions into 3 mm thick silicone samples resulted in puncture forces reaching approximately 8 N, when using a 18G needle [67, 68]. These results give an indication of the needle forces that can be reached during puncturing of thin silicone layers.

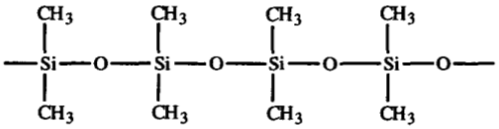

Figure 22 Structure of polydimethylsiloxane (PDMS), a common silicone. Retrieved from [63].

### 4.1.3 Polyurethane (PU)

Polyurethane is a synthetic polymer that is formed by reacting alcohols with two or more reactive hydroxyl groups per molecule, with isocyanates that have more than one reactive isocyanate group per molecule. An example of this process can be seen in Figure 23.

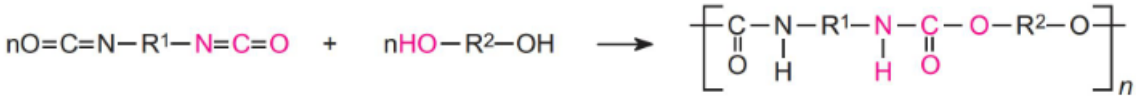

Figure 23 Example of the forming of a polyurethane. Retrieved from http://www.essentialchemicalindustry.org on September 26, 2018.

Polyurethane exists in a wide variety of forms, ranging from flexible foams to hard rubbers. For the purpose of finding a blood vessel mimicking material, the main focus is on PU-rubbers. Two-part PU-rubbers are easy to mold and can be cured at room temperature. They are available with a wide range of shore hardness options, that can surpass the hardness of silicone. In general, PU-rubbers are strong, have a good temperature resistance and negligible shrinkage. In literature, PU-rubbers are not commonly used for soft tissue mimicking. However, if the silicone results in puncture forces that are too low, PU-rubber might be interesting to experiment with.

### 4.1.4 Selecting materials for the experiments

PVA and silicone were selected to be used for the first experiments. PVA is chosen, because the connection with the PVA of the liver tissue is expected to be more easy when using the same material. The downsides are that it might be difficult to reach the desired needle puncture forces due to the gel-like substance of PVA. Silicone might be difficult to bond with the PVA liver tissue. However, due to its wide arrange of hardness options, it might be possible to find the right magnitude of needle forces. If the PVA and silicone do not result in the desired forces, PU is available in a higher hardness and might be an option then. PU will be difficult to bond with PVA as well.

Biopolymers such as gelatin, gellan gum and agarose were excluded at this stage, because it was expected that the needle insertion forces would be too low. In literature, latex tubes are used as a blood vessel during ultrasound needle guidance [69], although no force data are presented. However, the use of latex is somewhat laborious, because it has to be applied layer for layer and cannot be poured into a mold. Therefore it was excluded at this stage of the study. Finally, PVC is also used in literature as a tissue mimicking material. It is a hard material that can be softened by the addition of plasticizers, which can be toxic. Using the softened PVC, it is difficult to recreate the desired blood vessel structure and therefore the PVC was excluded at this stage.

## 4.2 Needle insertion forces

In the following sections, the needle insertion forces for PVA, silicone and PU rubber are presented and discussed. The main focus is thereby on the peak forces that arise during puncturing of the material. The desired range of peak forces, as mentioned in the introduction of this chapter, is shown in the figures by the red dotted lines. Furthermore, we looked at the entire force profile to ensure that, for example, the friction force is roughly in line with the experimental data on blood vessels. During all experiments, the same experimental setup and methods were used as in the experiments described in Section 3.1. Again, the samples were randomized and not the individual measurements.

### 4.2.1 PVA

For the experiments with PVA (Selvol PVOH 165, Sekisui Chemical Group, NJ, USA), multiple samples were made using a different amount of freeze-thaw cycles per sample (Figure 24). For all samples, 7m% of PVA was used, which is the highest recommended concentration of PVA by the producer. In general, a higher m% of PVA will result in higher needle forces [1], so therefore the highest concentration was used. The different PVA samples underwent 2, 4, 6 and 8 freeze-thaw cycles of 8 hours freezing and 8 hours thawing and the samples were between 2 mm and 4 mm thick. The results of the needle insertion experiments using the PVA samples are shown in Figure 24. The results clearly show that puncturing of the PVA samples results in puncture forces that are below the range of interest. Even when 8 freeze-thaw cycles were applied, the maximum needle force during a needle insertion into a 3-4 mm thick sample of PVA was not high enough to resemble the insertion force during a needle insertion into a human liver vein. This is even more so if we consider that the intended thickness of the blood vessel wall is 0.5-1.0 mm. More details on the PVA experiments are shown in Appendix D.

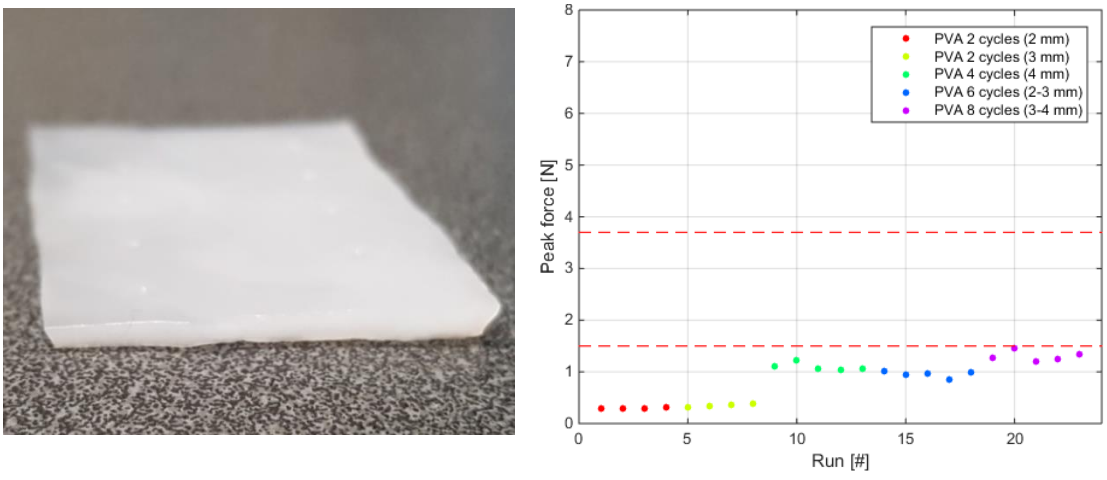


**Figure 24 Example of a PVA sample (left) and the peak forces during puncturing of PVA (7m%) samples with different freeze-thaw cycles.**

### 4.2.2 Silicone

Like mentioned in Section 4.1.2, silicone comes in a lot of varieties with different hardnesses. In this section, the needle insertion forces during experiments with silicone are discussed. Furthermore, the addition of Thi-Vex and the addition of a mesh fabric to the silicone are examined.

#### Thi-Vex

Thi-Vex (Smooth-On Inc., Macungie, PA, USA) can be added during the production process of silicone to increase the viscosity of the silicone. This makes it easier to apply the silicone to non-horizontal surfaces for example. This might be useful to create a blood vessel structure. It was examined if the addition of Thi-Vex influences the peak forces during needle insertions. The results, shown in Appendix D, showed that the addition of Thi-Vex did not result in different peak forces.

#### Dragon Skin 20

The first experiments with silicone were done using Dragon Skin 20 silicone (Smooth-On Inc., Macungie, PA, USA), with a Shore A hardness of 20. Samples were made with different thicknesses, ranging from 0.5 mm to 1.3 mm. Figure 25 shows an example of the samples and the results of the needle insertion experiments. The results show that puncturing the Dragon Skin 20 silicone does not result in the peak forces that are desired for the blood vessel mimicking material. Only one of the measurements resulted in a peak force in the desired range and all other peak forces were too low.

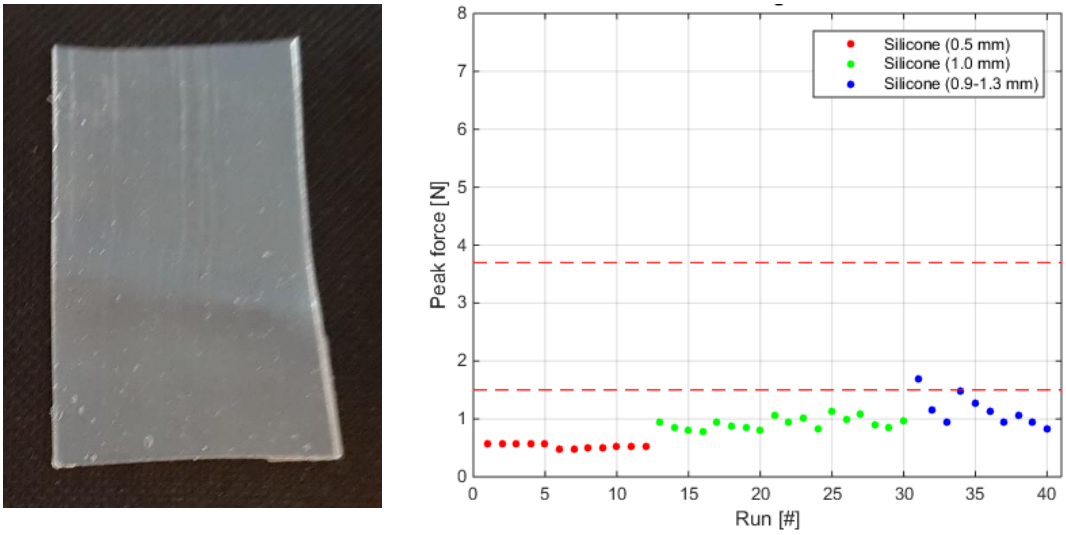


**Figure 25 (Left) Two samples of Dragon Skin 20 silicone. (Right) Results of the peak forces of Dragon Skin 20 silicone with different thicknesses.**

Based on these results, a harder type of silicone is needed to reach the desired peak forces. Preliminary needle insertion tests (Appendix D) indicated the suitability of Smooth-Sil 950 (Smooth-On Inc., Macungie, PA, USA), with a shore hardness of 50.

#### Smooth-Sil 950

For the experiments using Smooth-Sil 950, samples were made with a thickness varying between 0.6 mm and 1.8 mm. In Figure 26, an example of a Smooth-Sil 950 silicone sample and the results of the experiments are shown. When using the samples with a thickness of 0.6-0.8 mm, we see that the peak forces are still too low. However, when using a thickness of about 0.9-1.1 mm, we see that the forces fall in the desired range of peak forces. The silicone sample with a thickness of 1.8 mm results in peak forces that are close to the upper threshold.

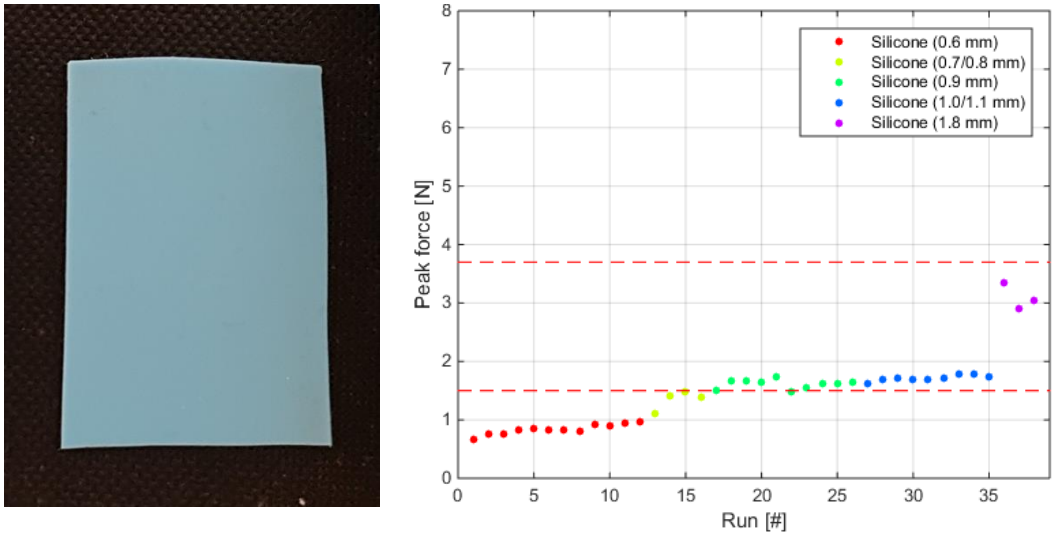


**Figure 26 (Left) Sample of Smooth-Sil 950 silicone. (Right) Results of the experiments using Smooth-Sil 950 silicone samples with different thicknesses.**

A typical force profile of a needle insertion into a 1.1 mm silicone sample is shown in Figure 27 on the left. The small and large peak during puncturing are expected to be due to the inner and outer part of the needle. This phenomenon can also be seen during measurements with a liver vein, as shown in Figure 27 on the right. The friction force seems to be a little higher during puncturing of silicone samples, compared to puncturing of liver veins. This could be due to the fact that veins are more moist than the silicone due to remainders of blood.

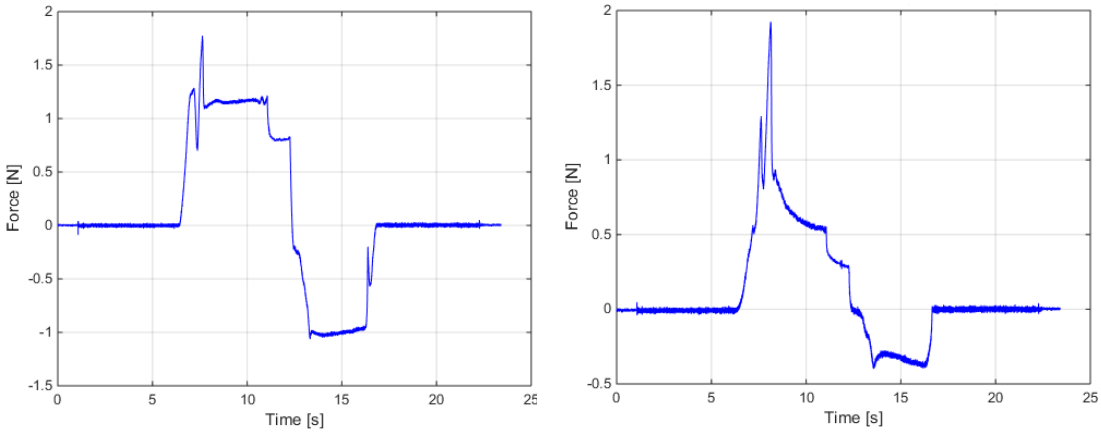


**Figure 27 Force profile during needle insertion in 1.1 mm Smooth-Sil 950 silicone sample (left) and a human liver vein (right).**

## Addition of mesh fabric (without glue)

Based on the aforementioned results, an increase in peak force was still needed for the desired blood vessel thickness of 0.5-1.0 mm. Therefore, a mesh fabric was added to the silicone. In addition to this feature, the mesh also enables proper bonding to the PVA (described in detail in Section 6.1). Samples were made using the Smooth-Sil 950 silicone with a thickness ranging between 0.6 mm and 1.3 mm. The mesh fabric was applied to the silicone during the hardening process. When the mesh fabric was applied too soon, it was fully absorbed in the silicone. Then, it is not possible to use the mesh fabric to bond the silicone and PVA. This can be prevented by adding Thi-Vex to the silicone or applying the mesh fabric later in the hardening process. The results of the experiments are shown in Figure 28. The addition of the mesh fabric increases the peak forces during needle insertion, to

within the desired range and even above. Furthermore, the variability in the peak forces increases due to the addition of the mesh fabric. This is beneficial for a blood vessel mimicking material, because there is a large variability in peak forces for blood vessels from the liver as well.

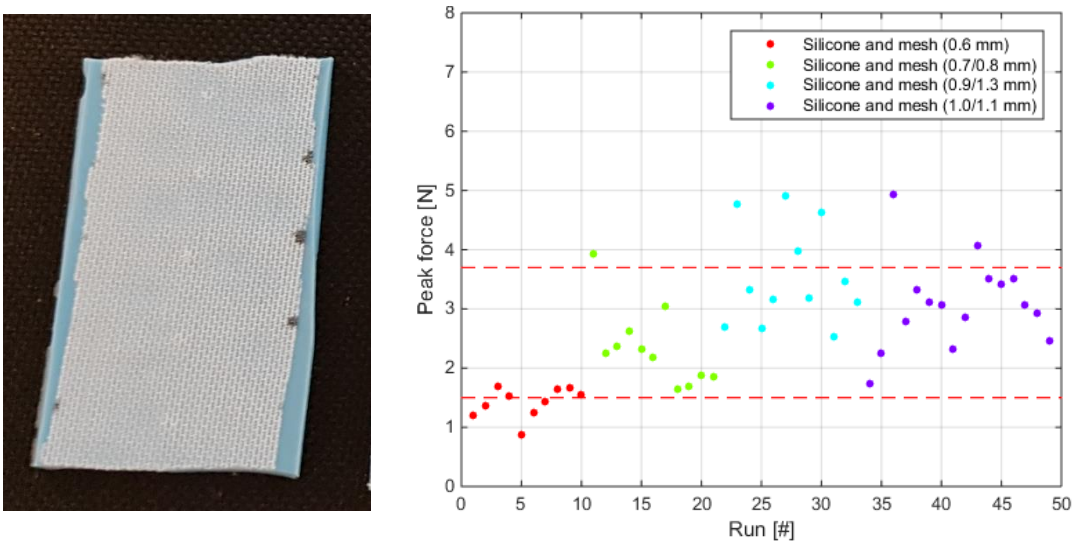


**Figure 28 (Left) Sample of Smooth-Sil 950 silicone with mesh fabric. (Right) Results of the experiments using Smooth-Sil 950 silicone samples with mesh fabric and different thicknesses.**

The addition of the mesh fabric does results in a somewhat different force profile. At the moment that the silicone is punctured, a double peak is shown. This can be seen in Figure 29 on the left. This pattern seems to be the result of the combination of the mesh fabric and the inner and outer needle. When we use only the inner needle in combination with the silicone and mesh fabric, the double peak does not appear. This is shown in Figure 29 on the right.

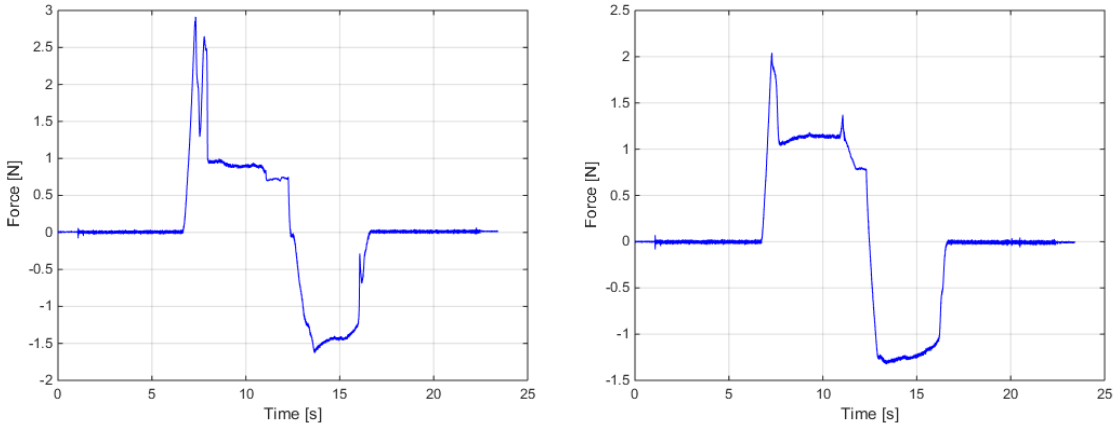


**Figure 29 Force profiles during needle insertion in a 1.3 mm Smooth-Sil 950 silicone sample with mesh fabric added, with both the inner and outer needle (left) and only the inner needle (right).**

### Addition of mesh fabric (with glue)

Another option for the addition of mesh fabric is to glue the fabric onto the silicone after the silicone has hardened. Silicone samples were made using Smooth-Sil 950 silicone and with a thickness of 0.6 mm and 1.1-1.2 mm. To glue the mesh fabric onto the silicone, Sil-Poxy silicone adhesive (Smooth-On Inc., Macungie, PA, USA) was used. An example of a sample and the results of the experiments are shown in Figure 30. For both the 0.6 mm silicone and the 1.1-1.2 mm silicone, we can see that the addition of glue does not clearly affect the peak forces. The peak forces are still inside the desired

range, with the 0.6 mm silicone close to the lower threshold and the 1.1-1.2 mm silicone in the middle of the range and reaching the upper threshold.

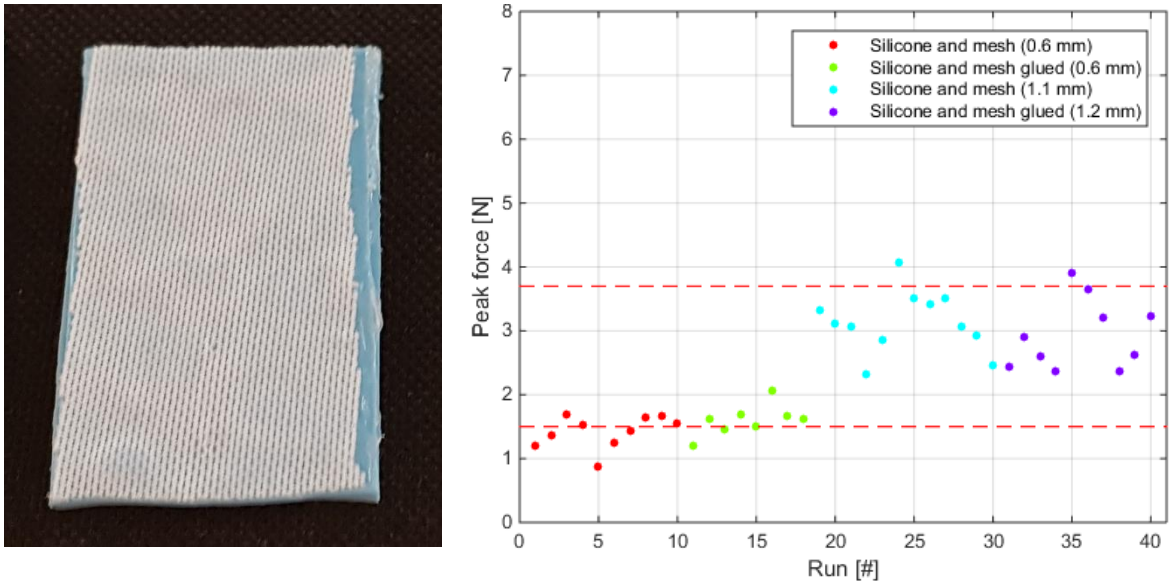


**Figure 30 (Left) Sample of Smooth-Sil 950 silicone with mesh fabric. (Right) Results of the experiments using Smooth-Sil 950 silicone samples with mesh fabric and different thicknesses.**

Both methods to apply the mesh fabric ensured a good bonding between the mesh fabric and the silicone. In addition, the orientation of the mesh fabric was examined, both with and without using Sil-Poxy glue. Details are shown in Appendix D. Finally, it needs to be considered that the addition of the mesh fabric might result in different forces when punctured under a different angle.

### 4.2.3 PU-rubber

During the experiments with only silicone, the peak forces were still somewhat low. Therefore further experiments were done using PU-rubber, which is available in a higher hardness than silicone. Using a PMC-780 Dry PU-rubber (Smooth-On Inc., Macungie, PA, USA) with a shore A hardness of 80, experiments were done to see if the PU could result in the desired forces when using only a 0.5-1.0 mm layer of PU-rubber. A downside of using this type of PU is that one of the parts is toxic and so it needs to be handled with care. A few samples were made with a thickness of 0.5 mm and 1.0 mm. Also a sample was made with mesh fabric on top, with a PU-rubber thickness of 0.6-0.8 mm. The results of the peak forces are shown in Figure 31. We can see that the 0.5 mm layer of PU results in peak forces that are in the desired range. The 1.0 mm

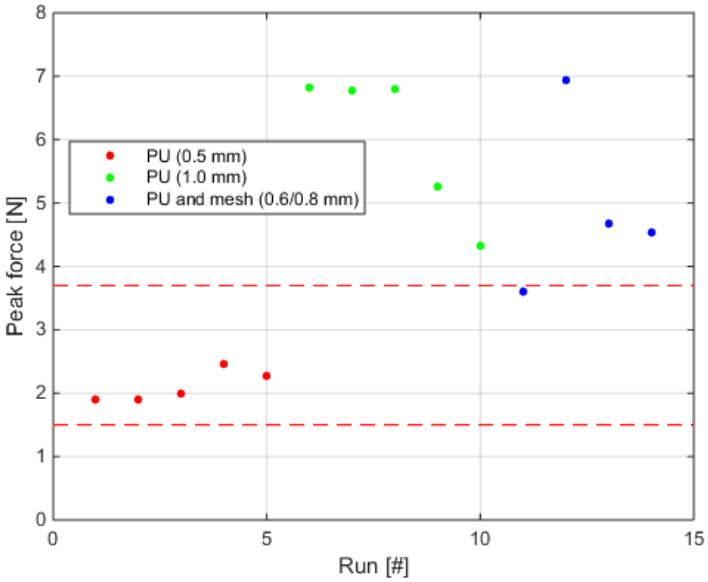


**Figure 31 Peak forces during puncturing of PMC-780 Dry PU samples with different thicknesses and the addition of mesh fabric.**

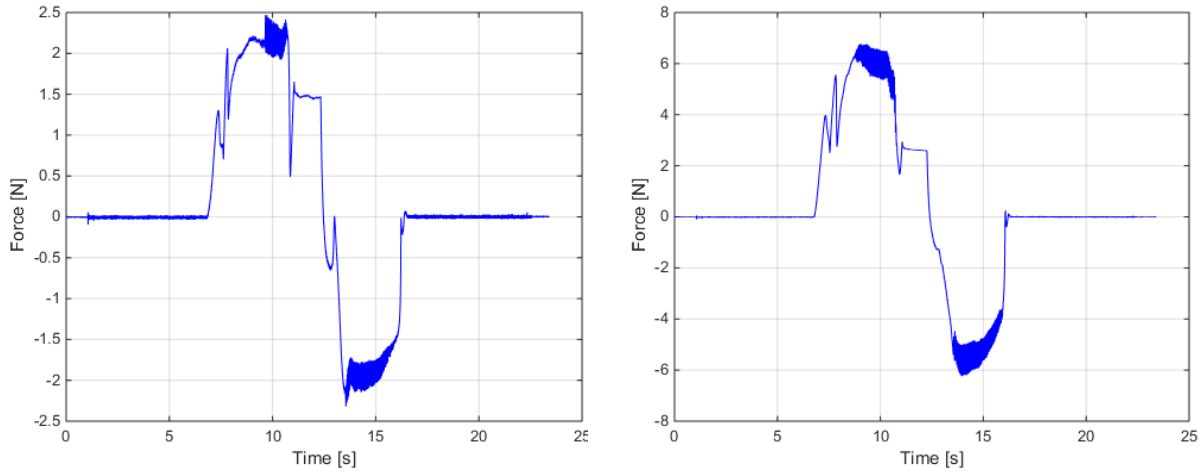


**Figure 32 Force profiles during needle insertion in PMC-780 Dry PU samples, with a thickness of 0.5 mm (left) and a thickness of 1.0 mm (right).**

layer results in forces that are too high and that is also the case when using the mesh fabric on a 0.6-0.8 mm layer. However, during the needle insertion into the PU, the force profile is not very similar to the force profile during needle insertion into a liver vein. This is shown in Figure 32 on the left, where the force profile of a needle insertion into a 0.5 mm PU sample is shown. We see that after the puncture the force keeps increasing do to a lot of friction. The typical force drop after the puncture is not present and therefore it does not resemble the force profile during a needle insertion into a liver vein. There is also a lot of fluctuation during the friction, if we compare it to the insertion into a liver vein or the silicone. The same phenomenon is observed when using the 1.0 mm PU sample, as can be seen in Figure 32 on the right.

## 4.3 Material selection

After the needle insertion experiments using the potential blood vessel mimicking materials, a materials must be selected to use for further steps. The results of the experiments using PVA, showed that the peak forces are not sufficient to mimic the human liver blood vessels. The forces during the PU experiments, were in the desired range when using a thickness of 0.5 mm. However, the force profile during a needle insertion in PU differs too much from the force profile of a needle insertion into a blood vessel. Therefore, the PU is not a suitable blood vessel mimicking material. The

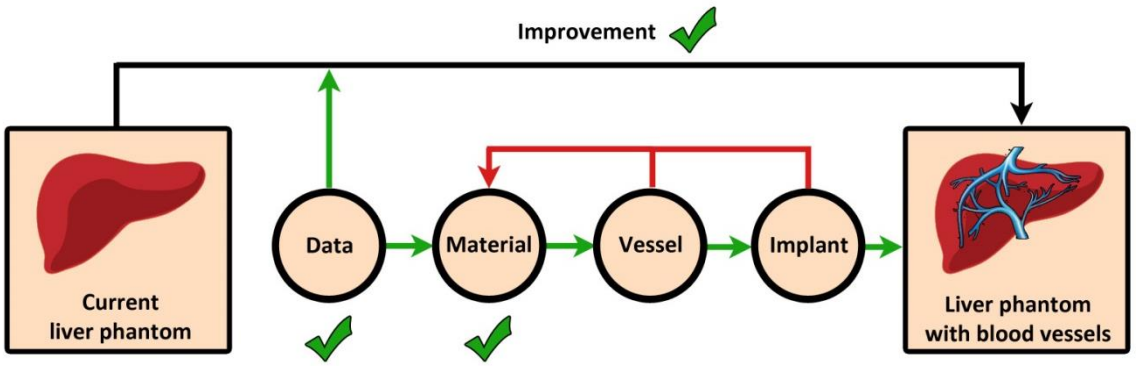


**Figure 33 The second step towards the improved liver phantom is completed by selecting a blood vessel mimicking material. The next step is to find recreate the blood vessel structure.**

Smooth-Sil 950 silicone reaches the lower threshold of the desired forces, when using a layer thickness of 1.0 mm without the mesh fabric. When adding the mesh fabric, the forces are almost all within the desired force range for a silicone thickness between 0.6 and 1.2 mm. The use of glue to attach the mesh fabric to the silicone does not affect the needle forces, so it can be used if necessary. Based on these results, the Smooth-Sil 950 silicone is chosen as the blood vessel mimicking material. It can now be tested for its ability to be formed in the shape of a human liver blood vessel. The current progress towards the improved liver phantom is shown in Figure 33.

# 5. Blood vessel recreation

This chapter presents methods that can be used to recreate the structure of the liver blood vessels. First a digital 3D-model of the liver blood vessels is made using a CT-scan of a liver. Then, two possibilities are discussed to create the 3D-model, using either a 3D-printer or modeling clay. Finally, both methods are compared and one of them is selected to create the blood vessel structure.

## 5.1 Modeling blood vessels

For our liver phantom we want our blood vessel structure to resemble the structure of the blood vessels in a human liver. Therefore, both the hepatic vein and portal vein need to be implanted into the phantom. We chose to focus only on the larger parts of both blood vessels, since these large vessels are expected to be punctured during procedures like TIPS. Besides that, the addition of small side branches makes the model more complex and therefore more difficult to produce.

The first step is to make a digital model of the liver, the portal vein and the hepatic vein. This was done via a semiautomatic segmentation process using a CT-scan of a human liver in 3D Slicer 4.8.1 [70]. The different steps of the segmentation process are shown in Figure 34.

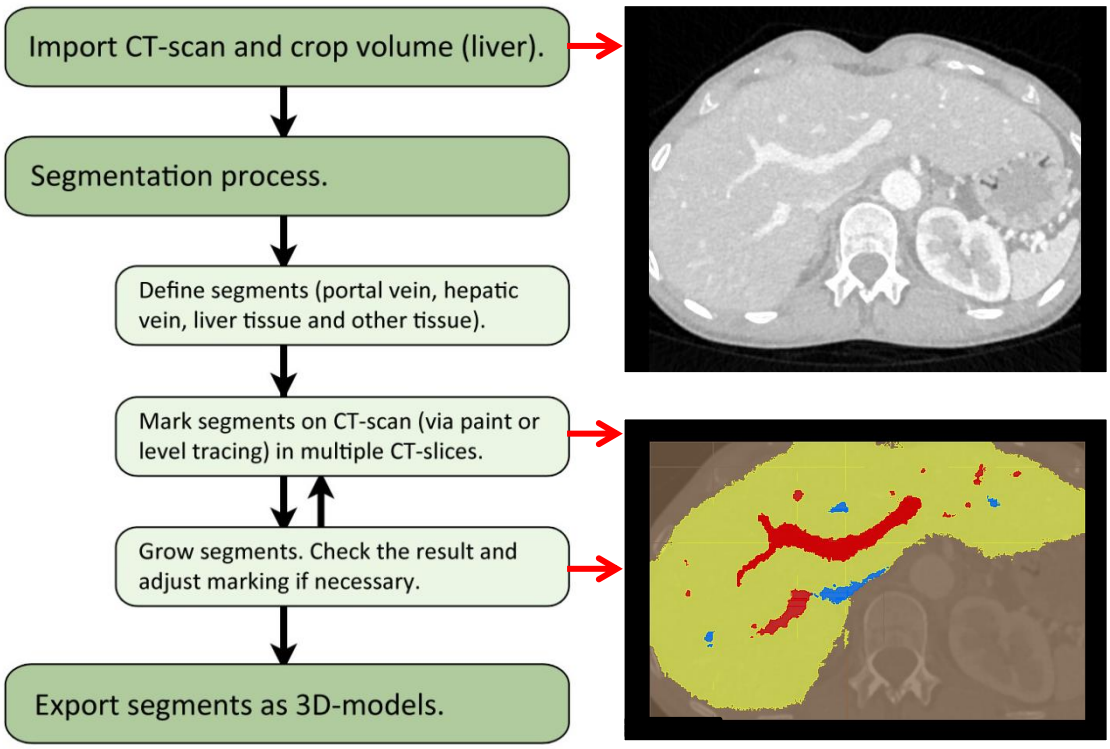


**Figure 34 Overview of the different steps of the segmentation process using 3D Slicer. Segmentation of portal vein (red), hepatic vein (blue), liver tissue (yellow) and other tissue (brown).**

The resulting 3D-models of the liver and both liver veins, are shown in Figure 35 using Meshlab [71]. On the left, we can see the posterior view of the entire liver model and the parts of the veins before entering and exiting the liver. On the right, we see the anterior view of the portal vein and hepatic vein, without the liver tissue. We can see that there are still a lot of side branches, even though the smallest branches are not taken into the model. Furthermore, we see that the left hepatic vein is partially missing. Appendix E shows more details on the segmentation process and the dimensions of the 3D-models of the veins.

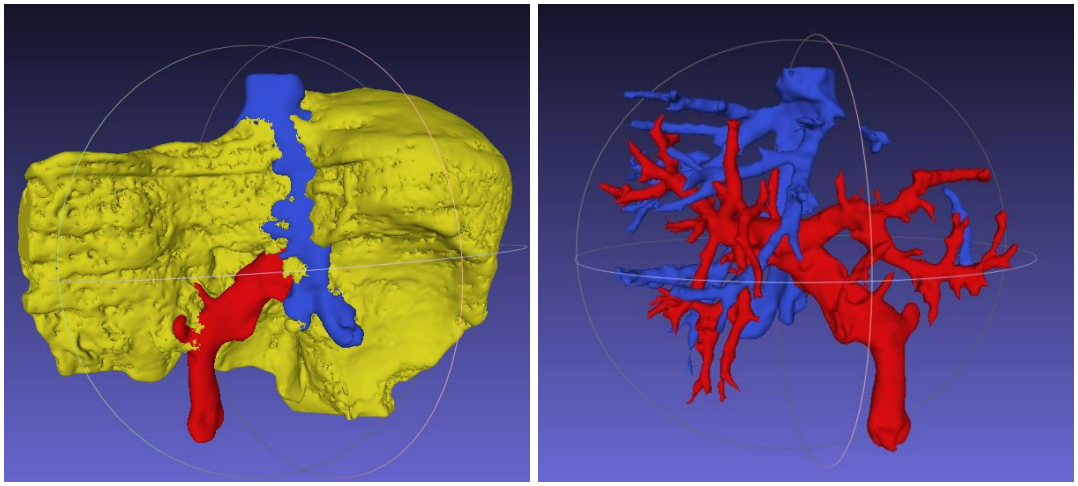

Figure 35 Posterior view of the entire liver model (left) and the anterior view of the portal vein (red) and hepatic vein (blue).

## 5.2 Creating blood vessel structure

To create a blood vessel structure, the silicone needs to be shaped into thin-walled hollow tubes. This was tested by applying a thin layer of silicone to a 5 mm diameter metal rod and a 10 mm diameter wooden rod (Figure 36). Both were coated with a silicone loosening agent, to ensure that the silicone could be easily removed after hardening. The silicone was smeared using a small brush and Thi-Vex was added to ensure that the silicone would not drip off the rods. On some of the samples, mesh fabric was added after about 20 minutes into the hardening process. This was to check if the mesh attached properly to the thin-walled tubes. After the silicone was hardened, it was removed from the rods to create the thin-walled hollow tubes.

The results of some of the samples are shown in Figure 36. The silicone vessels without mesh fabric did not have a constant thickness. This is due to the fact that the silicone was applied by a brush. The samples that included the mesh fabric, had a more even thickness. This is because pressure can be applied to the mesh and silicone, during the hardening process, to create a more even thickness along the tube. The mesh fabric was attached properly and remained attached during the removal of the rods.

Figure 36 Silicone and mesh fabric on a 10 mm diameter wooden rod (top) and thin-walled silicone tubes with and without mesh fabric (bottom).

From these test samples we concluded that it is possible to make thin-walled silicone tubes of 5-10 mm in diameter. However, the structure of a blood vessel is different than the straight rods used for the test samples. Therefore a method must be found to create a more complex blood vessel structure that can be removed after the silicone is hardened. Two different methods were examined: 3D-printing with water soluble PVA and modelling clay that can be melted.

### 5.2.1 Vessel structure: 3D Printing

One of the options to create a blood vessel structure based on the 3D-model, is using a 3D-printer. The structure of the blood vessel can be printed using water-soluble PVA. This way, the silicone can be applied on the 3D-printed model and after the silicone is hardened, the model can be placed in water. Then, the water-soluble PVA will dissolve and a thin-walled silicone structure will remain. A preliminary test was done using a small 5 mm diameter rod that was 3D-printed using water-soluble PVA. Silicone was applied on the rod and after it was hardened, it was placed in water. After about a week, the PVA was fully dissolved and a thin-walled silicone tube remained. The results of the test are shown in Figure 37. It shows that this method might be a viable option to create thin-walled blood vessel structure and an experiment was done using a more complex structure.

**Figure 37 3D-printed rod (5 mm diameter) made of water-soluble PVA (white) and a thin-walled silicone tube, created using a rod of water-soluble PVA (blue).**

First, a simplified version of the portal vein model was made using MeshLab. Like mentioned in Section 5.1, we focus on the larger parts of the veins. Therefore, the small side branches were removed and the model was reconstructed using the 'Screened Poisson Surface Reconstruction' function [72]. Furthermore, the surface of the blood vessel structure was smoothened to be able to apply an even layer of silicone. This simplification process is shown in Appendix E. Finally, two portal vein structures were 3D-printed, with one being more simplified than the other. The printing was done using an Ultimaker 3 3D-printer (Ultimaker Inc., Geldermalsen, The Netherlands), with a layer height of 0.2 mm. Then, using the most simplified structure, a silicone version of the portal vein was made. The silicone, without the addition of Thi-Vex, was applied with a brush.

The results of the 3D-printed, most simplified, portal vein structure and the silicone vein are shown in Figure 38. More details on the 3D-printed structures are shown in Appendix F.

**Figure 38 (Left) 3D-printed structure of the simplified portal vein. (Right) Silicone portal vein with the 3D-printed structure still inside the vein.**

Using a 3D-printer with water-soluble PVA has some advantages. A digital 3D-model of the blood vessel structure can be created precisely using a 3D-printer. Furthermore, the 3D-printed structure

can remain inside the silicone until the PVA liver phantom is complete. The water-soluble PVA can then be removed by placing the entire liver phantom in water. This ensures that the structure of the silicone blood vessels remains in the correct shape and position during pouring of the PVA in a liver phantom mold. The 3D-printing method also has some downsides. It takes time to dissolve all of the water-soluble PVA from the silicone vessels. Furthermore, it is difficult to remove the support structure, that is used during the 3D-printing, from the blood vessel structure. The main reason for this difficulty, is that the 3D-printer uses the same water-soluble PVA as a support material for the structure that is printed. Removal of the supports structure results in an rough surface on the structure and small branches are vulnerable for breaking. This problem might partially be solved by using different settings on the 3D-printer for the placement and structure of the support material.

### 5.2.1 Vessel structure: modelling clay

Another option to remove the inner blood vessel structure is to use a modelling clay, that can be melted out of the silicone structure. Two types of modeling clay were tested for their suitability: plasticine and Monster Clay (The Monster Makers Inc., Cleveland, OH, USA).

Plasticine is a relatively soft clay that has a melting point around 35°C. An addition type plasticine (Silicones and More, Geleen, The Netherlands) was chosen, which is recommended to use in combination with silicones. Monster clay is available in three different variants: soft, medium and hard. For this purpose the hard variant was chosen to ensure that the blood vessel structure stays in the correct shape while applying the silicone. Monster Clay has a melting point of about 60°C. Both materials were used to create a T-shaped blood vessel structure with a diameter of about 10 mm. The shapes of the structures are shown in Figure 39. The plasticine turned out to be too soft and it started to deform while applying the silicone. If the plasticine is used on an even more complex blood vessel structure, it would not be possible to retain the correct shape. Therefore, the plasticine was ruled out for further use. Monster Clay is very hard at room temperature and thus retained the correct shape while applying the silicone. After the silicone was hardened, the structure was placed in an oven and heated to approximately 75°C. After about half an hour, the Monster Clay started to melt and it slowly dripped out of the structure. However, a thin film of the molten clay remained on the inside of the silicone tube. Afterwards, the silicone was cooled so that the clay became hard again. By rubbing the silicone, it was possible to remove all of the clay from the inside of the tube. Another sample was made with mesh fabric added to the silicone.

**Figure 39 Two T-shaped samples to mimic a blood vessel structure, made of plasticine (left) and Monster Clay (right). The diameter of both structures is about 10 mm.**

The result of the T-shaped silicone structure that was made using Monster Clay, is shown in Figure 40. When using the mesh fabric, the mesh remained properly attached to the silicone during the entire production process.

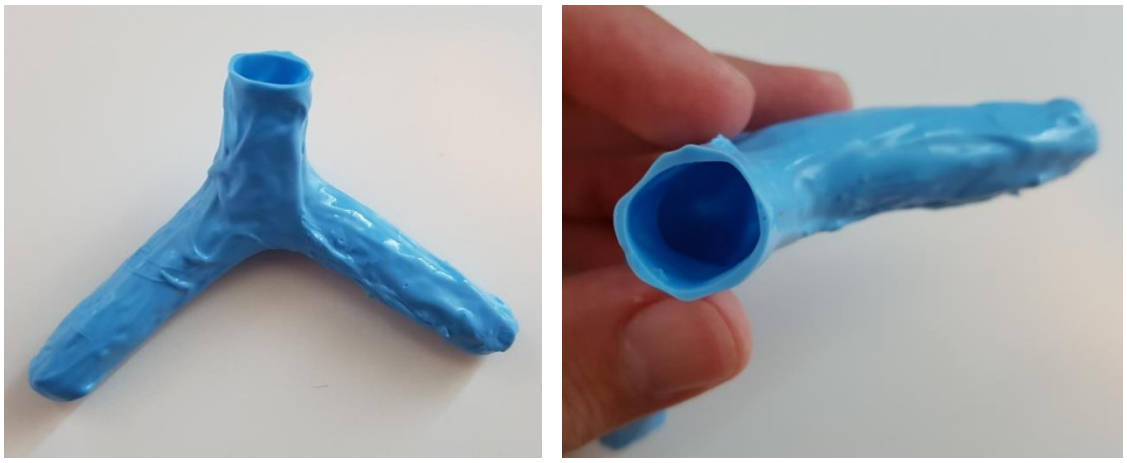

Figure 40 Thin-walled and T-shaped silicone tube, made using a Monster Clay structure.

With Monster Clay it is possible to create different kinds of structures with a smooth surface. The shaping of the clay is relatively fast and when at room temperature, the clay is hard so the structure remains in the correct shape. Furthermore, the removal of the clay is relatively fast. There are also some downsides of using this method. The clay must be removed from the silicone blood vessel before the PVA is poured into the liver phantom mold. Otherwise the entire PVA liver phantom needs to be heated afterwards, which dehydrates the PVA. When the clay is removed before the PVA is poured into the phantom mold, the liquid PVA might deform and displace the thin-walled silicone structure. Furthermore, a thin layer of clay remains on the inside of the silicone tube when melting the clay. When using a complex blood vessel structure, it is difficult to remove all of the clay. A final downside, is that the Monster Clay needs to be shaped by hand. Therefore it is difficult to attain a precise representation of a blood vessel model. However, a mold can be created in which the clay can be poured when heated.

## 5.3 Selection of vessel structure

To create a proper structure for the silicone blood vessels, we have two options: 3D-printing using water-soluble PVA and Monster clay. Both methods are described and discussed in Section 5.2. In Table 1 we see the main advantages and disadvantages of both methods once again.

| | | 3D-printing | Monster Clay |
|---|---|---|---|
| **Creating structure** | + | Very precise representation of structure | Smooth surface, without support structure |
| | - | Removing support structure | Made by hand and thus less precise |
| **Removal of structure** | + | After PVA is poured in liver phantom mold | Fast |
| | - | Slow | Before PVA is poured in liver phantom mold<br>Difficult to remove all clay in a complex structure |

Table 1 Pros and cons of both methods that can be used to create the blood vessel structure.

The method using the 3D-printed, water-soluble PVA is chosen as the best option to recreate the blood vessel structure for the liver phantom. The biggest advantages of the 3D-printing method, is that you can easily and precisely recreate the structure of a digital 3D-model of a blood vessel and that you can remove the 3D-printed structure after the PVA is poured into the liver phantom mold. This way the structure of the silicone blood vessel will remain in the correct shape and place during pouring of the PVA. The difficulty of removing the support material after 3D-printing might be

partially resolved using different settings on the 3D-printer. Now we have selected a method to create the vessel structure, we can go on to the next step: implanting the vessel in the existing PVA phantom, as can be seen in Figure 41.

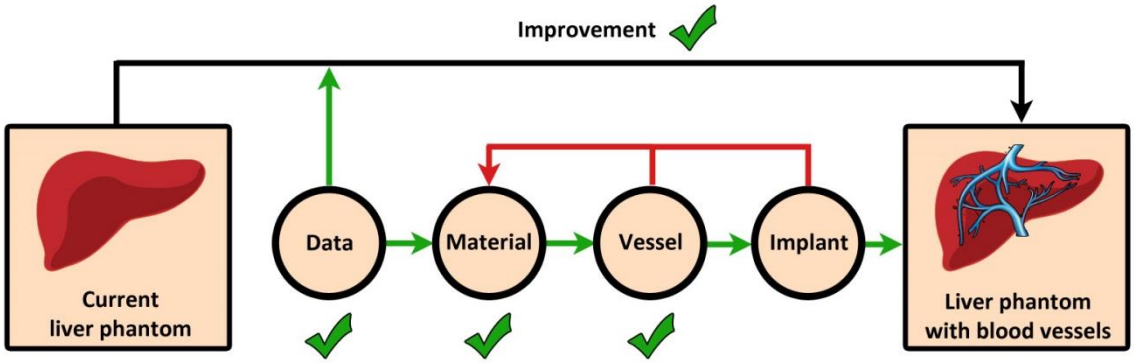


**Figure 41 The third step towards the improved liver phantom is completed by selecting a method to recreate the blood vessel structure. The next step is to implant the structure into PVA.**

# 6. Implantation in PVA

Using silicone as a blood vessel mimicking material, it is possible to create a thin-walled structure in the shape of a liver vein. The next step is to implant the silicone structure into PVA. In the first section of this chapter, the bonding between silicone and PVA is examined. Then, the force profile of a needle insertion into PVA and silicone is validated. Finally, the implantation of a silicone tube in PVA is tested for ultrasound needle guidance.

## 6.1 Bonding between PVA and silicone

The silicone needs to bond with the PVA to ensure that the blood vessel structure stays in place during needle interaction. First, experiments were done to see whether PVA bonds to silicone when poured onto the silicone. After the PVA was hardened, it was clear that there was no bonding at all between the silicone and the PVA. Another experiment was done using Sil-Poxy glue. The glue was applied to the silicone before the PVA was poured onto the silicone. Again, there was no bonding. Another option that was examined, was the use of a mesh fabric between the layers of silicone and PVA. The principle of using a mesh fabric is to create a physical link between both the silicone and the mesh and the PVA and the mesh.

Two methods were examined to apply the mesh fabric on the silicone. For the first method, a layer of mesh fabric was placed onto a flat layer of silicone after about 20 minutes into the hardening process. This process starts when both silicone components are mixed. Thi-Vex was added to the silicone to ensure that the mesh fabric was not absorbed into the silicone. For the second method, the mesh fabric was glued onto a flat layer of silicone after it was hardened. This was done using Sil-Poxy glue. For both methods, 4m% PVA was poured onto the silicone and mesh fabric after the silicone was hardened. Two freeze-thaw cycles were applied (8 hours freezing and 8 hours thawing) and then the bonding of the materials was examined. Another experiment was done using three silicone tubes with mesh fabric attached, both with and without Sil-Poxy glue. The tubes were placed in a small container, which was then filled with PVA (4m%). Then, two freeze-thaw cycles of 8 hours freezing and 8 hours thawing were applied. This experiment was done to test the implantation of a thin-walled tube, made from silicone and mesh fabric, into PVA. More details of the samples are shown in Appendix G.

Figure 42 shows the results of the bonding experiments. The left figure shows the bonding between a flat layer of silicone, including mesh fabric, and a layer of PVA. The right figure shows three silicone and mesh fabric tubes, embedded in PVA.

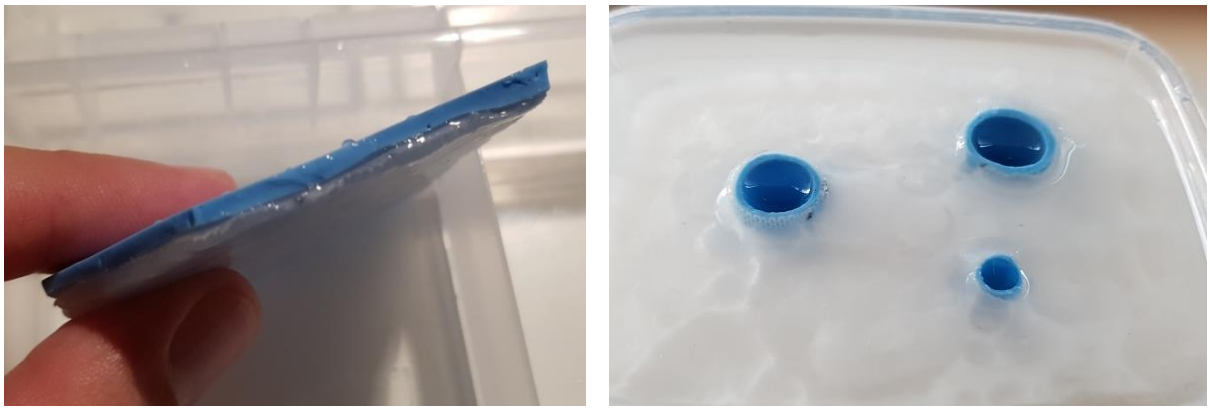

**Figure 42 (Left) Bonding between a layer of silicone and mesh fabric and a layer of PVA (4m%, 2 freeze-thaw cycles). (Right) three silicone tubes with mesh fabric embedded in PVA (4m%, 2 freeze-thaw cycles).**

The use of the mesh fabric ensured a proper bonding between the silicone and the PVA. This was the case for both methods, with and without glue, and for both silicone shapes, the flat layer and the tube. The silicone and PVA remained bonded during several needle insertions as well. When the flat layers of silicone and PVA were torn apart, the bonding between the silicone and the mesh was the first to loosen. From these results, we can concluded that the addition of a mesh fabric is an adequate way to bond the silicone and the PVA via a physical link. The mesh fabric was already tested for needle insertion forces in Section 4.2.2.

## 6.2 Force profile

In Section 4.2.2 it was shown that a thin layer of silicone and mesh fabric give a good representation of the peak forces during a needle puncture in a human blood vessel. Section 6.1 furthermore showed that the mesh fabric ensures bonding between the silicone and PVA. Now we have to check if the force profile of a needle insertion into a silicone layer with mesh fabric, attached to PVA, resembles the force profile during a needle insertion in a liver vein that is attached to liver tissue. Therefore another experiment was conducted.

First, needle insertions were done in human liver vein samples, using both the portal vein and hepatic vein. A layer of liver tissue of about 15 mm was still attached to the vein. The same experimental setup and methods were used as described in Section 3.1. Then, needle insertion experiments were done using phantom samples that consisted of a 15 mm layer of PVA (4m%, two freeze-thaw cycles of 8 hours freezing and 8 hours thawing) and a layer of silicone and mesh fabric. Figure 43 shows the experimental setup of both samples and more details are shown in Appendix H. Two different layer thicknesses were used for the silicone: 0.6 mm and 1.1 mm. Both were made with and without the use of Sil-Poxy glue to apply the mesh fabric. All needle insertions were done using the same orientation, with the liver tissue on top and the blood vessel wall on the bottom.

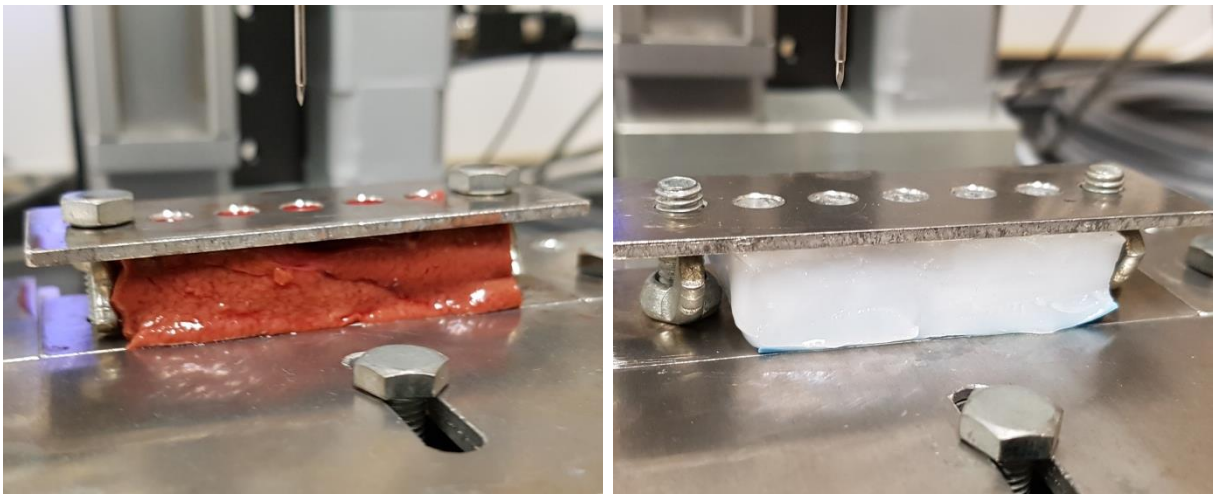

**Figure 43 Experimental setup during the force profile experiments. (Left) a 15 mm layer of liver tissue with a liver vein underneath. (Right) a 15 mm layer of PVA tissue with a silicone and mesh layer underneath.**

The results of the force profile experiments are shown in Figure 44 and Figure 45. The figures respectively show the force profiles of needle insertions into the phantom samples with a silicone layer of 1.1 mm and a silicone layer of 0.6 mm. Both are compared to the force profiles of needle insertions into the human liver vein samples.

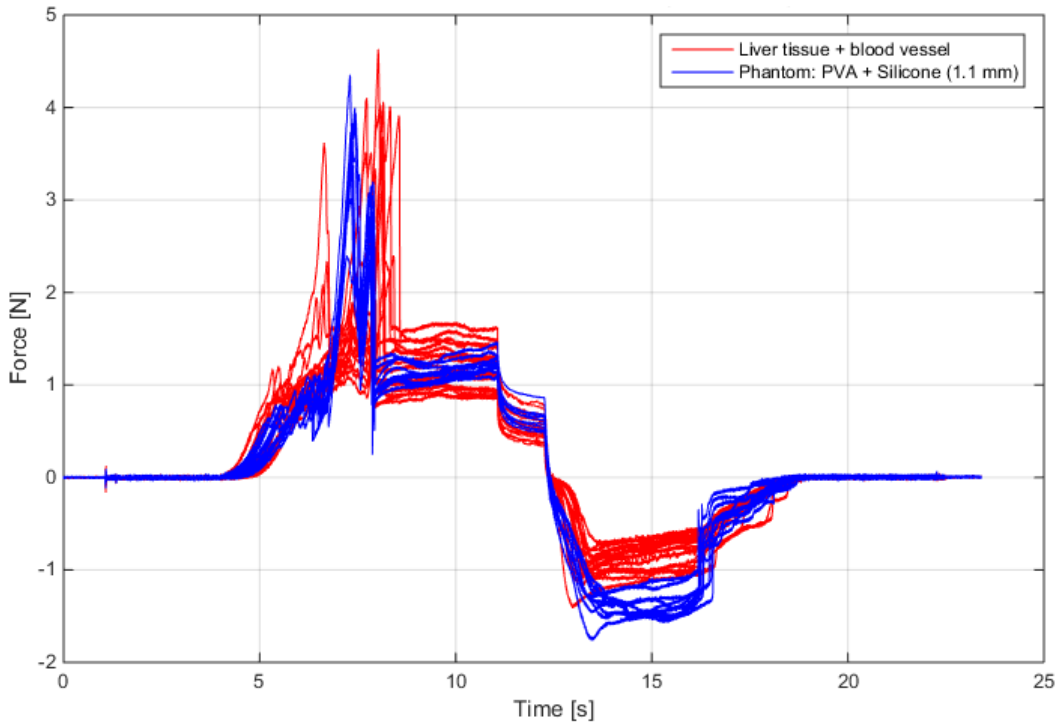


**Figure 44 Force profiles of needle insertions into human liver samples and phantom samples. The human liver samples consist of a 15 mm layer of liver tissue with a liver vein attached. The phantom samples consist of a 15 mm layer of PVA (4m%, 2 freeze-thaw cycles) with a 1.1 mm layer of silicone and mesh fabric.**

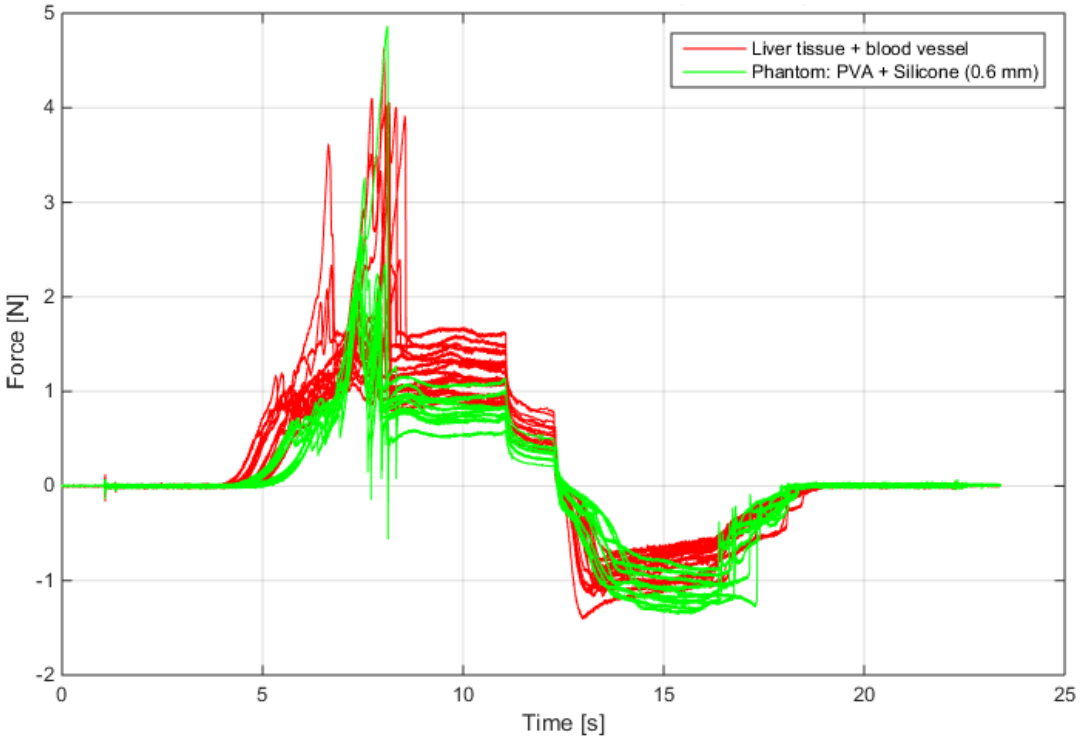


**Figure 45 Force profiles of needle insertions into human liver samples and phantom samples. The human liver samples consist of a 15 mm layer of liver tissue with a liver vein attached. The phantom samples consist of a 15 mm layer of PVA (4m%, 2 freeze-thaw cycles) with a 0.6 mm layer of silicone and mesh fabric.**

In general, we see that the force profiles of the phantom samples resemble the force profile of the human liver samples. The friction force during retraction of the needle is somewhat higher for the 1.1 mm phantom sample compared to the human liver sample. For the 0.6 mm silicone sample, the friction force during insertion is somewhat lower than the human liver samples. It needs to be mentioned that the layer of PVA in the 0.6 mm silicone sample was only 13 mm thick. Therefore it was approximately 2 mm thinner than the tissue on the human liver samples and the 1.1 mm silicone samples. This explains why the force starts to rise later during the 0.6 mm silicone samples, compared to the other samples. This might also have resulted in less friction force during insertion and retraction. The addition of glue does not influence the force profile as shown in Appendix H.

When we look closer at the force profile during the penetration of the phantom samples, we see some differences compared to the puncturing of the liver samples. In general, we see two peaks during the puncturing of the silicone (Figure 46, green circle). The double peak is already mentioned in Section 4.2.2 and is further discussed in Appendix H. Furthermore, we sometimes see a downward peak just after the penetration of the silicone, certainly with the 0.6 mm silicone samples (Figure 46, red circle). The downward peak might be due to the silicone oscillating up and down just after it is punctured. This would explain the fact that it is observed more frequently when using a the 0.6 mm layer of silicone, because a thin layer is more flexible and prone to oscillation. The magnitude of the peak forces in the phantom samples however, resembles the peak forces in the liver samples.

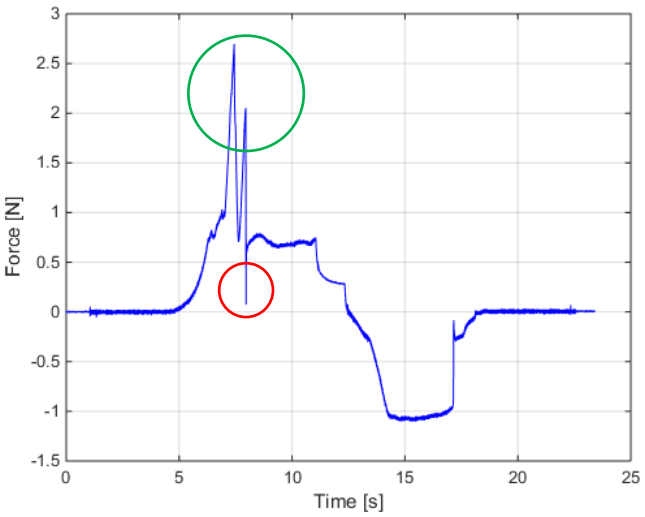


**Figure 46 Force profile of a needle insertion into a phantom sample consisting of a 15 mm layer of PVA (4m%, 2 freeze-thaw cycles) and a 0.6 mm silicone layer.**

## 6.3 Ultrasound guidance

The current liver phantom is intended to be used with ultrasound needle guidance. This means that the addition of blood vessels should not compromise this ability. Therefore both the blood vessels and the needle tip must be visible on the ultrasound image. Furthermore, the needle tip must remain visible during insertion into a blood vessel. Therefore an ultrasound test was done using a PVA sample including three silicone blood vessels, as shown in Figure 42 on the right. The vessels were filled with water during the scan.

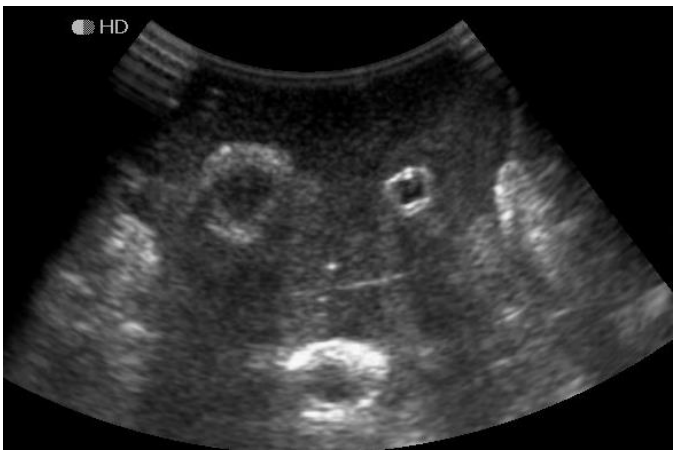


**Figure 47 Ultrasound scan of three silicone tubes with mesh embedded in PVA (4m%, 2 freeze-thaw cycles).**

The results of the ultrasound scan are shown in Figure 47, where we can clearly see three blood vessels in the PVA. The large vessel on the bottom was made using Sil-Poxy glue and the two vessels

on the top were made without glue. When puncturing the vessels with a needle, the needle could be seen during the entire puncture process. This is shown in Figure 48, showing the needle tip (in-pane) making contact with the blood vessel wall (left figure) and the needle tip (in-plane) after puncturing the vessel wall (right figure).

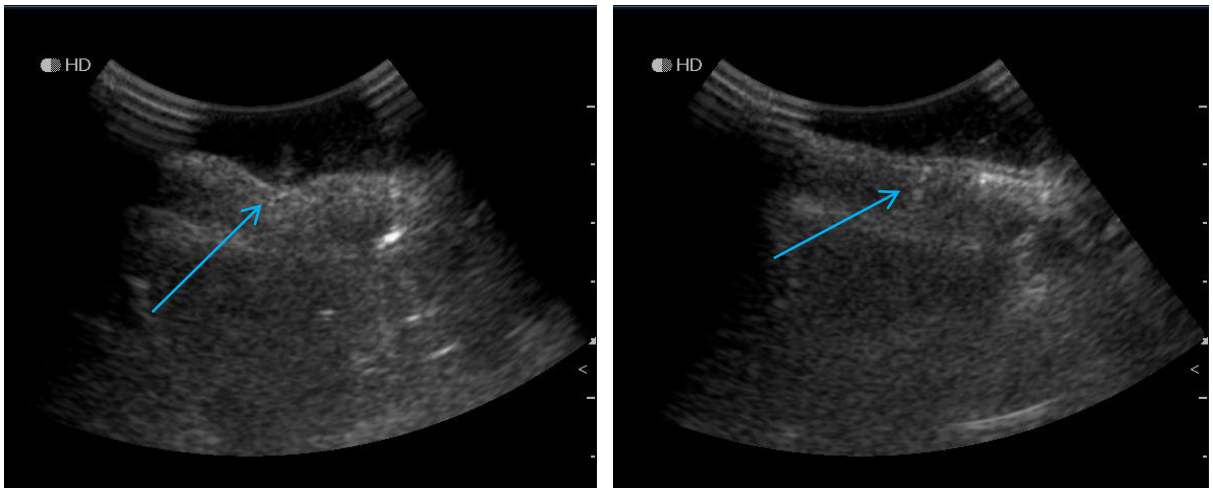


**Figure 48 Ultrasound scans of a needle puncturing a silicone tube with mesh, embedded in PVA (4m%, 2 freeze-thaw cycles). Left: the needle (in-plane) makes contact with the silicone tube. Right: the needle tip (in-plane) has punctured the silicone tube.**

The results of the ultrasound test show that it is both possible to identify the silicone blood vessels in the PVA and guide the needle tip during insertion in a blood vessel. The ability to use the improved liver phantom with ultrasound needle guidance is therefore not compromised. In Figure 47, it seems that the addition of glue makes the vessel wall more echogenic, although this difference in echogenicity was not as clear in other ultrasound scans.

With the combined results of the bonding between silicone and PVA, the force profiles and the ultrasound scan, we can conclude that it is possible to implant silicone blood vessels in PVA liver tissue. This means that all steps towards the improved liver phantom, can be taken. This is shown in Figure 49.

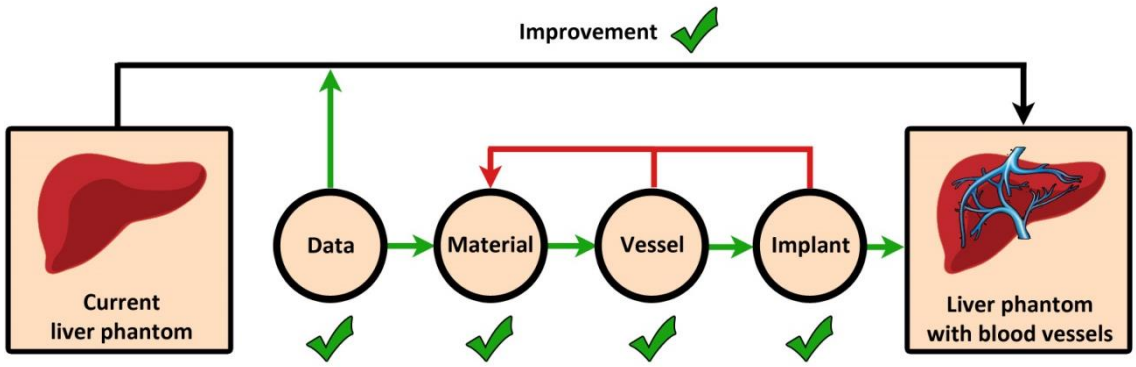


**Figure 49 The fourth step towards the improved liver phantom is completed by selecting a method implant the blood vessel structure in PVA. All these steps can now be used to produce liver phantom with blood vessels.**

# 7. Discussion

The goal of the study was to provide insight into the needle forces during puncturing of blood vessels from the human liver. The resulting force data are used for the improvement of a PVA liver phantom, intended for needle development and training purposes. In this chapter, the main results of the study and the steps towards the improved liver phantom are discussed.

In literature, no data were found on needle interaction forces in blood vessels from the human liver. Therefore a needle insertion experiment was done to collect these data. Peak forces were examined during needle insertions in portal veins, hepatic veins, hepatic arteries and liver tissue. The results indicated that puncturing of liver blood vessels results in higher peak forces than puncturing of the surrounding liver tissue. This means that it is necessary to implant an artificial blood vessel wall in the liver phantom. The resulting force data were used to find a blood vessel mimicking material. Smooth-Sil 950 silicone, with the addition of a mesh fabric, resulted in the desired peak forces. It needs to be considered that the force data were collected using fresh-frozen livers that were expected to be healthy. For the liver phantom, it needs to be considered that puncturing of blood vessels from in vivo livers or sick livers might result in different needle forces. Furthermore, the needles were inserted perpendicular to the tissue during all experiments. The addition of a mesh fabric might have more influence on the needle forces when puncturing under a different angle.

For the production of the improved liver phantom, a couple of steps need to be taken. First, it must be determined which parts of the veins need to be included in the liver phantom. Most of the small branches might not be necessary to include in the phantom. Then, a 3D-model of the veins must be designed, which can be done by segmenting the veins using a CT-scan of a liver. The next step is to fabricate the 3D-models with a 3D-printer using water-soluble PVA. Thereby, the support structure must be designed in such a way that it can be removed easily from the blood vessel structure after printing. Then, a layer of silicone can be applied to the water-soluble PVA vein structures. This can be done using a brush, but with the addition of Thi-Vex it is hard to create an even layer of silicone. Other methods can therefore be considered. Without using Thi-Vex, the silicone is more easy to apply in an even layer. However, it will drop off because of its lower viscosity. If the entire structure is kept in rotational motion, it might be possible to prevent that from happening. Instead of using a brush, the entire structure can be submerged in silicone to create a more even layer. Another option is to develop a mold in which the water-soluble PVA structure can be placed. This mold can then be used to pour the silicone around the structure to ensure a constant thickness of the silicone layer. On the other hand, creating an exactly even layer of silicone might not be necessary. This is because there is a large variability of the peak forces during puncturing in liver veins.

For the addition of the mesh fabric, there are two options. The mesh can either be glued onto the silicone after it is hardened, or it can be put on the silicone during the hardening process. The latter is time-dependent and might therefore be more difficult to accomplish. This is certainly the case when using a large structure, because then it takes more time to apply the silicone when using a brush Therefore, less time remains available to apply the mesh fabric. However, this method has an advantage as well. The mesh fabric is placed on top of the silicone and it is possible to put some pressure on the mesh to create a more even thickness of the silicone layer. This way the silicone does not stick to your hands or tools. Furthermore, it needs to be considered that it is difficult to apply the

mesh to the more curvy parts of the silicone vein. This is less of a problem when using Sil-Poxy glue, because you have time to properly fit the mesh fabric to the vein shape.

The final step is to implant the silicone and mesh blood vessel structure into a PVA liver phantom. Therefore, first a special liver mold has to be designed in which the blood vessel structures can be placed. It needs to be ensured that the blood vessels remain in the correct shape and position during the pouring of the PVA into the liver mold. After the PVA has been poured into the mold, it can be placed in the freezer to apply the appropriate amount of freeze-thaw cycles. When the PVA liver tissue is completed, the entire liver phantom can be placed in water to dissolve the water-soluble PVA inside the blood vessels. What remains, is the improved liver phantom with implanted silicone veins.

# 8. Conclusion

Needle insertion experiments were done to collect data on the needle forces during puncturing of blood vessels from the liver. These force data can be used to improve an existing PVA liver phantom, by implanting artificial blood vessels. This liver phantom mimics the forces during needle insertions in the liver and is intended for needle development and training purposes. The results of the experiment showed that puncturing of liver blood vessels results in higher needle peak forces than puncturing of liver tissue. The collected force data were used to find a blood vessel mimicking material, that mimics the forces during needle insertion in human liver veins. A silicone layer between 0.6 mm and 1.2 mm, with the addition of a mesh fabric, resulted in the desired peak forces. The addition of the mesh fabric furthermore ensures that the silicone bonds with the PVA tissue used in the liver phantom. A digital model of the liver blood vessels was made using a CT-scan of the liver. Using this model, a simplified structure of the portal vein was created with a 3D-printer using water soluble PVA. That structure was used to create a silicone blood vessel. The methods described in this thesis, can be used to implant artificial veins in a PVA liver phantom.

# Appendices

## Appendix A: Articles on needle interaction forces in blood vessels

Different text colors indicate different experiments presented in the same article.

| Article | | | | Tissue characteristics | | Needle geometry | | Insertion methods | | | | Needle forces |
|---|---|---|---|---|---|---|---|---|---|---|---|---|
| Ref. | Authors | Year | Title | Tissue type | Vessel type | Diameter [mm] or [G] | Needle type | Velocity [mm/s] | Angle [°] | Samples [#] | Manual/automatic | Peak force [N] |
| [11] | Elgezua et al. | 2013 | Survey on Current State-of-the-Art in Needle Insertion Robots: Open Challenges for Application in Real Surgery. | Porcine (ex vivo) | Liver vein | 18G-1 1/2" | - | 0.75-6 | 90 | - | Automatic | 1 (based on one sample?) |
| [12] | Elgezua et al. | 2013 | Event Classification in Percutaneous Treatments based on Needle Insertion Force Pattern Analysis. | Porcine (ex vivo) | Liver artery | 18G-1 1/2" | - | 0.75-6 (steps of 0.75) | 90 | 65 | Automatic | 0.55-0.87 |
| [13] | Elgezua et al. | 2016 | Online Event Classification for Liver Needle Insertion Based on Force Patterns | Porcine (ex vivo) | Liver vein/artery | 18G-1 1/2" | - | - | - | - | Automatic | 0.4-1.3 |
| [14] | Jiang et al. | 2014 | Experimental study of needle–tissue interaction forces: Effect of needle geometries, insertion methods and tissue characteristics. | Porcine (ex vivo) | Liver vein/artery | - | - | - | - | - | - | 0.59 (based on one sample?) |
| [15] | Okuno et al. | 1998 | Development of an automatic blood sampling system: control of the puncturing needle by measuring forces | Human (in vivo)<br>Rabbit | Vena mediana cubiti<br>Ear vein | 0.4 and 0.8 mm<br>0.4 mm | - | 15<br>2.5 | 15<br>15-30 | 10<br>10 | Manual<br>Automatic | 0.23±0.09 (0.4 mm needle)<br>0.64±0.23 (0.8 mm needle)<br>0.11±0.01 |
| [16] | Healey et al. | 2005 | In vivo force during arterial interventional radiology needle puncture procedures. | Human (in vivo) | Femoral artery | - | - | - | - | 10 | Manual | 0.13-8.89 (mean: 3.76 SD: 3.32) |
| [8] | Zhai et al. | 2012 | A sensor for needle puncture force measurement during interventional radiological procedures. | Human (in vivo) | Femoral artery | 19G | Vascular access needle | - | - | only 1 example is shown | Manual | 2.1 |
| [17] | Pepley et al. | 2017 | Measurement of Syringe Needle Forces for a Haptic Robotic Training Device. | Human (fresh frozen) | Jugular vein | 18G | Introducer needle (to mimic CVC needle) | - | - | 5 | Manual | 1.35-2.02 |
| [18] | Kobayashi et al. | 2012 | Development of a needle insertion manipulator for central venous catheterization. | Porcine | Jugular vein | 18G (article: 2.4 mm) | Short bevel, puncture needle with outer sheath | 4 | 10, 20, 30, 40, 50, 60, 70, 80 | 5 insertions per angle | Automatic | 0.3-1.3 (puncture force for different angles)<br>0.10-0.50 (force drop for different angles) |
| [19] | Kobayashi et al. | 2013 | Use of puncture force measurement to investigate the conditions of blood vessel needle insertion. | Porcine | Jugular vein | 18G (article: 1.36 mm) | Short bevel | 1,3,5,7,9<br>3 | 15<br>10, 20, 30, 40, 50, 60, 70, 80 | 5 insertions per condition | Automatic | 0.10-0.50 (force drop) |
| [20] | Kobayashi et al. | 2014 | Preliminary in vivo evaluation of a needle insertion manipulator for central venous catheterization. | Porcine (in vivo) | Jugular vein | 18G? (article: 2.4 mm)?<br>*Not really clear...* | - | 3 | 15 | 2 x 5 insertions | Automatic | 1.4 (opened skin)<br>3.7 (unopened skin) |
| [21] | Saito et al. | 2005 | Detection of needle puncture to blood vessel using puncture force measurement. | Rabbit | Ear vein | 27G | Bevelled in three planes | 2.5 | 15 | 30 | Manual + automatic | 0.15-0.20 |
| [22] | Saito et al. | 2006 | Detection of needle puncture to blood vessel by using electric conductivity of blood for automatic blood sampling. | Rabbit (in vivo) | Ear vein | 27G | - | 2.5 | 15 | 18 | Automatic | 0.10-0.20 |
| [23] | Clement et al. | 2016 | Effects of Axial Vibration on Needle Insertion into the Tail Veins of Rats and Subsequent Serial Blood Corticosterone Levels | Rat | Tail vein | 25G | Hypodermic needle | - | 15 | 18<br>18 | Manual | 0.2-0.4 (with needle vibration)<br>0.5-1.5 (without needle vibration) |

# Appendix B: Articles on needle interaction forces in the liver

Different text colors indicate different experiments presented in the same article. Matching colored authors indicate very similar articles.

| Article | | | | Tissue | Needle geometry | | Insertion methods | | | Needle forces | | Other info |
|---|---|---|---|---|---|---|---|---|---|---|---|---|
| Ref. | Authors | Year | Title | Liver type | Diameter [mm] or [G] | Type | Velocity [mm/s] | Samples [#] | Manual/ automatic | Type of force | Force [N] | |
| [1] | De Jong et al. | 2017 | PVA matches human liver in needle-tissue interaction | Human (ex vivo) | 18G | Triangular tip, trocar needle | 5 | 173<br>39 | Automatic | Peak forces<br>Friction slope | 0-0.65<br>0.01 (in N/mm) | During insertion and retraction, forces were characterized by friction, peak forces and number of peak forces per unit length. Peak forces in boxplot: median = 0.18 N, Q1 = 0.10 N, Q3 = 0.34N and outliers reach 1.7 N. |
| [8] | Zhai et al. | 2012 | A sensor for needle puncture force measurement during interventional radiological procedures. | Porcine (in vitro)<br>Human (in vivo) | 19G<br>18G | Vascular access needle<br>Kimal needle with trocar | 3.33<br>? | only 1 example is shown | Automatic<br>Manual | Puncture force (with capsule)<br>Force profile during liver biopsy | 0.42<br>0-8 (from force plot) | Force plots are shown of needle insertion in porcine liver and liver biopsy in patient. |
| [24] | Maurin et al. | 2004 | In vivo study of forces during needle insertions | Porcine (in vivo) | 18G | bevel tip, biopsy needle | ?<br>15 | - | Manual<br>Automatic | Maximum force | 3.73 (sd:0.59, 'with skin')<br>0.7 (sd:0.29, direct access)<br>1.89 (sd:0.36, 'with skin')<br>0.59 (sd:0.17, direct access) | Also liver 'removal' forces are mentioned. Unclear what this means (friction during removal?). Also liver capsule force mentioned. Stiffness force and friction force parameters are also determined and compared to values in Simone and Okamura. |
| [25] | Barbe et al. | 2007 | In Vivo Model Estimation and Haptic Characterization of Needle Insertions | Porcine (in vivo) | - | - | - | only 1 example is shown | Manual | Puncture force (through opened skin, including fat, muscle tissue and liver capsule) | 1.2 | Force plots given of needle inertion through opened and unopened skin. No real clear data on puncture force, due to unclarity of what tissue is punctured. |
| [26] | Washio et al. | 2004 | Needle Force Sensor, Robust and Sensitive Detection of the Instant of Needle Puncture | Porcine (in vivo) | 2 mm | Coaxial needle | 5 | 45 | Automatic | Puncture force | 0.4 | Friction force and tip force are measured independently. When combined the peak force during puncturing is about 0.5 N. |
| [27] | Shah et al. | 2008 | Robotically assisted needle driver: evaluation of safety release, force profiles, and needle spin in a swine abdominal model | Porcine (in vivo) | 18G | Diamond tip needle | - | 16 | Automatic | Insertion force | 0-1.5 (in force profile) | Three different needle rotation speeds were used: 0, 90 and 180 rpm. Also nozzle forces were mentioned, which are due to contact of the tissue on the needle shaft. |
| [13] | Elgezua et al. | 2015 | Online Event Classification for Liver Needle Insertion Based on Force Patterns | Porcine (ex vivo) | 18G-1 1/2" | - | - | 75-250 per liver and 5 livers. | Automatic | Puncture force | 0.1-0.4 | Puncture forces are shown in graph. |
| [12] | Elgezua et al. | 2013 | Event Classification in Percutaneous Treatments based on Needle Insertion Force Pattern Analysis | Porcine (ex vivo) | 18G-1 1/2" | - | 0.75-6 | 200 | Automatic | Puncture force | 0.16-0.20<br>(means for different velocities) | |
| [11] | Elgezua et al. | 2013 | Survey on Current State-of-the-Art in Needle Insertion Robots: Open Challenges for Application in Real Surgery | Porcine (ex vivo) | 18G-1 1/2" | - | 0.75-6 | - | Automatic | "Force to cut liver" | 0.4 | |
| [28] | Kobayashi et al. | 2008 | Modeling of conditions where a puncture occurs during needle insertion considering probability distribution. | Porcine (ex vivo) | 17G | biopsy needle | 0.5, 1, 2, 3, 4, 6, 8 | 63<br>(9 per insertion velocity) | Automatic | Puncture force | 0.35 (between 0.15 and 0.6 for different velocities) | Most variation in the forces is seen at lower insertions speeds. Mean value of 0.35 N is almost equal for all velocities. |
| [29] | Kobayashi et al. | 2008 | In Vitro Validation of Viscoelastic and Nonlinear Physical Model of Liver for Needle Insertion Simulation | Porcine (ex vivo) | 17G | biopsy needle | 0.5, 1, 2, 3, 4, 6, 8 | 63<br>(9 per insertion velocity) | Automatic | Puncture force | 0.35 (between 0.15 and 0.6 for different velocities) | Most variation in the forces is seen at lower insertions speeds. Mean value of 0.35 N is almost equal for all velocities. |
| [30] | Kobayashi et al. | 2009 | Developing a planning method for straight needle insertion using probability-based condition where a puncture occurs | - | - | - | 5 | - | Automatic | Puncture force | 0.9 and 1.7 (it is unclear what kind of tissue is punctured) | Only a single force plot and it is unclear what kind of liver is used and what kind of tissue is punctured in the force plot. |

| Article | | | | Tissue | Needle geometry | | Insertion methods | | | Needle forces | | Other info |
|---|---|---|---|---|---|---|---|---|---|---|---|---|
| Ref. | Authors | Year | Title | Liver type | Diameter [mm] or [G] | Type | Velocity [mm/s] | Samples [#] | Manual/ automatic | Type of force | Force [N] | |
| [31] | Wang et al. | 2015 | Experimental analysis of robot-assisted needle insertion into porcine liver. | Porcine (ex vivo) | 1.5 mm<br>8 mm | bevel tip<br>conic tip (custom made) | - | all data are based on 10 tests | Manual and robot-assisted | Maximum insertion force | 1.88 (manual) 1.65 (robot-ass.)<br>4.85 (manual) 4.22 (robot-ass.) | "The force data collected is a summation of stiffness, friction, and cutting forces". It is also concluded that the robotic needle insertion causes less oscillation than the manual insertion. |
| [32] | Wang et al. | 2014 | Optimal needle design for minimal insertion force and bevel length | Porcine (ex vivo) | 11G | lancet point needles (three different shaped) | 1.5 | 30 (10 per needle type) | Automatic | Initial peak needle insertion force | 0.81-1.02 (different needles) | Different lancet needle geometries are evaluated. |
| [33] | Wang et al. | 2013 | The Needle With Lancet Point: Geometry for Needle Tip Grinding and Tissue Insertion Force. | Porcine (ex vivo) | 11G | lancet point and bevel (see other info for details) | 1.5 | 40 (10 per needle type) | Automatic | Puncture force | 0.83-1.43 (different needles) | Three different lancet point needles were fabricated, starting from a bevel needle, and these needles were compared to a bevel needle. |
| [34] | Kobayashi et al. | 2005 | Physical Properties of the Liver and the Development of an Intelligent Manipulator for Needle Insertion | Porcine (ex vivo) | 17G | bevel tip, biopsy needle | 2 | 1 | Automatic | Puncture force | 0.55 | Also a friction force is metioned and in the graph it is shown to be about 0.2 N during insertion or -0.15 during retraction (unclear). |
| [35] | Kobayashi et al. | 2004 | Physical properties of the liver for needle insertion control. | Porcine (ex vivo) | 17G | bevel tip, biopsy needle | 2 | 1 | Automatic | Puncture force | 0.55 | Also a friction force is metioned and in the graph it is shown to be about 0.2 N during insertion or -0.15 during retraction (unclear). |
| [36] | Hing et al. | 2006 | Reality-Based Needle Insertion Simulation for Haptic Feedback in Prostate Brachytherapy | Porcine (ex vivo) | 18G | Prostate seeding needle (two part trocar) | 1.2, 12.7, 25.4 | 45 (5 samples * 3 velocities * 3 livers) | Automatic | Punture force<br>Cutting force | 0.53-0.72 (mean for different velocities)<br>0.36-0.46 (mean for different velocities) | Cutting force is determined by subtracting the withdrawal force (due to friction) from the total needle insertion force. |
| [37] | Hing et al. | 2007 | A biplanar fluoroscopic approach for the measurement, modeling and simulation of needle and soft-tissue interaction | Porcine (ex vivo) | 18G | Prostate seeding needle (two part trocar) | 1.2, 12.7, 25.4 | 45 (5 samples * 3 velocities * 3 livers) | Automatic | Punture force<br>Cutting force | 0.53-0.72 (mean for different velocities)<br>0.36-0.46 (mean for different velocities) | Cutting force is determined by subtracting the withdrawal force (due to friction) from the total needle insertion force. Also a force profile is shown of a needel insertion and withdrawal, including multiple puncures of liver structures. |
| [14] | Jiang et al. | 2014 | Experimental study of needle–tissue interaction forces: Effect of needle geometries, insertion methods and tissue characteristics. | Porcine (in vitro) | - | - | - | - | - | Stiffness force /puncture force of capsule | 0.1623 | Different needle geometries and insertion methods are also evaluated using PVA. Very little about porcine liver forces and needle/insertion characteristics are unclear for porcine experiments. |
| [38] | Bao et al. | 2016 | Experiment study on puncture force between MIS suture needle and soft tissue | Porcine (ex vivo)<br>Rabbit (ex vivo) | (see other info for details) | MIS Suture needles (see other info for details) | 1<br>0.17-1.7<br>1<br>1 | 10 repetitions per velocity<br>for other experiments unclear... | Automatic | Puncture force<br>Puncture force: diff. velocities<br>Puncture force: diff. angles (45-90°)<br>Puncture force | 0.20-0.28 (different needles)<br>0.05-0.40 (different needles)<br>0.10-0.26 (different needles)<br>0.028-0.033 (different needles) | Suture needles: Δ1/2 10x28, O1/2 10x28, Δ1/2 8x20 and O1/2 8x20. Δ and O are cross-section shape of needle (triangular and circular respectively). 8 and 10 refer do needles diameter. |
| [39] | Yang et al. | 2014 | Identification of tissue types and boundaries with a fiber optic force sensor | Porcine (ex vivo) | 16G | Bevel tip needle (with fiber optic force sensor) | - | only 1 example is shown | - | Puncture force | 0.5 | Only one example of a force plot is given. |
| [40] | Mahvash et al. | 2010 | Mechanics of Dynamic Needle Insertion into a Biological Material | Porcine (ex vivo) | 18G | Bevel needle | 1 | only 1 example is shown | Automatic | Puncture force | 0.6-1.6 (different punctures) | A force profile is shown of a singel insertion into a porcine liver. It is unclear what kind of tissue is punctured. |
| [41] | Okamura et al. | 2004 | Force modeling for needle insertion into soft tissue | Bovine (ex vivo) | 18G | bevel tip, surgical needle | 3<br>3 | 19 measurements into two livers.<br>5 insertions (1 liver) | Automatic | Puncture force (with capsule)<br>Cutting force<br>Friction | 2.30 (sd: 0.83)<br>0.94 (sd: 0.36)<br>Different friction coefficients | Drop in force mentioned after puncture (0.66 N). Non-linear stiffness equation determined (at 3 mm/s). Friction force parameters determined (at sinusoidal motion, 20 mm/s). Effects of needle diameter and tip type also investigated, but on phantoms. |
| [42] | Simone et al. | 2002 | Modeling of needle insertion forces for robot-assisted percutaneous therapy. | Bovine (ex vivo) | 18G | bevel tip, surgical needle | 3<br>3 | 19 measurements<br>5 insertions | Automatic | Puncture force (with capsule)<br>Cutting force<br>Friction | 2.30 (sd: 0.83)<br>0.94 (sd: 0.36)<br>Different friction coefficients | Drop in force mentioned after puncture (0.66 N). Non-linear stiffness equation determined (at 3 mm/s). Friction force parameters determined (at sinusoidal motion). |
| [43] | Simone | 2002 | Modeling of needle insertion forces for percutaneous therapies | Bovine (ex vivo) | - | bevel tip and diamond tip<br>blunt needle | 4<br>2.5 | 21 for liver one and 14 for liver two. More livers used...?<br>7 | Automatic | Stiffness/puncture (with capsule)<br>Internal stiffness/Cutting (no capsule)<br>Friction | 0.5-2.4 (different needles)<br>0.09 (maximum is 0.24)<br>Different friction coefficients | Stiffness and friction/damping were also measured under fluoroscopic imaging so that the deformation of the tissue can be observed. |

| Article | | | | Tissue | Needle geometry | | Insertion methods | | | Needle forces | | Other info |
|---|---|---|---|---|---|---|---|---|---|---|---|---|
| Ref. | Authors | Year | Title | Liver type | Diameter [mm] or [G] | Type | Velocity [mm/s] | Samples [#] | Manual/ automatic | Type of force | Force [N] | |
| [44] | Sahlabadi et al. | 2017 | Novel Design of Honeybee-inspired Needles for Percutaneous Procedure | Bovine (ex vivo) | 2 mm<br>3 mm | barbed and conventional bevel needles | 1.5 | only 4 examples are shown | Automatic | Insertion force | 0-2 (in force profile)<br>0-4 (in force profile) | The results show a 46% decrease of insertion force when using barbed needles compared to conventional needles. |
| [45] | Vidal et al. | 2008 | Simulation of ultrasound guided needle puncture using patient specific data with3D textures and volume haptics | Bovine (in vitro) | - | Chiba needle | 8.3 | only one plot with a mean, min and max. | Automatic | Puncture force | 2 (range: 1.5-3.5) | In the force-displacement diagram, a linear slope is shown that is most likely due to friction and cutting force. |
| [46] | Gokgol et al. | 2012 | Estimation of fracture toughness of liver tissue: Experiments and validation | Bovine (ex vivo) | 2, 3, 4, 5 mm | Custom made needles | 3 | 4 per needle | Automatic | Penetration peak forces | 2.5-4 (different needles) | The 5 mm diameter needle doesn't show a clear peak |
| [16] | Healey et al. | 2005 | In vivo force during arterial interventional radiology needle puncture procedures. | Bovine (ex vivo) | 15G, 17G, 19G<br>18G | coaxial biopsy trocar needle<br>biopsy needle, spinal needle and Kimal needle | 8.33<br>8.33 | - | Automatic | Insertion force<br>Insertion force | 0-3.5<br>0-3 | The results show two force-displacement profiles using different needle types and different needle diameters. It is unclear what kind of tissue is punctured. |

# Appendix C: Needle insertion experiment results

*Peak forces per liver*

In Figure 50 the results of the needle insertion experiments are shown per liver. The number behind the blood vessel or tissue type indicates the number of the liver. In total three different livers were used for the experiments.

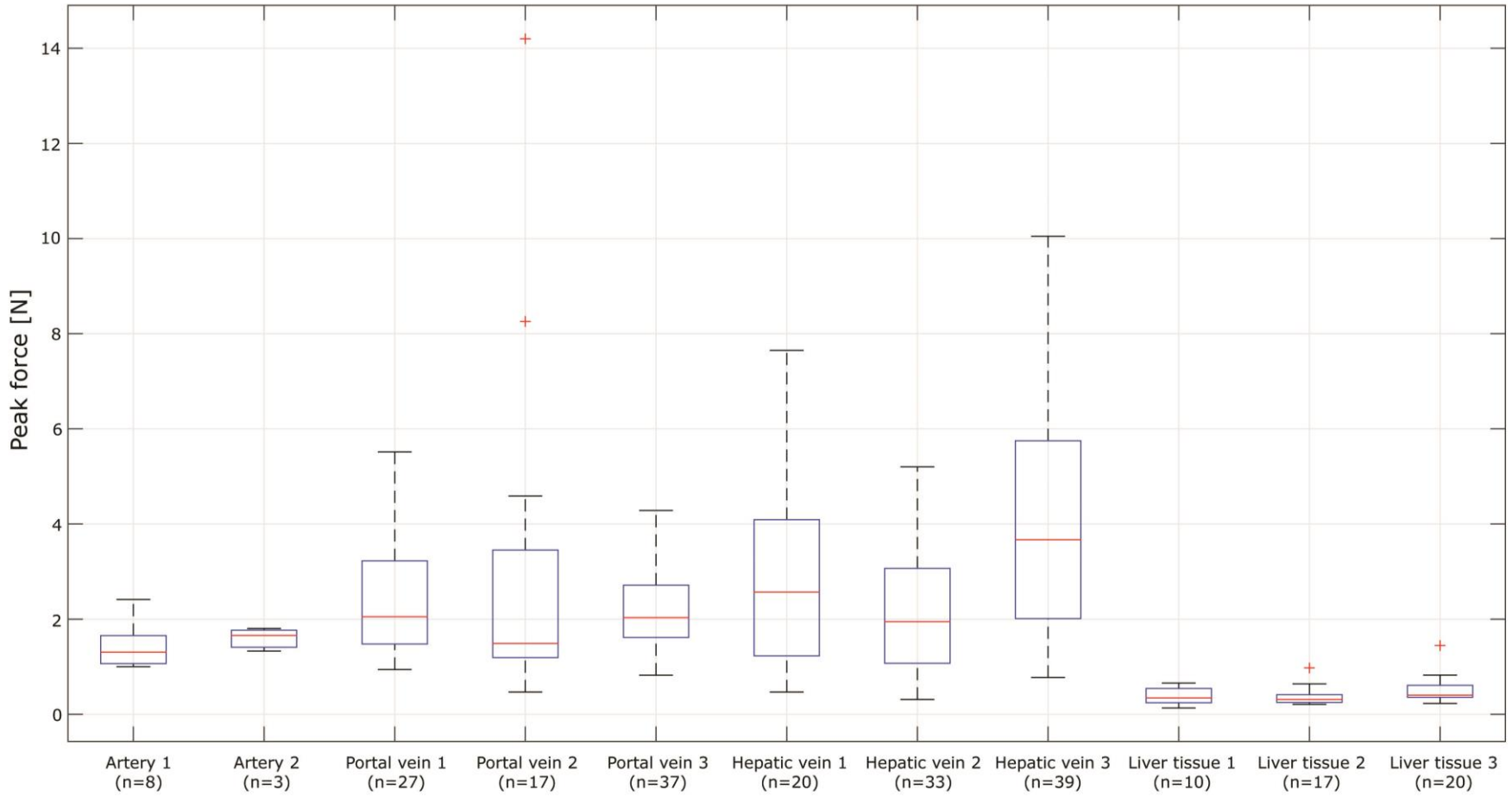


**Figure 50 Boxplot of the peak forces per liver and per blood vessel type or tissue.**

## *Peak forces in relation to the blood vessel location – Liver 1*

In Figure 53 we see the approximate locations of the vein samples that were retrieved from liver 1. In Figure 51 we see a boxplot of the peak forces for the hepatic vein samples and in Figure 52 a boxplot of the peak forces of the portal vein samples. When looking at the results of both the hepatic vein and portal vein, in general, the proximal samples result in slightly higher forces than the distal samples. However, it is definitely not the case that all proximal measurements resulted in higher forces than distal measurements.

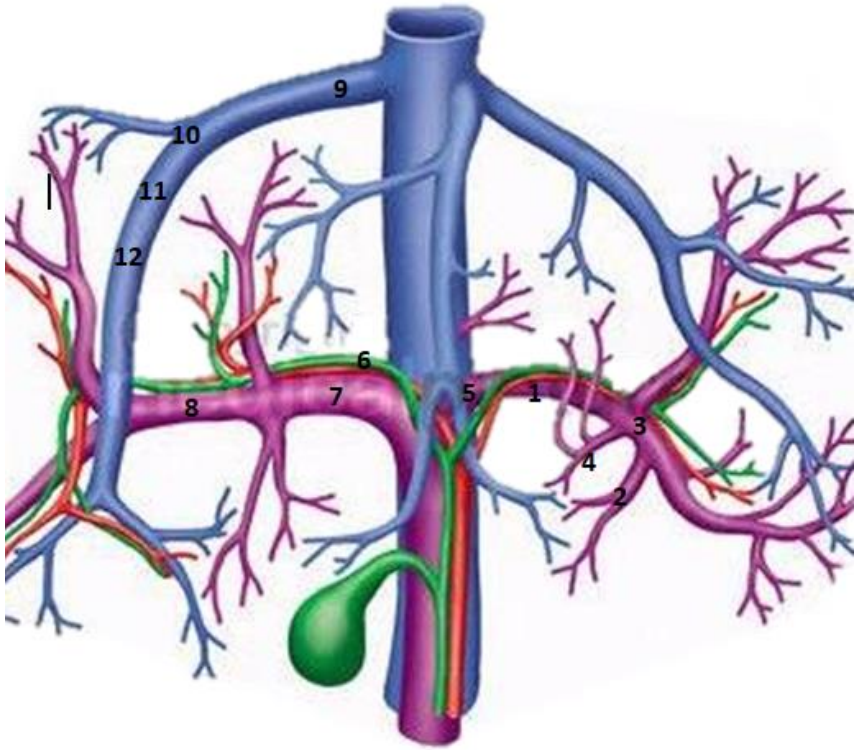


**Figure 53 Locations of the vein samples retrieved from liver 1.**

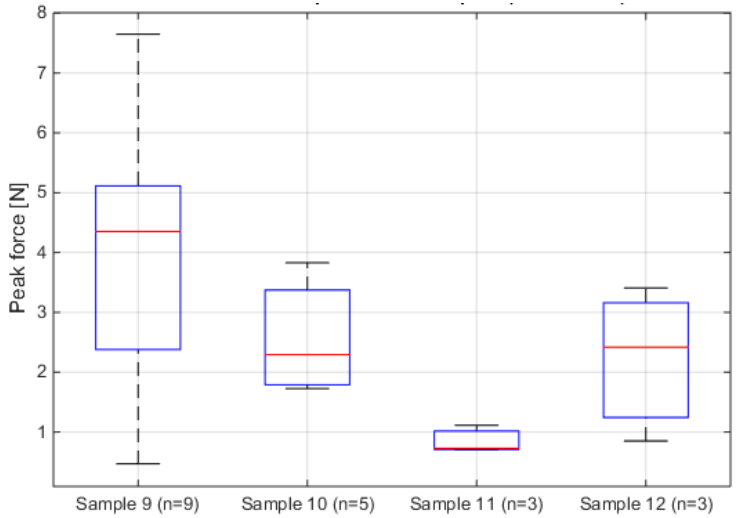


**Figure 51 Boxplot of the peak forces of the hepatic vein samples of liver 1**

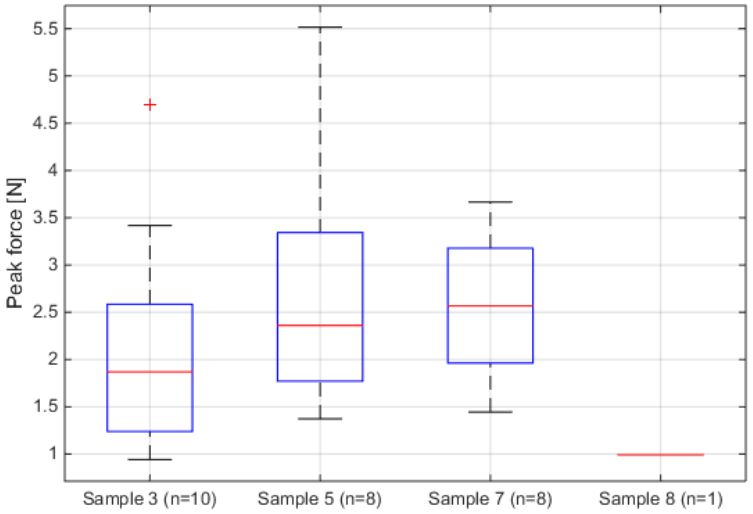


**Figure 52 Boxplot of the peak forces of the portal vein samples of liver 1.**

### *Peak forces in relation to the blood vessel location – liver 2*

Figure 56 we see the approximate locations of the vein samples that were retrieved from liver 2. In Figure 54 we see a boxplot of the peak forces for the hepatic vein samples and in Figure 55 a boxplot of the peak forces of the portal vein samples. When looking at the results the hepatic vein, it is difficult to compare the samples because different braches were used. The results of the portal vein show that sample 9, which was more distal, resulted in the highest forces. This might be due to the fact that multiple braches came together here and might have been punctured at the same time.

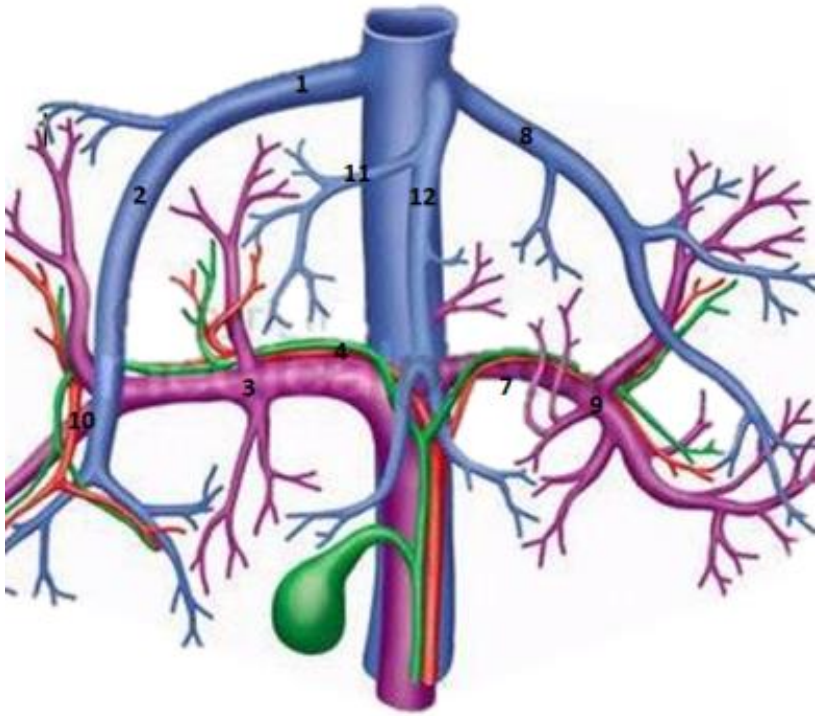


**Figure 56 Locations of the vein samples retrieved from liver 2.**

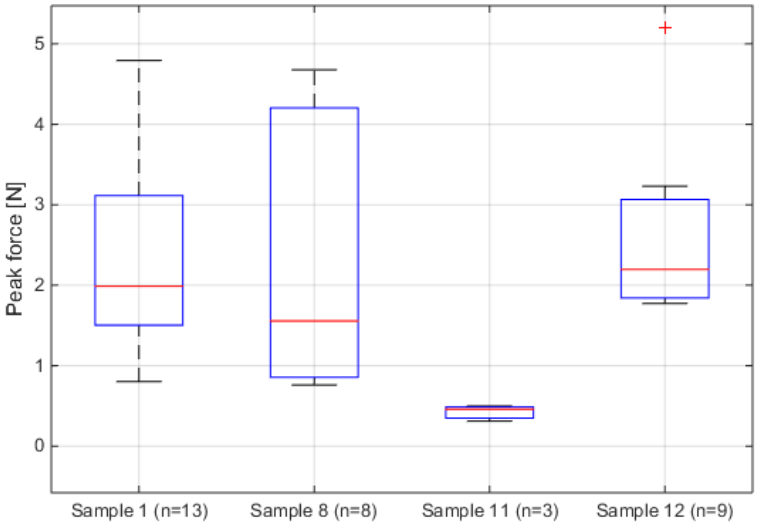


**Figure 54 Boxplot of the peak forces of the hepatic vein samples of liver 2.**

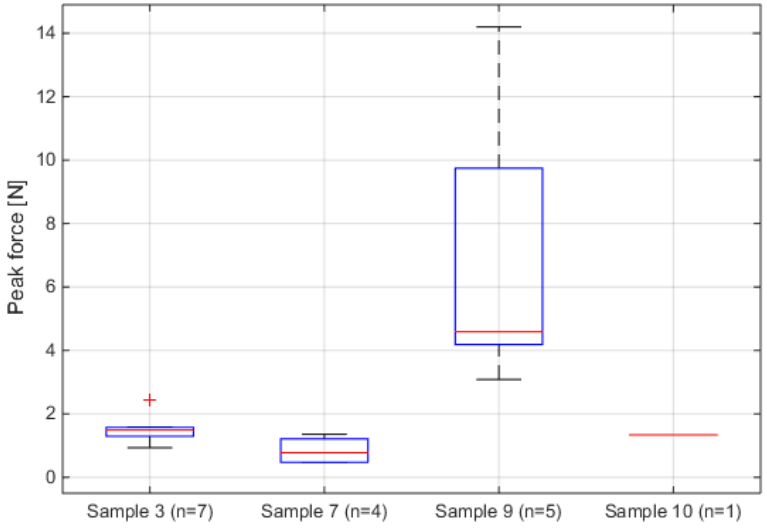


**Figure 55 Boxplot of the peak forces of the portal vein samples of liver 2.**

### *Peak forces in relation to the blood vessel location – liver 3*

Figure 59 we see the approximate locations of the vein samples that were retrieved from liver 3. In Figure 57 we see a boxplot of the peak forces for the hepatic vein samples and in Figure 58 a boxplot of the peak forces of the portal vein samples. When looking at the results of the hepatic vein, sample 3 (proximal) resulted in higher forces than sample 4 (distal) The other samples are difficult to compare, because different branches were used. The results of the right portal vein (in the figure on the left) show slightly higher forces for proximal samples. However, for the left portal vein (in the figure on the right) it is the other way around.

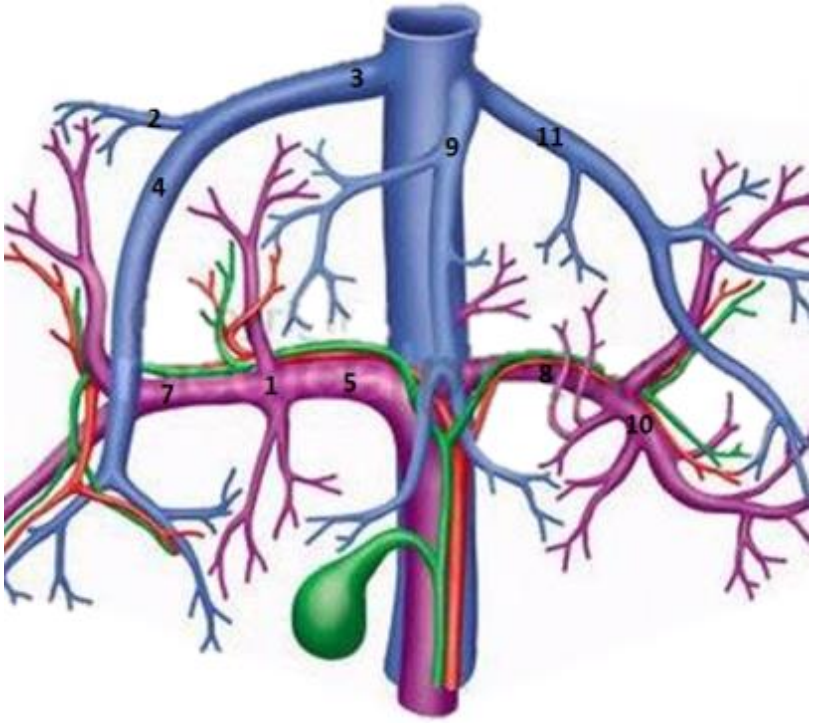


**Figure 59 Locations of the vein samples retrieved from liver 3.**

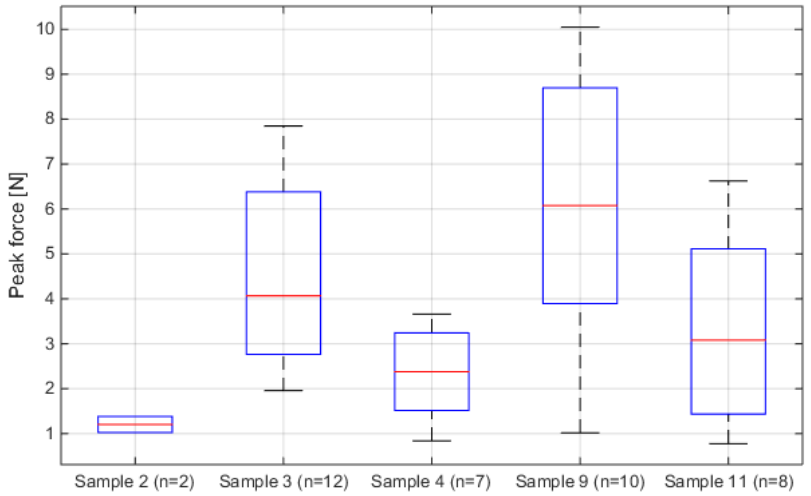


**Figure 57 Boxplot of the peak forces of the hepatic vein samples of liver 3.**

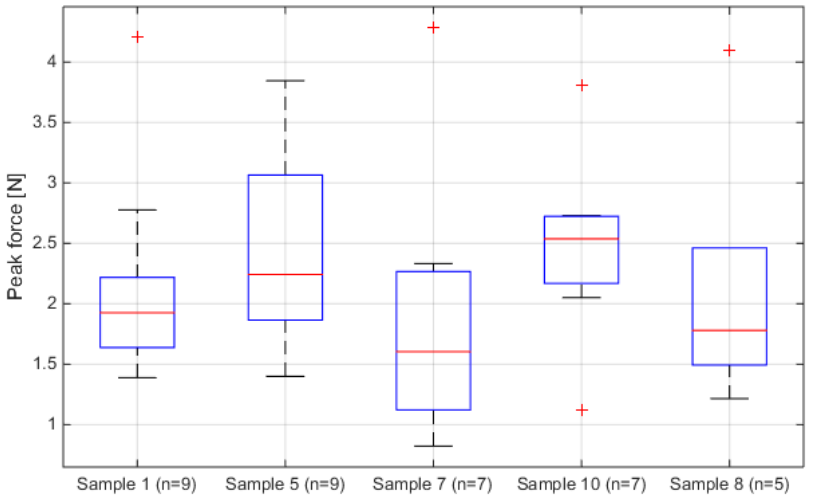


**Figure 58 Boxplot of the peak forces of the portal vein samples of liver 3.**

# Appendix D: Needle insertion experiments with blood vessel mimicking materials.

In this appendix, some extra information and data are presented on the experiments with blood vessel mimicking materials. The main results of the experiments can be found in Section 4.2.

## *PVA*

For the needle insertion experiments using blood vessel mimicking materials, PVA (7m%) was used with different freeze-thaw cycles. The results of the peak forces are already shown in Section 4.2 of the thesis. After 8 freeze-thaw cycles the PVA had shrunk as can be seen in Figure 61. Mesh was also added to the PVA to check whether this would result in the desired puncture forces. The mesh was absorbed in the PVA when the PVA was poured over the mesh. It furthermore deformed inside the PVA. When the mesh was placed on top of the PVA it would remain in place and it could be used for measurements. In Figure 60, the results are shown when puncturing a needle through the 15 mm thick PVA sample with the mesh fabric on the bottom. The resulting peak forces are too low. The mesh inside the other PVA sample was also punctured and these forces were in the range we were looking for. However, the shape and position of the mesh fabric cannot be controlled when the mesh is inside the PVA. Therefore, using the mesh as a blood vessel wall inside the PVA liver tissue does not seem like a viable method.

**Figure 61 Shrinking of a PVA (7m%) sample after 8 freeze-thaw cycles (8 hours freezing and 8 hours thawing).**

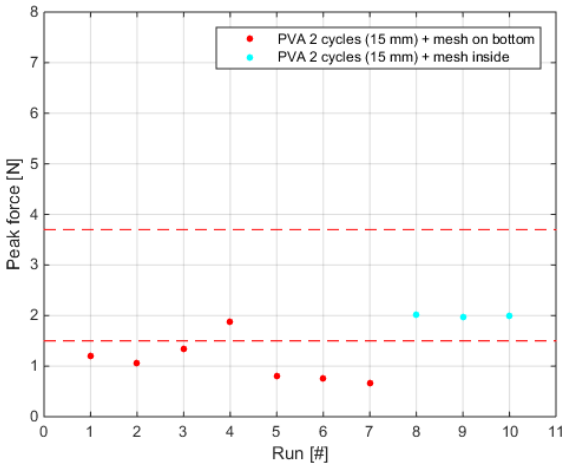


**Figure 60 (Left) sample consisting of 15 mm thick PVA (7m%, 2 freeze-thaw cycles) with mesh fabric on top. (Right) results of the peak forces during needle insertions into 15 mm thick PVA with mesh fabric.**

## *Silicone and other materials*

During one of the first experiments, different materials were used to measure puncture forces. This was done to get an indication of the materials that could be used. The results of that experiment are shown in Figure 62. The silicone that was used during this experiment, was Dragon Skin 20 (Figure 25). Samples with different thicknesses were made. The peak forces were too low when using this type of silicone. Therefore other silicones were examined for their suitability.

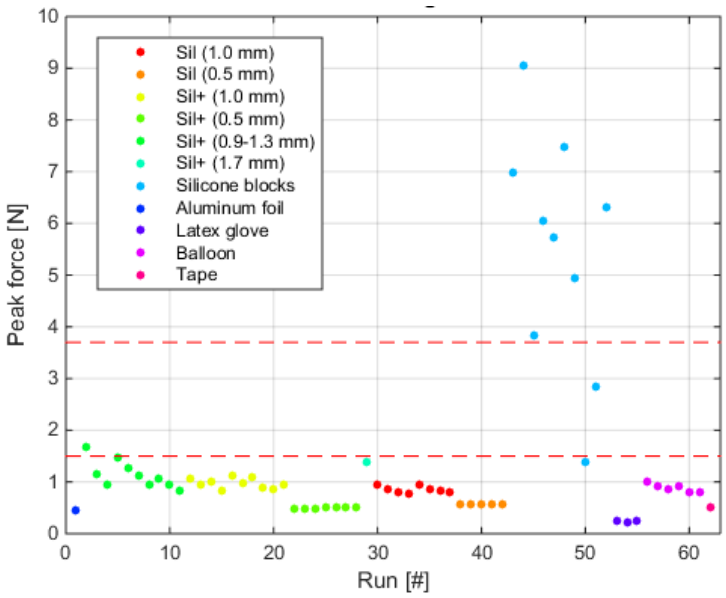


**Figure 62 Peak forces during the first test using different materials. Sil indicates Dragon Skin 20 silicone and Sil+ indicates Dragon Skin 20 silicone with the addition of Thi-Vex.**

Different silicone sample blocks from producer Smooth-On (Smooth-On Inc., Macungie, PA, USA), shown in Figure 63, were used to check whether an increasing shore hardness increases the puncture force. These sample blocks were punctured and the peak forces were examined. The results, shown in Figure 63, showed that a higher shore hardness generally results in a higher peak force. It needs to be mentioned that not all silicone blocks had the same thickness. The Smooth-Sil 950 silicone resulted in the highest peak force and was selected for further experiments.


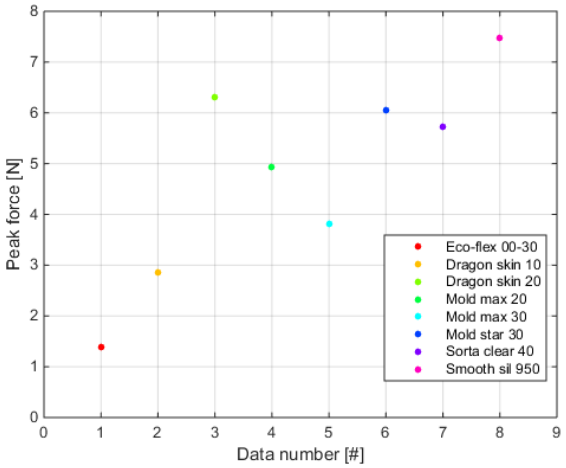


**Figure 63 (Left) Blocks of silicone types by Smooth-On. (Right) peak forces during puncturing of the different blocks.**

### *Thi-Vex*

In Figure 64 we can see that the addition of Thi-Vex does not clearly influence the peak forces for the Dragon Skin 20 silicone (left figure) and the Smooth-Sil 950 silicone (right figure).

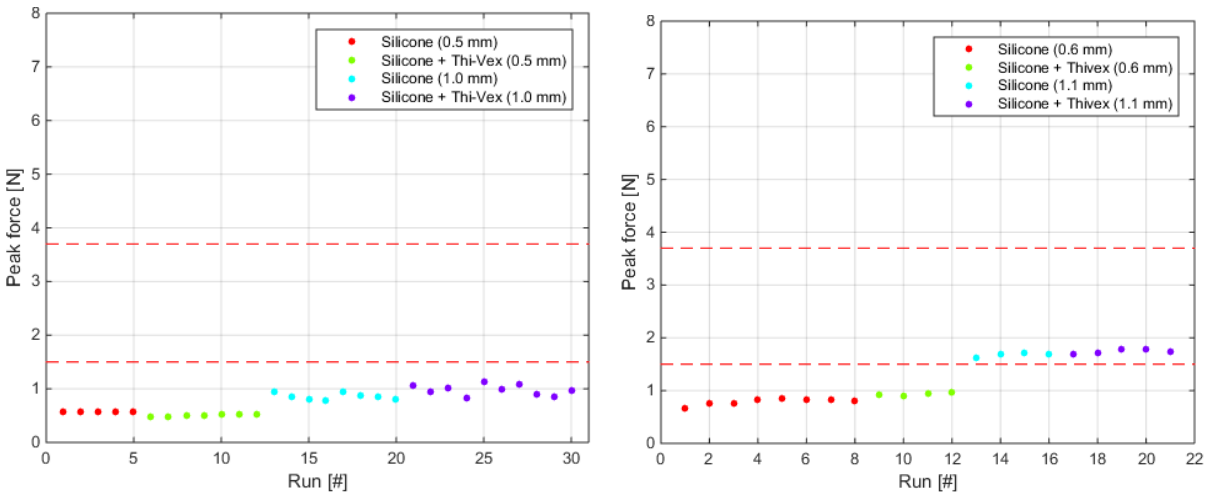


**Figure 64 Influence of Thi-Vex on the peak forces for the Dragon Skin 20 silicone (left) and the Smooth-Sil 950 silicone (right).**

### *Mesh fabric orientation*

When the mesh fabric is added to the silicone, the silicone can be punctured both with the mesh fabric on the top and on the bottom. The orientation was examined both with and without glue. The results are shown in Figure 65. For the samples without glue, it seems that the orientation does not influence the peak force during insertion into the 0.6 mm samples. For the 1.1 mm samples however, it seems that the peak forces are slightly higher when the mesh fabric was positioned at the bottom of the silicone. For the samples with glue, the orientation of the mesh fabric doesn't seem to affect the peak forces. However, it needs to be considered that only little measurements were done.

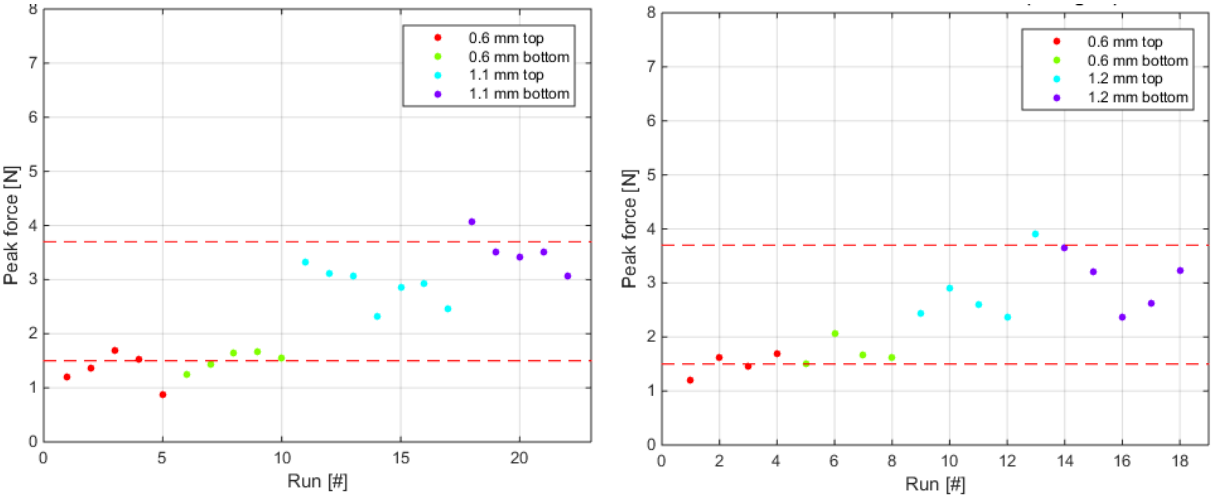


**Figure 65 Peak forces during puncturing of Smooth-Sil 950 silicone samples with different thicknesses and with addition of mesh fabric. The effect of the orientation of the mesh on the peak force was examined, both without glue (left) and with glue (right).**

# Appendix E: Modelling liver blood vessels

## *Creating 3D-models*

A 3D-model of the liver blood vessels and the liver itself was made using a CT-scan of the abdomen and 3D Slicer 4.8.1. Figure 67 shows the CT-scan with the blood vessels of the liver. In Figure 66, the results of the segmentation process of the portal vein, hepatic vein and liver tissue are shown.

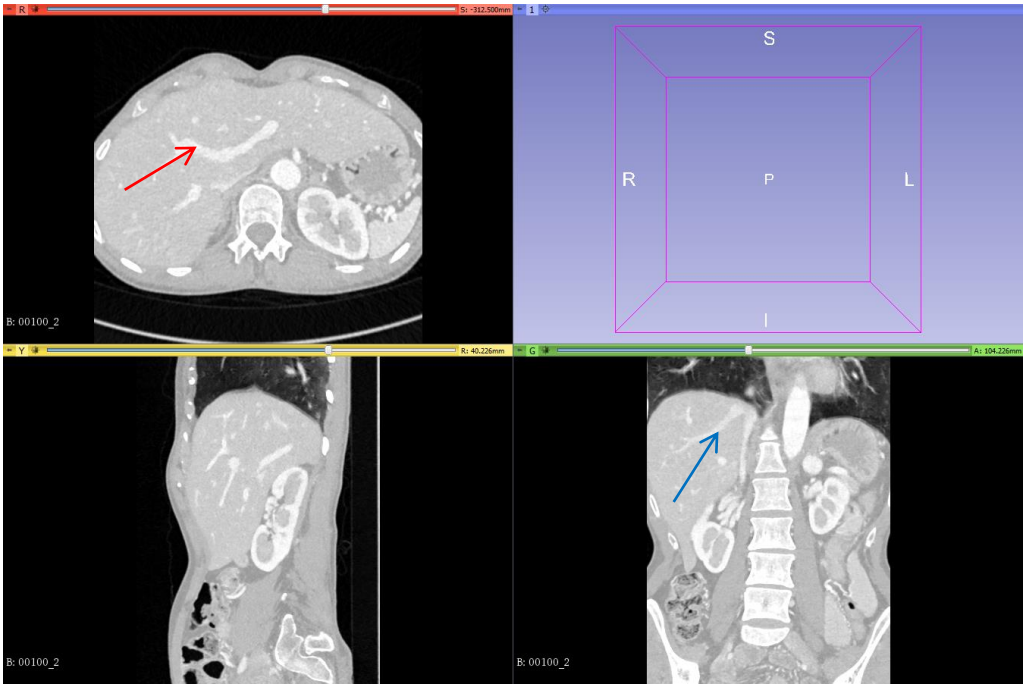


**Figure 67 CT scan of the human abdomen in 3D-slicer 4.8.1, showing the portal vein (red arrow) and hepatic vein (blue arrow).**

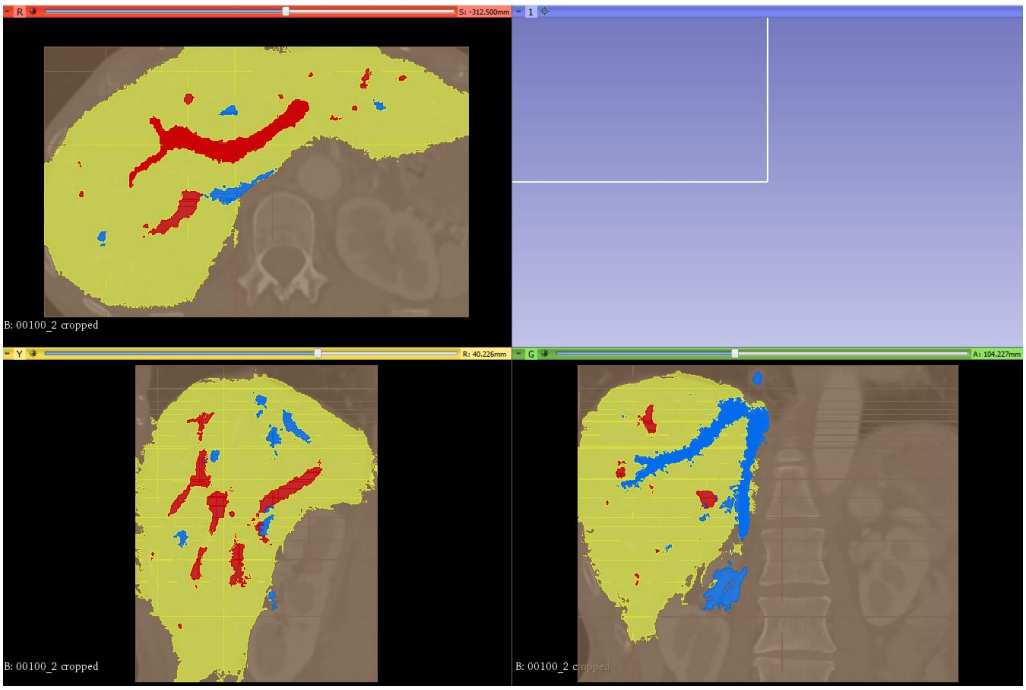


**Figure 66 Marking the liver tissue (yellow), the portal vein (red) and the hepatic vein (blue) using a CT-scan of the abdomen in 3D-Slicer 4.8.1.**

## *Results of the 3D-models*

The results of the 3D-models of the portal vein and hepatic vein are shown in Figure 68. The left hepatic vein is partially missing. Furthermore, the dimensions of the portal vein model are roughly shown as an indication of the portal vein size.

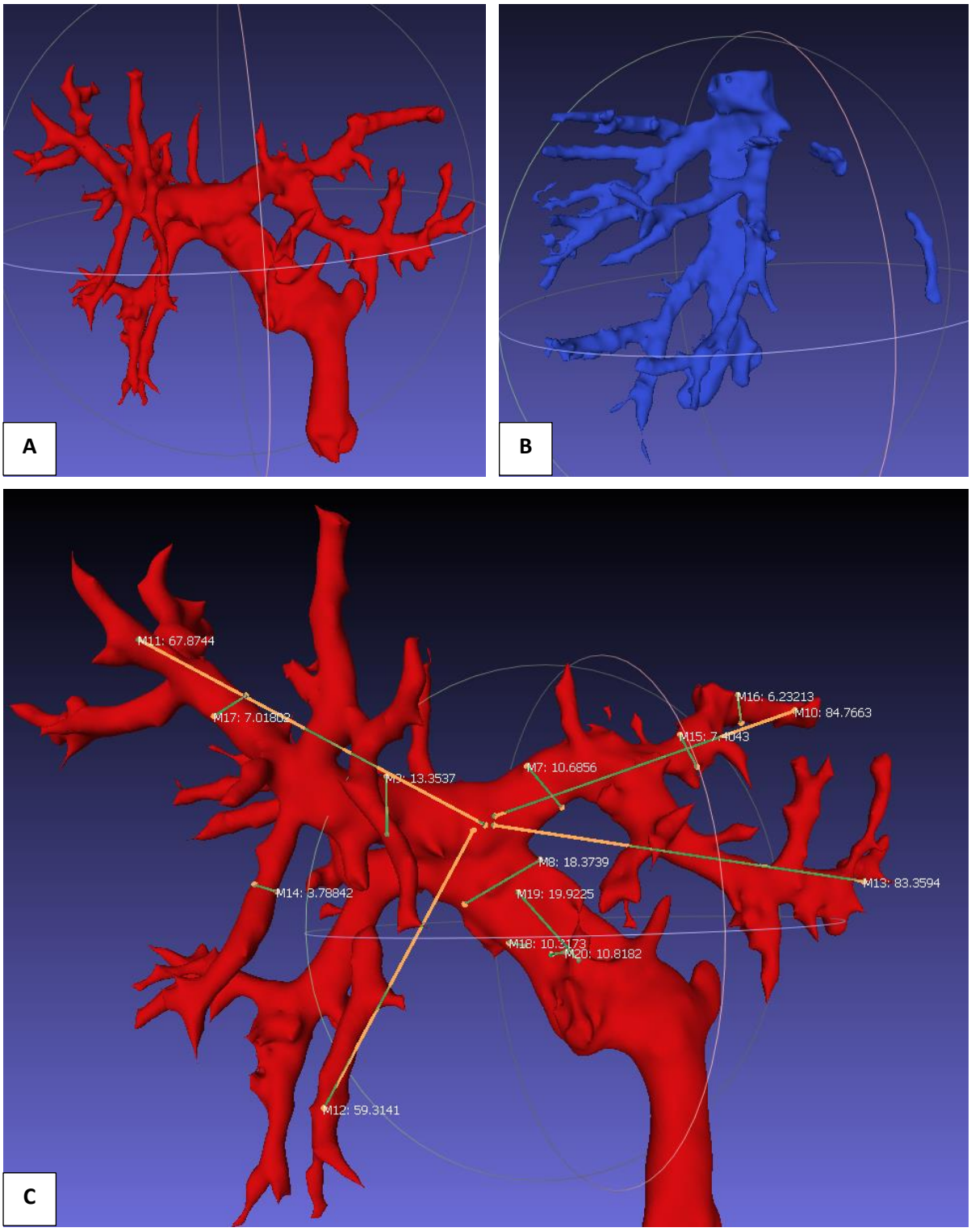


**Figure 68 (A) Anterior view of the 3D-model of the portal vein. (B) Anterior view of the 3D-model of the hepatic vein. (C) Dimensions of the portal vein model in mm.**

### *Simplification of the portal vein model*

The 3D-model of the portal vein was simplified using Meshlab, before it was 3D-printed. First all small side branches were deleted (Figure 69A). Then the model surface was restructured ('Screened Poisson Surface Reconstruction' function) and smoothened ('Smooths normal on a point sets' function). The result is shown in Figure 69B. The portal vein model was even more simplified by deleting more side branches. The result of that model is shown in Figure 69C.

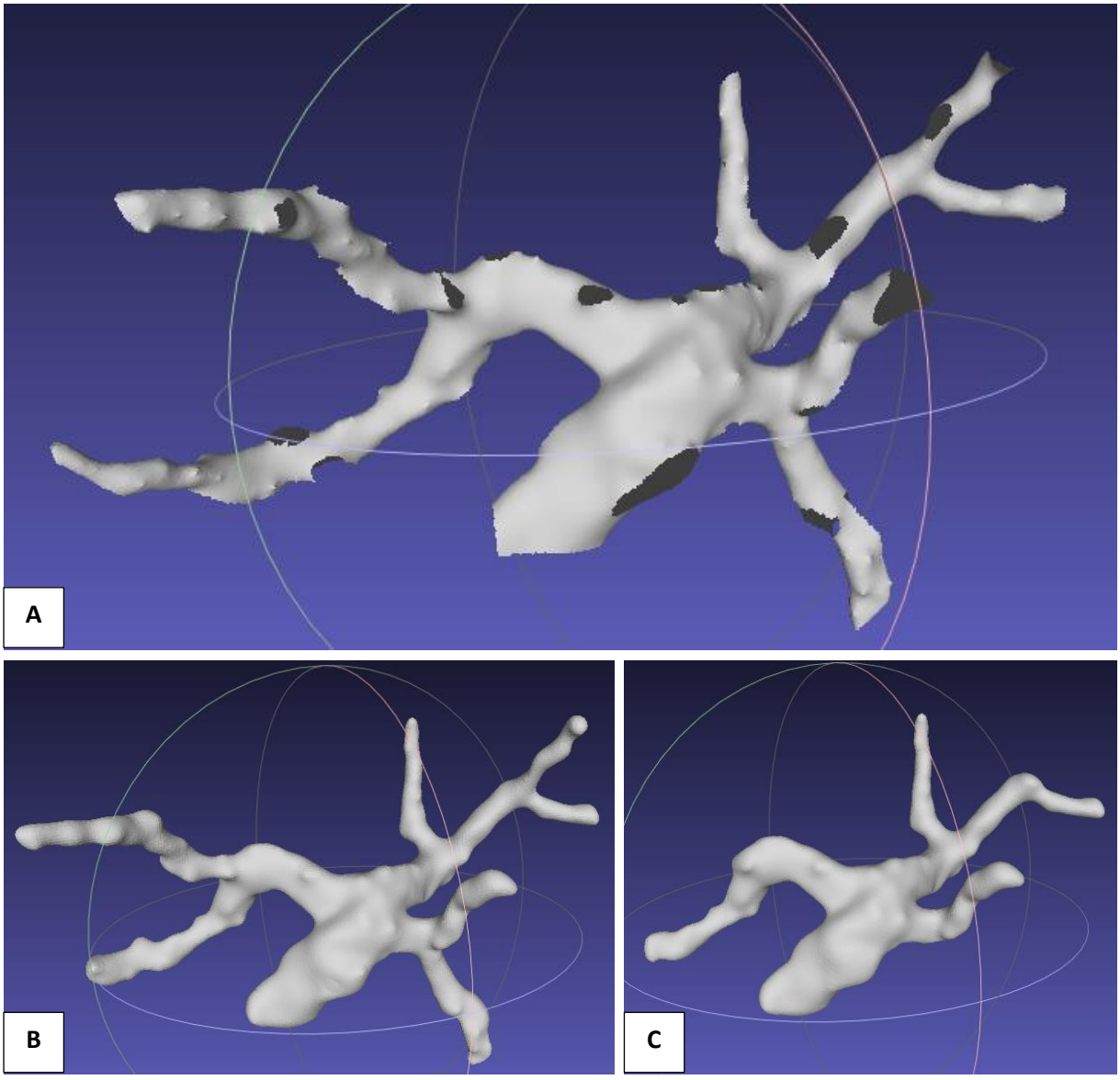


**Figure 69 (A) The small side branches of the portal vein model were deleted in MeshLab. (B) Structure of the portal vein after simplification. (C) Structure of the portal vein that is even more simplified.**

# Appendix F: 3D-printing blood vessel structure

Both simplified portal vein models were 3D-printed using a Ultimaker 3 and Cura 3.4.1 (Ultimaker Inc., Geldermalsen, The Netherlands). Figure 70 shows the most simplified portal vein model in Cura, with and without the support structure visualized.

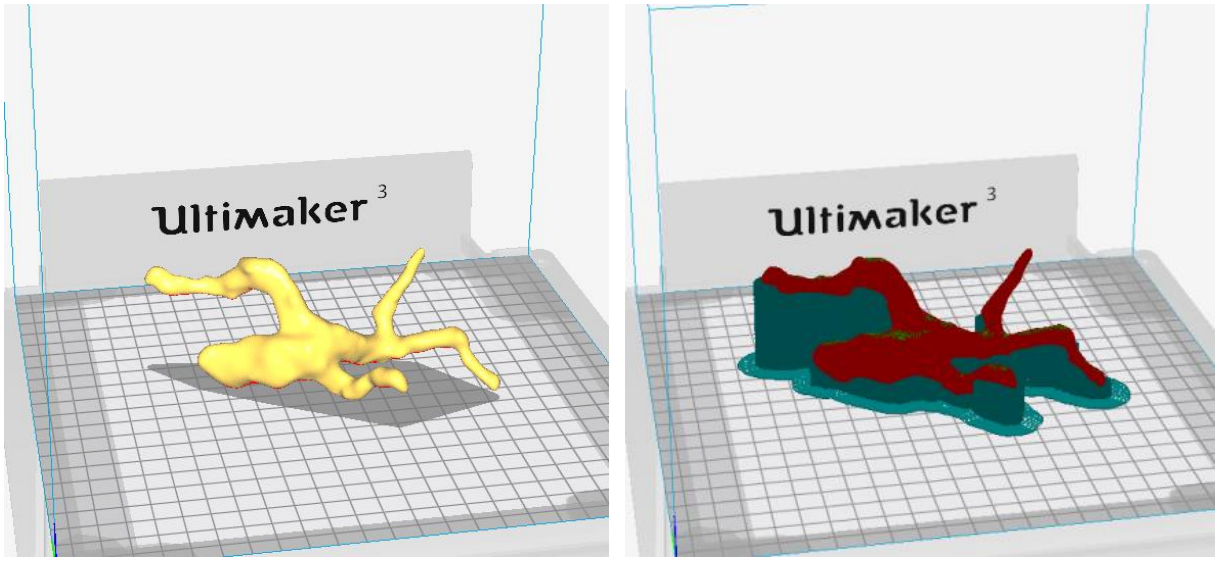


**Figure 70 Simplified model of the portal vein in Cura (left). The right figure shows the portal vein model (red) and the support structure (blue).**

The results of the 3D-printing of both portal vein models are shown in Figure 71. More details of the 3D-printed vein structures are shown in Figure 72. The support structure is made of the same material as the vein model (water-soluble PVA). Therefore it is hard to remove the support structure from the vessel model, without damaging the model.

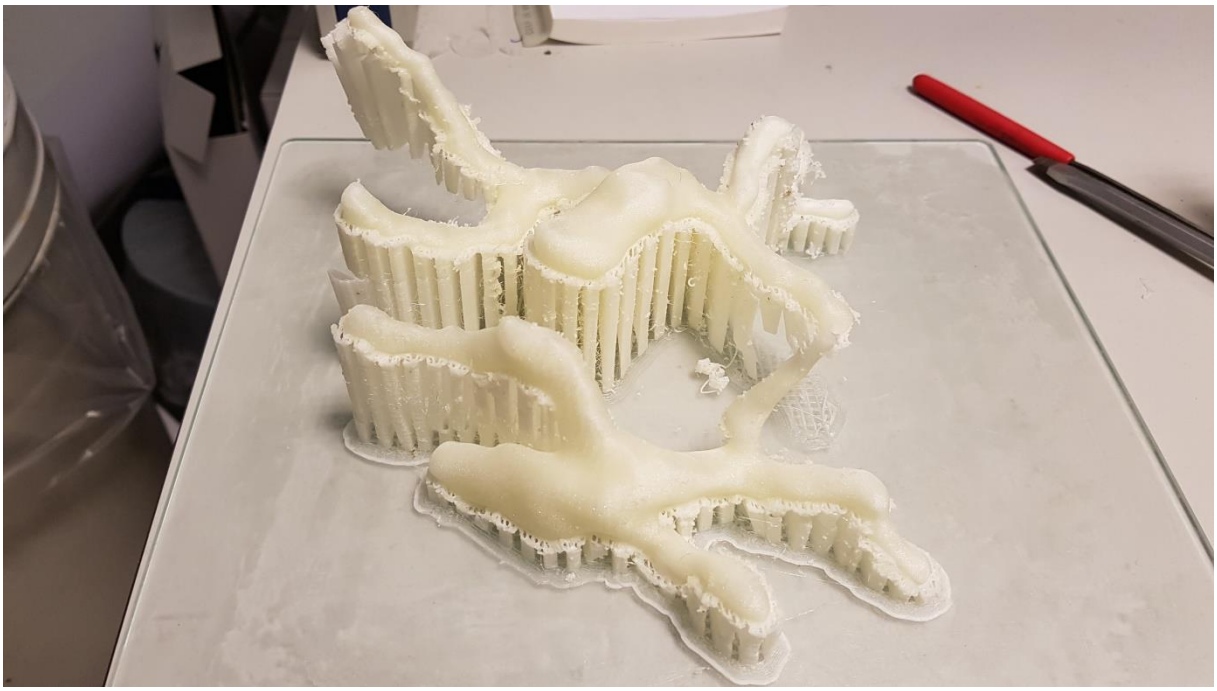

**Figure 71 Results of the 3D-printed portal vein models including the support structure on the bottom.**

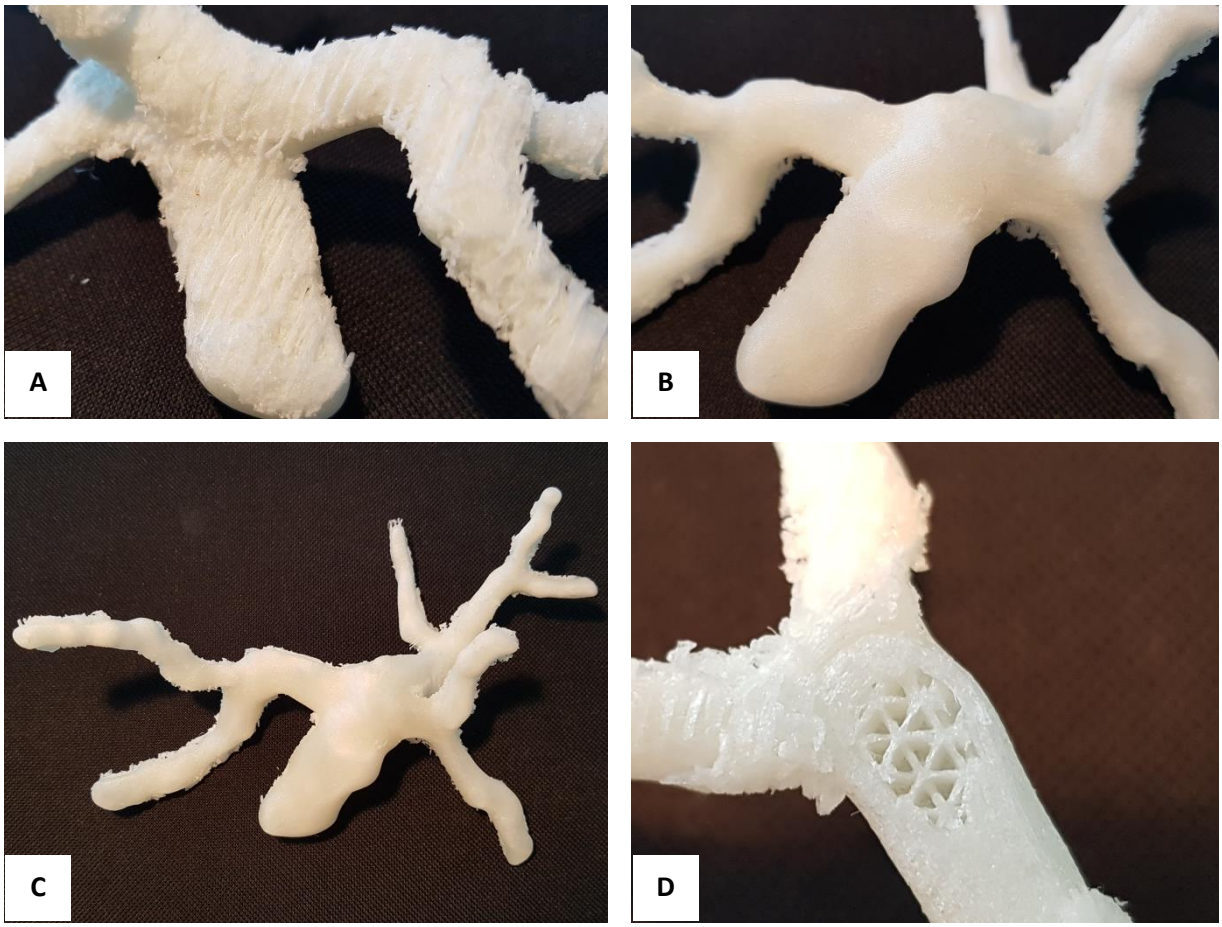


**Figure 72 Details of the 3D-printed portal vein models. (A) Remainders of the support structure that are attached on the bottom of the vein model. (B) The surface on the top of the vein model. (C) The less simplified model of the portal vein, showing remainders of the support structure. (D) Part of the triangular structure inside the vein model.**

# Appendix G: Silicone and PVA connection

Experiments were done to check whether silicone and PVA bond by adding a mesh fabric to the silicone. The mesh is applied both with and without Sil-Poxy glue. The samples are shown in Figure 73. Without the addition of glue, we can see that the mesh fabric is partially absorbed into the silicone (Figure 73A).

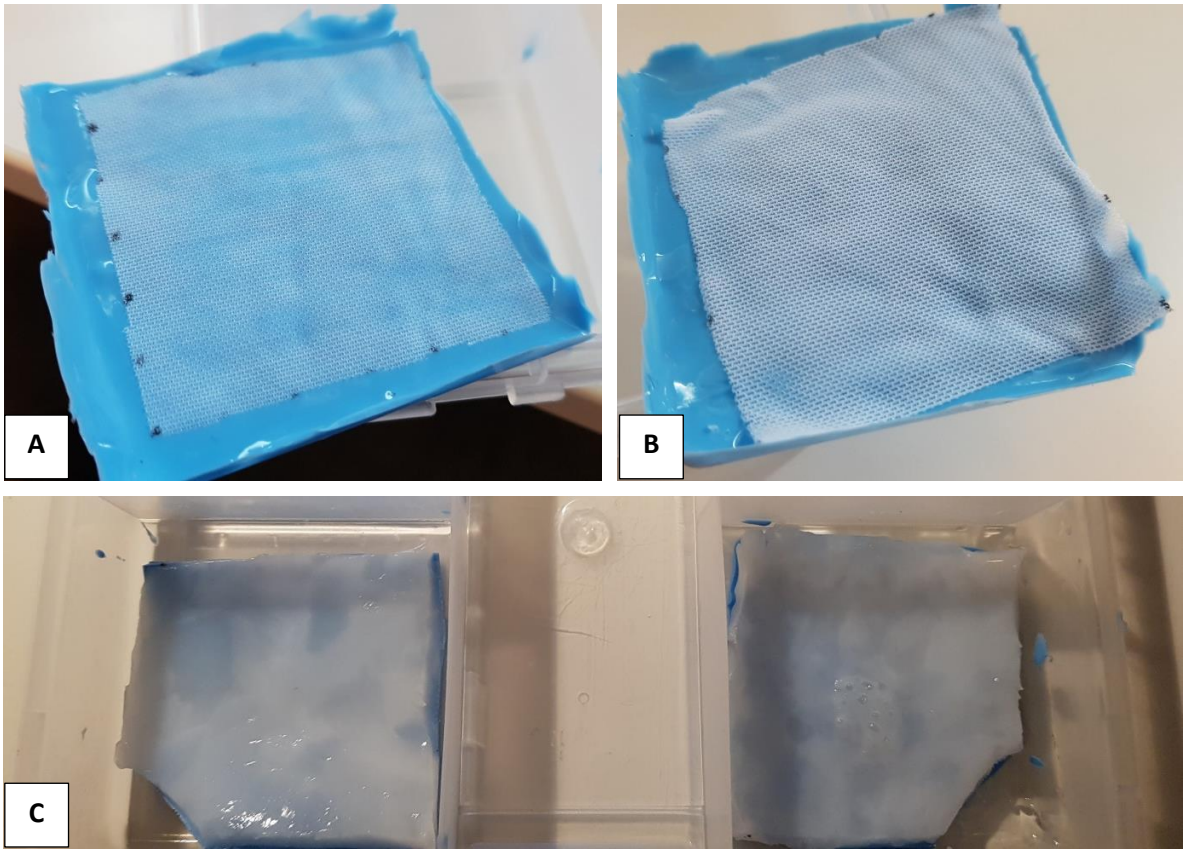


**Figure 73 (A) Sample of silicone layer with mesh fabric added during hardening of the silicone. (B) Sample of silicone layer with mesh fabric glued onto the silicone. (C) Samples of PVA, silicone and mesh fabric to test bonding.**

A sample was made using silicone tubes with layer of mesh fabric, as well. The tubes were then embedded in PVA to test the bonding. Figure 74 shows the sample, just after the liquid PVA was poured around the silicone tubes. The silicone tubes need to be held in place when the PVA is liquid.

**Figure 74 Silicone tubes embedded in liquid PVA, just after it was poured into the container.**

# Appendix H: Force profile experiment (human liver and phantom)

## *Human liver samples*

A human liver sample consisted of a 15 mm layer of liver tissue with a liver vein attached. Figure 75 shows the process of a measurement using a human liver sample. The liver vein is first located and cut open, then carved out of the liver and finally placed in the experimental setup.

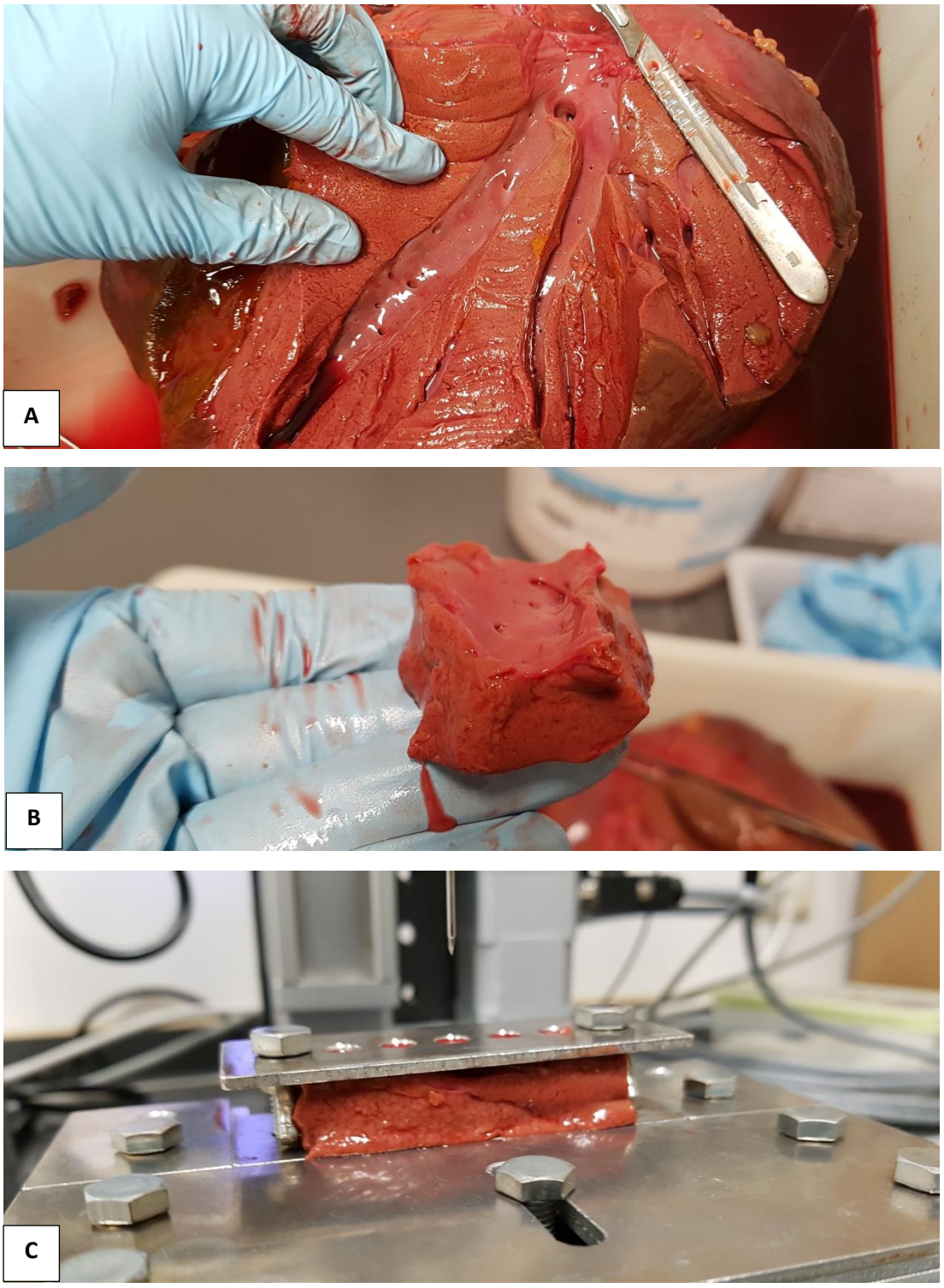


**Figure 75 (A) Locating the liver vein by cutting it open. (B) Retrieval of a sample containing a liver vein and 15 mm liver tissue. (C) Experimental setup for a measurement using a human liver sample.**

### *Phantom samples*

The phantom samples consisted of a 15 mm layer of PVA (4m% and 2 freeze-thaw cycles) and a silicone layer with mesh fabric. Figure 76 shows examples of the samples and a measurement.

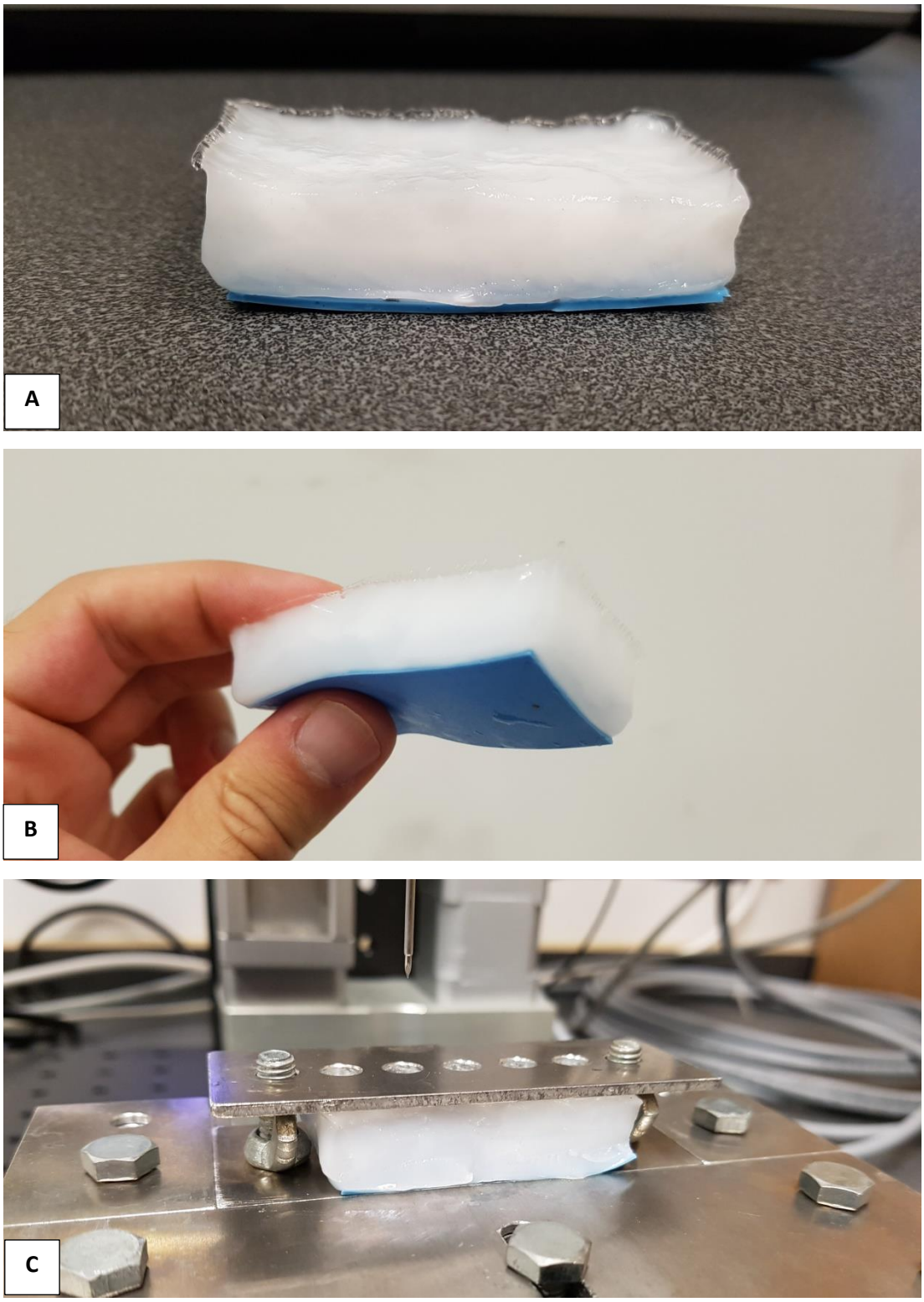


**Figure 76 (A,B) Examples of the phantom samples. (C) Experimental setup for a measurement using a phantom sample.**

### *Force profiles of phantom samples with and without glue*

It was examined if the addition of Sil-Poxy glue influences the force profile during a needle insertion in a phantom sample consisting of a 15 mm layer of PVA and silicone with mesh fabric. The results of the 1.1 mm silicone layer samples are shown in Figure 77 and the 0.6 mm silicone layer samples in Figure 78. The results show that the addition of glue does not clearly influence the force profiles. The layer of PVA was slightly larger for the glued samples. Therefore the force starts to rise sooner for the samples containing glue. At the 0.6 mm silicone samples there is one outlier in the peak forces. It is unclear what caused this outlier. It might be due to the fact that the needle was inserted exactly at a string of the mesh fabric.

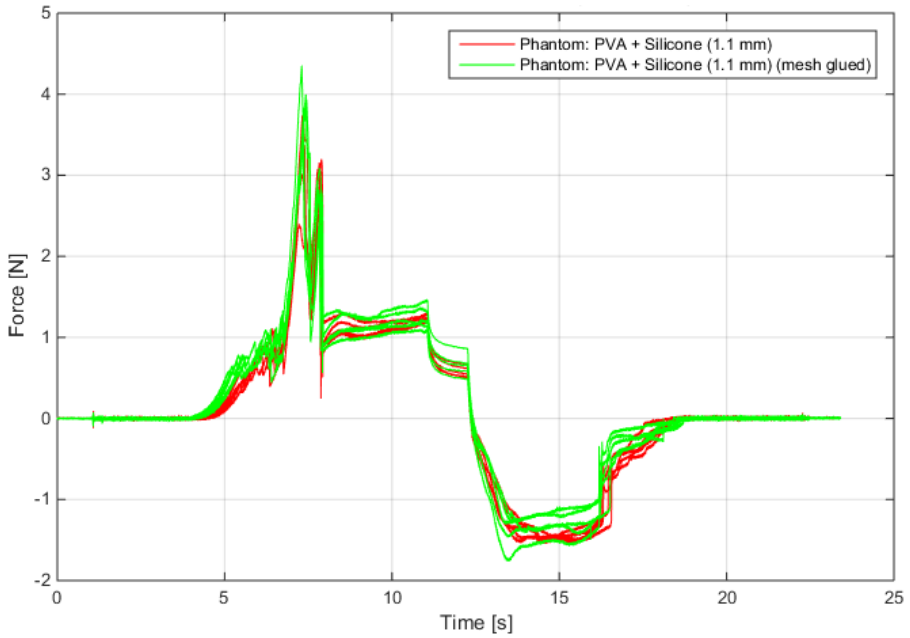


**Figure 77 Force profiles of phantom samples, consisting of PVA and a 1.1 mm silicone layer with mesh fabric, both with and without glue.**

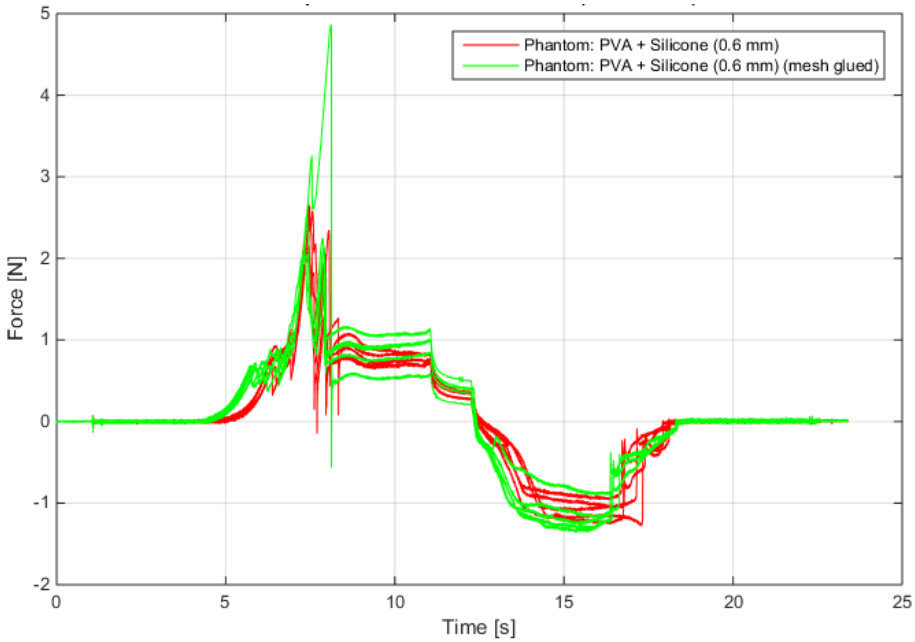


**Figure 78 Force profiles of phantom samples, consisting of PVA and a 0.6 mm silicone layer with mesh fabric, both with and without glue.**

### *Force profile with and without mesh fabric*

During the experiment it was checked whether the mesh fabric is the reason for the double force peak during the insertion of the needle. In Figure 79 a measurement is shown using both silicone with and without mesh fabric. The results indicate that the double peak can also occur when the mesh fabric is not applied to the silicone. Thus, it is not really clear what causes the double peak.

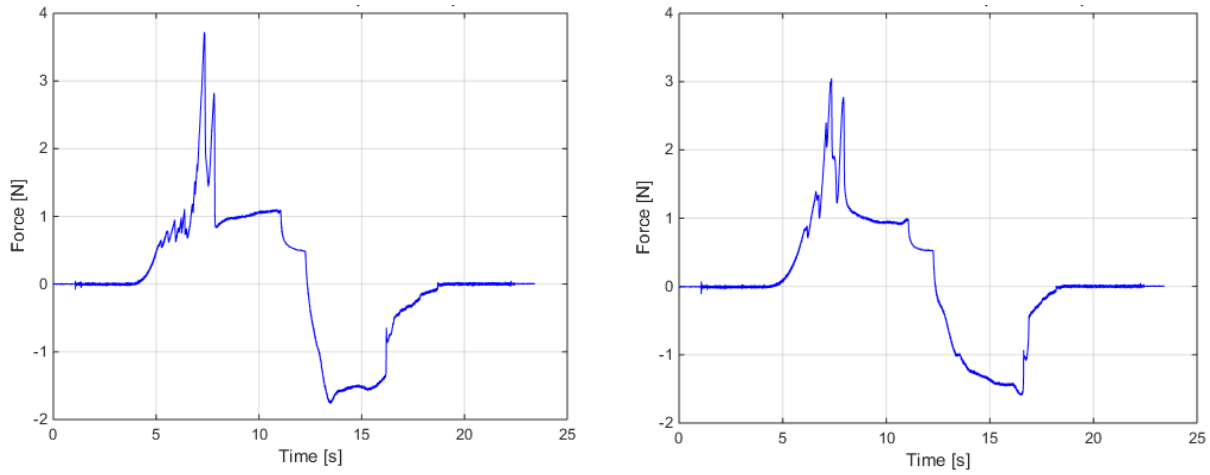


**Figure 79 Examples of force profiles of needle insertions in silicone, both with mesh fabric (left) and without mesh fabric (right).**

# References


1. De Jong, T.L., et al., *PVA matches human liver in needle-tissue interaction.* Journal of the mechanical behavior of biomedical materials, 2017. **69**: p. 223-228.
2. De Jong, T.L., et al., *Design of a PVA liver phantom with respiratory motion for simulation of needle interventions*, in *CARS*. 2018: Berlin, Germany. p. (extended abstract in: Int J CARS Proceedings, S66 -67).
3. Van der Velden, S., *Needle forces during interaction with blood vessels and the liver: Literature research towards the development of a liver phantom*. 2018.
4. Marieb, E.N. and K. Hoehn, *Human anatomy & physiology*. 2014: Pearson Education.
5. Siriwardena, A.K., et al., *Management of colorectal cancer presenting with synchronous liver metastases.* Nature reviews Clinical oncology, 2014. **11**(8): p. 446.
6. OpenStax. *Anatomy and physiology*. 2013 [cited 2018 March 15]; Available from: http://cnx.org/contents/14fb4ad7-39a1-4eee-ab6e-3ef2482e3e22@8.108.
7. van Gerwen, D.J., J. Dankelman, and J.J. van den Dobbelsteen, *Needle–tissue interaction forces–A survey of experimental data.* Medical Engineering and Physics, 2012. **34**(6): p. 665-680.
8. Zhai, J., et al., *A sensor for needle puncture force measurement during interventional radiological procedures.* Medical Engineering and Physics, 2013. **35**(3): p. 350-356.
9. Sigma-Aldrich. *Syringe Needle Gauge Chart*. [cited 2018 March 15]; Available from: https://www.sigmaaldrich.com/chemistry/stockroom-reagents/learning-center/technical-library/needle-gauge-chart.html.
10. Fung, Y.-c., *Biomechanics: mechanical properties of living tissues*. 2013: Springer Science & Business Media.
11. Elgezua, I., Y. Kobayashi, and M.G. Fujie, *Survey on current state-of-the-art in needle insertion robots: Open challenges for application in real surgery.* Procedia CIrP, 2013. **5**: p. 94-99.
12. Elgezua, I., et al. *Event classification in percutaneous treatments based on needle insertion force pattern analysis*. in *Control, Automation and Systems (ICCAS), 2013 13th International Conference on*. 2013. IEEE.
13. Elgezua, I., et al., *Online Event Classification for Liver Needle Insertion Based on Force Patterns*, in *Intelligent Autonomous Systems 13*. 2016, Springer. p. 1145-1157.
14. Jiang, S., et al., *Experimental study of needle–tissue interaction forces: effect of needle geometries, insertion methods and tissue characteristics.* Journal of biomechanics, 2014. **47**(13): p. 3344-3353.
15. Okuno, D., et al. *Development of an automatic blood sampling system: control of the puncturing needle by measuring forces*. in *Engineering in Medicine and Biology Society, 1998. Proceedings of the 20th Annual International Conference of the IEEE*. 1998. IEEE.
16. Healey, A.E., et al., *In vivo force during arterial interventional radiology needle puncture procedures.* Stud Health Technol Inform, 2005. **111**: p. 178-84.
17. Pepley, D., et al. *Measurement of syringe needle forces for a haptic robotic training device*. in *2017 Design of Medical Devices Conference*. 2017. American Society of Mechanical Engineers.
18. Kobayashi, Y., et al., *Development of a needle insertion manipulator for central venous catheterization.* The International Journal of Medical Robotics and Computer Assisted Surgery, 2012. **8**(1): p. 34-44.
19. Kobayashi, Y., et al., *Use of puncture force measurement to investigate the conditions of blood vessel needle insertion.* Medical Engineering and Physics, 2013. **35**(5): p. 684-689.
20. Kobayashi, Y., et al., *Preliminary in vivo evaluation of a needle insertion manipulator for central venous catheterization.* ROBOMECH Journal, 2014. **1**(1): p. 18.
21. Saito, H. and T. Togawa, *Detection of needle puncture to blood vessel using puncture force measurement.* Medical and Biological Engineering and Computing, 2005. **43**(2): p. 240-244.

22. Saito, H., K. Mitsubayashi, and T. Togawa, *Detection of needle puncture to blood vessel by using electric conductivity of blood for automatic blood sampling.* Sensors and Actuators A: Physical, 2006. **125**(2): p. 446-450.
23. Clement, R.S., et al., *Effects of axial vibration on needle insertion into the tail veins of rats and subsequent serial blood corticosterone levels.* Journal of the American Association for Laboratory Animal Science, 2016. **55**(2): p. 204-212.
24. Maurin, B., et al., *In vivo study of forces during needle insertions*, in *Perspective in Image-Guided Surgery*. 2004, World Scientific. p. 415-422.
25. Barbé, L., et al., *In vivo model estimation and haptic characterization of needle insertions.* The International Journal of Robotics Research, 2007. **26**(11-12): p. 1283-1301.
26. Washio, T. and K. Chinzei. *Needle force sensor, robust and sensitive detection of the instant of needle puncture*. in *International Conference on Medical Image Computing and Computer-Assisted Intervention*. 2004. Springer.
27. Shah, S., et al., *Robotically assisted needle driver: evaluation of safety release, force profiles, and needle spin in a swine abdominal model.* International Journal of Computer Assisted Radiology and Surgery, 2008. **3**(1-2): p. 173-179.
28. Kobayashi, Y., et al. *Modeling of conditions where a puncture occurs during needle insertion considering probability distribution*. in *Intelligent Robots and Systems, 2008. IROS 2008. IEEE/RSJ International Conference on*. 2008. IEEE.
29. Kobayashi, Y., et al. *In vitro validation of viscoelastic and nonlinear physical model of liver for needle insertion simulation*. in *Biomedical Robotics and Biomechatronics, 2008. BioRob 2008. 2nd IEEE RAS & EMBS International Conference on*. 2008. IEEE.
30. Kobayashi, Y., et al. *Developing a planning method for straight needle insertion using probability-based condition where a puncture occurs*. in *Robotics and Automation, 2009. ICRA'09. IEEE International Conference on*. 2009. IEEE.
31. Wang, W., et al., *Experimental analysis of robot-assisted needle insertion into porcine liver.* Bio-medical materials and engineering, 2015. **26**(s1): p. S375-S380.
32. Wang, Y., et al., *Optimal needle design for minimal insertion force and bevel length.* Medical Engineering and Physics, 2014. **36**(9): p. 1093-1100.
33. Wang, Y., et al., *The needle with lancet point: geometry for needle tip grinding and tissue insertion force.* Journal of Manufacturing Science and Engineering, 2013. **135**(4): p. 041010.
34. Kobayashi, Y., J. Okamoto, and M.G. Fujie. *Physical properties of the liver and the development of an intelligent manipulator for needle insertion*. in *Robotics and Automation, 2005. ICRA 2005. Proceedings of the 2005 IEEE International Conference on*. 2005. IEEE.
35. Kobayashi, Y., J. Okamoto, and M.G. Fujie. *Physical properties of the liver for needle insertion control*. in *Intelligent Robots and Systems, 2004.(IROS 2004). Proceedings. 2004 IEEE/RSJ International Conference on*. 2004. IEEE.
36. Hing, J.T., A.D. Brooks, and J.P. Desai. *Reality-based needle insertion simulation for haptic feedback in prostate brachytherapy*. in *Robotics and Automation, 2006. ICRA 2006. Proceedings 2006 IEEE International Conference on*. 2006. IEEE.
37. Hing, J.T., A.D. Brooks, and J.P. Desai, *A biplanar fluoroscopic approach for the measurement, modeling, and simulation of needle and soft-tissue interaction.* Medical image analysis, 2007. **11**(1): p. 62-78.
38. Bao, X., et al., *Experiment study on puncture force between MIS suture needle and soft tissue.* Biosurface and Biotribology, 2016. **2**(2): p. 49-58.
39. Yang, T., et al., *Identification of tissue types and boundaries with a fiber optic force sensor.* Science China Information Sciences, 2014. **57**(12): p. 1-7.
40. Mahvash, M. and P.E. Dupont, *Mechanics of dynamic needle insertion into a biological material.* IEEE Transactions on Biomedical Engineering, 2010. **57**(4): p. 934-943.
41. Okamura, A.M., C. Simone, and M.D. O'leary, *Force modeling for needle insertion into soft tissue.* IEEE transactions on biomedical engineering, 2004. **51**(10): p. 1707-1716.

42. Simone, C. and A.M. Okamura. *Modeling of needle insertion forces for robot-assisted percutaneous therapy*. in *Robotics and Automation, 2002. Proceedings. ICRA'02. IEEE International Conference on*. 2002. IEEE.
43. Simone, C., *Modeling of needle insertion forces for percutaneous therapies*. 2002, Citeseer.
44. Sahlabadi, M. and P. Hutapea, *Novel Design of Honeybee-inspired Needles for Percutaneous Procedure.* Bioinspiration & biomimetics, 2017.
45. Vidal, F.P., et al., *Simulation of ultrasound guided needle puncture using patient specific data with 3D textures and volume haptics.* Computer Animation and Virtual Worlds, 2008. **19**(2): p. 111-127.
46. Gokgol, C., C. Basdogan, and D. Canadinc, *Estimation of fracture toughness of liver tissue: Experiments and validation.* Medical Engineering and Physics, 2012. **34**(7): p. 882-891.
47. O'Rourke, M.F., et al., *Clinical applications of arterial stiffness; definitions and reference values.* American journal of hypertension, 2002. **15**(5): p. 426-444.
48. Boesen, M.E., et al., *A systematic literature review of the effect of carotid atherosclerosis on local vessel stiffness and elasticity.* Atherosclerosis, 2015. **243**(1): p. 211-222.
49. Lim, J., et al., *Interrelationships among various measures of central artery stiffness.* American journal of hypertension, 2016. **29**(9): p. 1024-1028.
50. Burton, A.C., *Relation of structure to function of the tissues of the wall of blood vessels.* Physiological reviews, 1954. **34**(4): p. 619-642.
51. Pearson, A.C., et al., *Transesophageal echocardiographic assessment of the effects of age, gender, and hypertension on thoracic aortic wall size, thickness, and stiffness.* American heart journal, 1994. **128**(2): p. 344-351.
52. Tao, J., et al., *Reduced arterial elasticity is associated with endothelial dysfunction in persons of advancing age: comparative study of noninvasive pulse wave analysis and laser Doppler blood flow measurement.* American journal of hypertension, 2004. **17**(8): p. 654-659.
53. Sehmbi, H. and A. Perlas, *Basics of ultrasound imaging*, in *Regional Nerve Blocks in Anesthesia and Pain Therapy*. 2015, Springer. p. 27-56.
54. Majewicz, A., et al., *Behavior of tip-steerable needles in ex vivo and in vivo tissue.* IEEE Transactions on Biomedical Engineering, 2012. **59**(10): p. 2705-2715.
55. Hungr, N., et al., *A realistic deformable prostate phantom for multimodal imaging and needle-insertion procedures.* Medical physics, 2012. **39**(4): p. 2031-2041.
56. Callister, W.D. and D.G. Rethwisch, *Fundamentals of materials science and engineering*. Vol. 471660817. 2000: Wiley London, UK:.
57. Surry, K., et al., *Poly (vinyl alcohol) cryogel phantoms for use in ultrasound and MR imaging.* Physics in Medicine & Biology, 2004. **49**(24): p. 5529.
58. Jiang, S., S. Liu, and W. Feng, *PVA hydrogel properties for biomedical application.* Journal of the mechanical behavior of biomedical materials, 2011. **4**(7): p. 1228-1233.
59. King, D.M., et al., *Development of a vessel-mimicking material for use in anatomically realistic Doppler flow phantoms.* Ultrasound in medicine & biology, 2011. **37**(5): p. 813-826.
60. Nadkarni, S.K., et al., *A pulsating coronary vessel phantom for two-and three-dimensional intravascular ultrasound studies.* Ultrasound in medicine & biology, 2003. **29**(4): p. 621-628.
61. Chu, K.C. and B.K. Rutt, *Polyvinyl alcohol cryogel: An ideal phantom material for MR studies of arterial flow and elasticity.* Magnetic Resonance in Medicine, 1997. **37**(2): p. 314-319.
62. Kosukegawa, H., et al., *Measurements of dynamic viscoelasticity of poly (vinyl alcohol) hydrogel for the development of blood vessel biomodeling.* Journal of Fluid Science and Technology, 2008. **3**(4): p. 533-543.
63. LeVier, R.R., et al., *What is silicone?* Plastic and reconstructive surgery, 1993. **92**(1): p. 12-167.
64. Balter, M.L., et al., *Adaptive kinematic control of a robotic venipuncture device based on stereo vision, ultrasound, and force guidance.* IEEE Transactions on Industrial Electronics, 2017. **64**(2): p. 1626-1635.

65. Li, Z., et al. *A robotic system for investigation on mis-alignment force of needle and vein needle insertion into blood vessel*. in *Intelligent Robot Systems (ACIRS), 2017 2nd Asia-Pacific Conference on*. 2017. IEEE.
66. De Lorenzo, D., et al. *Experimental evaluation of a coaxial needle insertion assistant with enhanced force feedback*. in *Engineering in Medicine and Biology Society, EMBC, 2011 Annual International Conference of the IEEE*. 2011. IEEE.
67. Naemura, K., Y. Uchino, and H. Saito. *Effect of the needle tip height on the puncture force in a simplified epidural anesthesia simulator*. in *Engineering in Medicine and Biology Society, 2007. EMBS 2007. 29th Annual International Conference of the IEEE*. 2007. IEEE.
68. Naemura, K. *Comparative phantom study on epidural anesthesia needle*. in *Engineering in Medicine and Biology Society, 2006. EMBS'06. 28th Annual International Conference of the IEEE*. 2006. IEEE.
69. Kendall, J.L. and J.P. Faragher, *Ultrasound-guided central venous access: a homemade phantom for simulation.* Canadian Journal of Emergency Medicine, 2007. **9**(5): p. 371-373.
70. Kikinis, R., S.D. Pieper, and K.G. Vosburgh, *3D Slicer: a platform for subject-specific image analysis, visualization, and clinical support*, in *Intraoperative imaging and image-guided therapy*. 2014, Springer. p. 277-289.
71. Cignoni, P., et al. *Meshlab: an open-source mesh processing tool*. in *Eurographics Italian chapter conference*. 2008.
72. Kazhdan, M. and H. Hoppe, *Screened poisson surface reconstruction.* ACM Transactions on Graphics (ToG), 2013. **32**(3): p. 29.